UNIVERSITÉ DU QUÉBEC

VARIABILITÉ SAISONNIÈRE ET INTERANNUELLE DES EAUX DOUCES DANS LES MERS ARCTIQUES : LE CAS DE LA BAIE D'HUDSON

THÈSE

PRÉSENTÉE À

L'UNIVERSITÉ DU QUÉBEC À RIMOUSKI

comme exigence partielle

du programme de doctorat en océanographie

PAR

PIERRE ST-LAURENT

Juin, 2010

REMERCIEMENTS

I would like to thank the members of my thesis committee and jury, Dr. M. Gosselin (chair, ISMER–UQAR), Dr. S.J. Déry (examiner on jury, UNBC), Dr. K.F. Drinkwater (examiner on committee, IMR), and my thesis supervisors, Dr. F. Straneo (advisor, WHOI), Dr. J.-F. Dumais (co-advisor, ISMER–UQAR), and Dr. D.G. Barber (co-advisor, Univ. Manitoba). They provided precious insight into the scientific questions examined, and the thesis highly benefited from their constructive and helpful comments. Dr. Straneo in particular was a dedicated and enthusiastic advisor, and it was a joy to work with her over the last two years.

The Dr. F.J. Saucier was the instigator and first advisor of this research project. His contagious passion for science, as well as the exuberant spirit he exhibited whenever I came up with novel results and ideas on Hudson Bay, were a constant inspiration and motivation over the first year of the project. I can hardly express how sorry I was to see him leave the institute, and ultimately lose his fight against cancer. The thesis is dedicated to his memory.

Plusieurs personnes m'ont aidé et supporté dans mon travail au fil des dernières années : tout d'abord Simon Senneville, par sa compréhension profonde du modèle de François, son souci pour la réussite des étudiants, et sa bonne humeur contagieuse ; James Caveen, qui partage mon goût pour les systèmes d'exploitation dignes de ce nom et les écrans noirs avec de gros caractères blancs ; Marcelle Martin et l'équipe de la bibliothèque de l'UQAR, qui ont poussé leurs recherches jusqu'en Australie pour obtenir les livres dont j'avais besoin ; le personnel de soutien de l'ISMER, qui ont tout fait pour m'accommoder dans mes requêtes...

...et tous mes collègues et amis du laboratoire et de l'UQAR en général !
« *If I never meet you in this life, let me feel the lack* », écrivait James Jones.
Ça a été un plaisir de vous côtoyer, et je ne vous oublierai pas de sitôt.

RÉSUMÉ

[1]The Arctic seas are characterized by the presence of a sea ice cover, a large river input and a net precipitation rate that make them fresh relative to the rest of the ocean, and a net export of freshwater via Fram Strait and the Canadian Arctic Archipelago. Recent studies highlight the substantial variability in the freshwater content of these seas and in their freshwater export to the nordic and subarctic seas. The goal of this work is to better understand the controls and impacts of the variability in Arctic sea's freshwaters. The thesis specifically focuses upon Hudson Bay, a large and shallow basin characterized by low salinity waters, a seasonal ice cover, and a large seasonal river input. The body of the thesis has three chapters whose objective, method, and main results, are summarized in the following lines.

The objective of the first chapter is to examine the impacts of the seasonal ice cover upon the ocean flow. The study specifically focuses on what effect the friction against the sea ice cover has on the barotropic tidal currents. The analysis makes use of new observations collected from eight different moorings successfully deployed over one complete seasonal cycle or longer. The instrument records reveal significant seasonal variations in Foxe Basin, Hudson Strait, and Hudson Bay. Multi-year records confirm the recurrent nature of this variability, and numerical simulations with a 3–D sea ice-ocean coupled model confirm the definite role played by friction in this variability. Regions of the basin where the flow is most affected are identified. The chapter was published in the Journal of Geophysical Research.

The objective of the second chapter is to investigate the processes controlling the fate of the river waters of Hudson Bay. To circumvent the lack of year-round surveys of these waters, the study makes use of a highly realistic 3–D sea ice-ocean coupled model whose results are consistent with the available observations. Most of the river waters are found to be transported by the general cyclonic circulation although a significant fraction is diverted to the interior of the basin. Ekman dynamics control the seasonal cross-shore exchange of river waters, with a variability that follows the curl of the wind stress over the basin. A tracer experiment confirms that a significant volume of river water is stored in the interior. Thus, this area can act as a reservoir that can substantially modulate the amount of freshwater released downstream to the subarctic seas. The chapter has been submitted to the Journal of Marine Systems.

The objective of the third chapter is to examine what controls the interannual variability in the storage and export of freshwater. A conceptual model of an Arctic sea is designed and applied to the case of Hudson Bay. Following the results from previous chapters and other studies, the model makes use of highly realistic forcing for the rivers and winds. A

[1]Notez que les sections Résumé, Introduction Générale, et Conclusion Générale, sont présentées en anglais et en français dans la thèse. Dans toutes ces sections la version anglaise précède celle en français, le passage d'une langue à l'autre étant souligné par le symbôle ∴.

hindcast simulation is conducted over the past 28 years and it shows substantial interannual variability in both storage and export of freshwater. In agreement with recent observations from the Beaufort Sea, the storage is controlled by Ekman pumping events, and its long-term evolution is related to the large-scale variability of the atmosphere (the Arctic Oscillation). The model results are compared to historical and previously unpublished observations, and the simulation is found consistent with the data. The chapter will soon be submitted to a peer-reviewed journal.

∴

Les mers arctiques sont caractérisées par la présence d'une couverture de glace, un grand apport des rivières et un bilan précipitation–évaporation positif qui les rendent peu salées par rapport au reste des océans, et enfin, un net export d'eau douce via le détroit de Fram et via l'Archipel arctique canadien. Des études récentes mettent en lumière la variabilité substantielle dans le contenu en eau douce de ces mers et dans leur export d'eau douce vers les mers nordiques et subarctiques. Le but de ce travail est de mieux comprendre les impacts de cette variabilité et les processus qui la contrôle. La thèse se concentre sur la baie d'Hudson, un grand bassin peu profond caractérisé par des eaux peu salées, une couverture glacielle saisonnière, et un grand apport saisonnier des rivières. Le corps de la thèse comporte trois chapitres dont les objectifs, méthode, et principaux résultats, sont soulignés dans les lignes suivantes.

L'objectif du premier chapitre est d'examiner les impacts de la couverture glacielle saisonnière sur l'écoulement océanique. L'étude se concentre plus spécifiquement sur l'effet de la friction à l'interface glace–océan sur les courants de marée barotropes. L'analyse fait usage de nouvelles observations provenant de huit différents mouillages déployés avec succès durant un cycle saisonnier complet ou plus. Les relevés des instruments révèlent des variations saisonnières significatives dans le bassin de Foxe, le détroit d'Hudson, et la baie d'Hudson. Des séries temporelles pluriannuelles confirment la nature récurrente de cette variabilité saisonnière, et les simulations numériques d'un modèle 3–D océan–glace de mer confirment le rôle important joué par la friction océan–glace dans cette variabilité. Les régions du bassin où l'écoulement est le plus affecté sont identifiées. Le chapitre a été publié dans le Journal of Geophysical Research.

L'objectif du second chapitre est d'examiner les processus contrôlant le devenir des eaux des rivières de la baie d'Hudson. Étant donné le peu de mesure disponibles hors de la courte période libre de glace, l'étude fait usage d'un modèle 3–D couplé océan–glace de mer réaliste dont les résultats sont cohérents avec les observations disponibles. Alors que la majeure partie des eaux des rivières est transportée par la circulation générale cyclonique, une proportion significative est détournée vers l'intérieur du bassin. La dynamique d'Ekman contrôle cet échange saisonnier des eaux des rivières entre la zone côtière et l'intérieur, en

suivant la variabilité du rotationnel des contraintes appliquées à la surface de l'eau. Une expérience avec un traceur numérique confirme qu'un volume important d'eau des rivières est stocké dans l'intérieur, cette région pouvant agir tel un réservoir qui peut moduler de façon substantielle l'export d'eau douce vers les mers subarctiques situées en aval. Ce chapitre a été soumis au Journal of Marine Systems.

L'objectif du troisième chapitre est d'examiner les processus contrôlant la variabilité interannuelle du stockage et de l'export de l'eau douce. Un modèle conceptuel d'une mer arctique est développé et appliqué au cas de la baie d'Hudson. Le modèle fait notamment usage de forçages hautement réalistes pour les rivières et les vents. Une simulation des 28 dernières années montre une variabilité interannuelle substantielle pour le stockage et l'export de l'eau douce. En accord avec de récentes observations de la mer de Beaufort, le stockage est contrôlé par les événements de pompage d'Ekman, et son évolution à long-terme est mise en relation avec la variabilité atmosphérique de grande-échelle (l'oscillation arctique). Les résultats du modèle sont comparés avec des observations historiques et d'autres présentées pour la première fois. De façon générale la simulation est cohérente avec ces observations. Le chapitre sera bientôt soumis à un journal revu par les pairs.

TABLE DES MATIÈRES

REMERCIEMENTS iii

RÉSUMÉ v

TABLE DES MATIÈRES ix

LISTE DES TABLEAUX xii

LISTE DES FIGURES xiii

INTRODUCTION GÉNÉRALE 1

ARTICLE I
ON THE MODIFICATION OF TIDES IN A SEASONALLY ICE-COVERED SEA . . 23

1.1 Abstract 23

1.2 Introduction 24

1.3 Method 27

1.3.1 Observations 27

1.3.2 Numerical Simulations 30

1.4 Results from Observations 34

1.5 Results from Numerical Experiments 39

1.5.1 Comparison with Observations 39

1.5.2 The Role of the Ice-Ocean Friction in the Modification of Tides . . . 40

1.5.3 Local and Remote Effects of the Ice-Ocean Stress upon Tides 41

1.5.4 The Effects of the Tides upon the Ice Cover 43

1.6 Discussion 45

1.7 Conclusions 47

1.8 Acknowledgements 47

ARTICLE II
WHAT IS THE FATE OF THE RIVER WATERS OF HUDSON BAY? 49

2.1 Abstract 49

2.2 Introduction 50

2.3 Method 54

2.4 Results 59
2.4.1 The Baseline: the Annual Freshwater Budget 59
2.4.2 The Role of Sea Ice Growth and Melt 61
2.4.3 The Fate of the River Waters 62
2.4.4 Exchanges between the Boundary and Interior Regions 66
2.4.5 What Regulates the Freshwater Stored in the Interior? 67
2.4.6 The Residence Time of the River Waters 73
2.5 Discussion 77
2.6 Conclusions 79
2.7 Acknowledgements 80
ARTICLE III
STORAGE AND EXPORT OF FRESHWATER IN ARCTIC SEAS: THE CASE OF HUDSON BAY 81
3.1 Abstract 81
3.2 Introduction 82
3.3 Method 84
3.3.1 The Conceptual Model 84
3.3.2 Forcing used in the Simulations 85
3.4 Results 91
3.4.1 General Features from the Model Simulation and Comparison with Observations 91
3.4.2 Storage and Export of Freshwater in Hudson Bay 96
3.4.3 The Formation of the Fresh Bursts 101
3.4.4 Is the Freshwater Balance in Phase with Climatic Indices? 104
3.5 Discussion 107
3.6 Conclusions 110
3.7 Acknowledgements 111
CONCLUSION GÉNÉRALE 113
RÉFÉRENCES 130

APPENDICE A
EXPANDED DESCRIPTION OF THE CONCEPTUAL MODEL 141

APPENDICE B
CALCULATION OF RIVER RUNOFF WITHIN HUDSON BAY 155

LISTE DES TABLEAUX

1	Location, period and depth of the pressure records used in the first article. . .	28
2	Comparison between observed and modeled values for the amplitude and phase of the M_2 tide.	33
3	Annual budget for the freshwater and volume of Hudson Bay.	60
4	Parameters and Forcing Used in the Numerical Simulation of Hudson Bay. . .	86
5	List of the numerical simulations conducted with the conceptual model. . . .	90
6	Size of gauged and ungauged areas within the drainage basin of Hudson Bay.	157

LISTE DES FIGURES

1 Map of Hudson Bay (HB) within the Arctic region. 2

2 Sea surface salinity in the Arctic and subarctic seas. 3

3 Pathway of liquid freshwater from the Arctic seas to the subarctic seas. 4

4 Spatial distribution of liquid freshwater within the Arctic and subarctic seas. . 6

5 Map of the Hudson Bay System. 26

6 Amplitude and phase of the M_2 tide in September 2003 (ice-free period) in the control simulation. 32

7 Monthly elevation of the M_2 tide from observations, the control simulation, and the experiment without ice-ocean stress. 35

8 Monthly phase of the M_2 tide from observations, the control simulation, and the experiment without ice-ocean stress. 37

9 Multiyear timeseries of amplitude and phase of the M_2 tide from observations. 38

10 Meridional M_2 velocity profile at station 7 from observations and the control simulation. 38

11 Difference between ice covered and ice free periods for the M_2 tide in the control simulation. 42

12 Tidal ice drift and under-ice barotropic energy dissipation during maximum ice cover. 44

13 Thickness of sea ice and peak-to-peak amplitude of the internal ice stress during maximum ice cover. 46

14 Map of Hudson Bay within the Arctic. 52

15 Salinity at the surface and along 61°N during the summer according to observations and the simulation. 56

16 Volume of freshwater in Hudson Bay over the year. 63

17 Spatial distribution of the river tracer, location and mean discharge of the rivers, surface salinity, and streamfunction of the mean surface currents. . . . 65

18 Freshwater budget for the interior region and seasonal cycle of the wind stress curl. 68

19 Stress at the ocean surface and Ekman transport for two contrasting periods. . 72

20 Gradual release of the river waters of 2004. 75

21 Schematic for the fluxes of river water after the injection period. 76

22 Top and side views of the conceptual model. 86

23 Climatologic seasonality of the hydrologic, cryospheric, and atmospheric forcing. 88

24 Map of Hudson Bay and the surrounding basins. 89

25 Mean depth of the interface and mean velocities in the boundary current. . . . 92

26 Comparison between observed and modeled velocities upstream of the boundary current. 94

27 Comparison between observations and model results downstream of the boundary current. 95

28 Interannual variability of the river runoff, wind stress curl, export of freshwater out of the basin, and volume of freshwater within the boundary region and interior. 97

29 Vertical profiles of freshwater concentration in the interior region. 99

30 Comparison between the modeled and observed freshwater flux downstream of the boundary current. 100

31 Sensitivity of the model to changes in hydrological and atmospheric forcing. . 103

32 Comparison between climate indices and the storage of freshwater. 106

33 Schematic for the relations between the Arctic Oscillation index, river runoff, and the storage/release of freshwater. 109

34 Comparison between the wind stress curl and observed along-shore velocities. 144

35 Period over which observed daily river runoff data is available for the ten largest rivers of Hudson Bay. 157

INTRODUCTION GÉNÉRALE

Background: On Freshwater in the Arctic seas

[2]The Arctic seas are a series of basins located north of the Arctic Circle (66°N, see Fig. 1 and IHO, 1953). These seas are characterized by waters of relatively low salinity (Fig. 2) and are sometimes collectively described as an estuary of the saltier North Atlantic Ocean (Britannica, 1984) in reference to the brackish zone found downstream of a river and upstream of the salty ocean.

A number of sources of freshwater contribute to the low salinity of the Arctic seas: water coming from the Pacific through Bering Strait (Melling et al., 2008, Pacific waters being generally fresher than their Atlantic counterpart), a positive precipitation minus evaporation rate (Dickson et al., 2007), and a relatively large river runoff both on the Eurasian and American sides (Lammers et al., 2001). The influence of the latter is clearly visible in the nearshore areas (Fig. 2).

On long timescales, the budget of Arctic freshwater must be close to a balance where sources of freshwater are cancelled by a net outflow of freshwater. The outflow occurs on the western and eastern sides of Greenland (white arrows, Fig. 3) and crosses the Nordic Seas (Greenland and Norwegian seas) and subarctic seas (Irminger and Icelandic basins, Labrador Sea; see Fig. 1). The signature of this fresh Arctic outflow is noticeable in maps of the surface salinity (Fig. 2), especially on the eastern side of Greenland and on the western side of the Labrador Sea. The latter region holds the Labrador Current (Fig. 1), a fresh and cold current extending down to the mid-Atlantic Bight (Chapman and Beardsley, 1989).

The Arctic seas thus appear conceptually as (1) a region holding a large amount of fresh

[2]Notez que les sections Résumé, Introduction Générale, et Conclusion Générale, sont présentées en anglais et en français dans la thèse. Dans toutes ces sections la version anglaise précède celle en français, le passage d'une langue à l'autre étant souligné par le symbôle ∴.

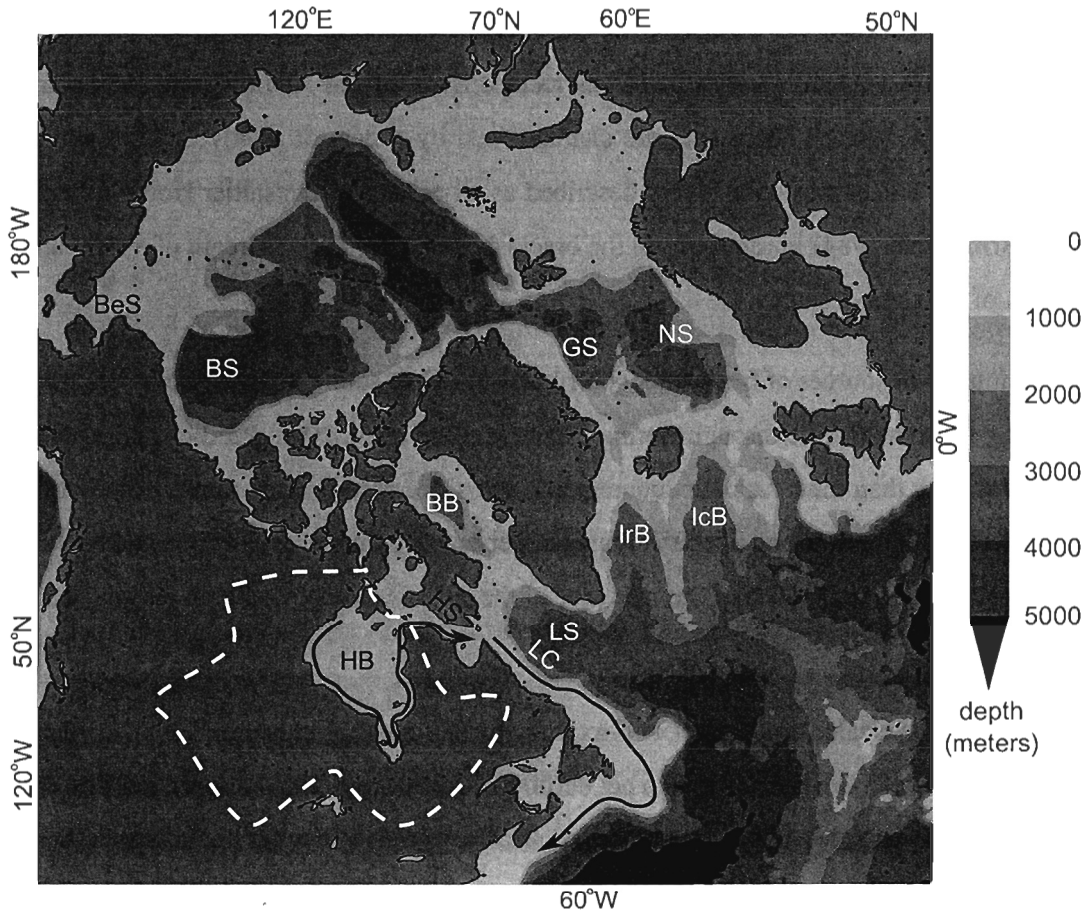

Figure 1: Map of Hudson Bay (HB) within the Arctic region. The drainage basin of HB is delimited by the white dashed line. The circulation of HB's surface waters and the Labrador Current (LC) are schematized by the magenta and black arrows, respectively. Also indicated are Bering Strait (BeS), Beaufort Sea (BS), Baffin Bay (BB), Hudson Strait (HS), Greenland Sea (GS), Norwegian Sea (NS), Irminger Basin (IrB), Icelandic Basin (IcB), and the Labrador Sea (LS).

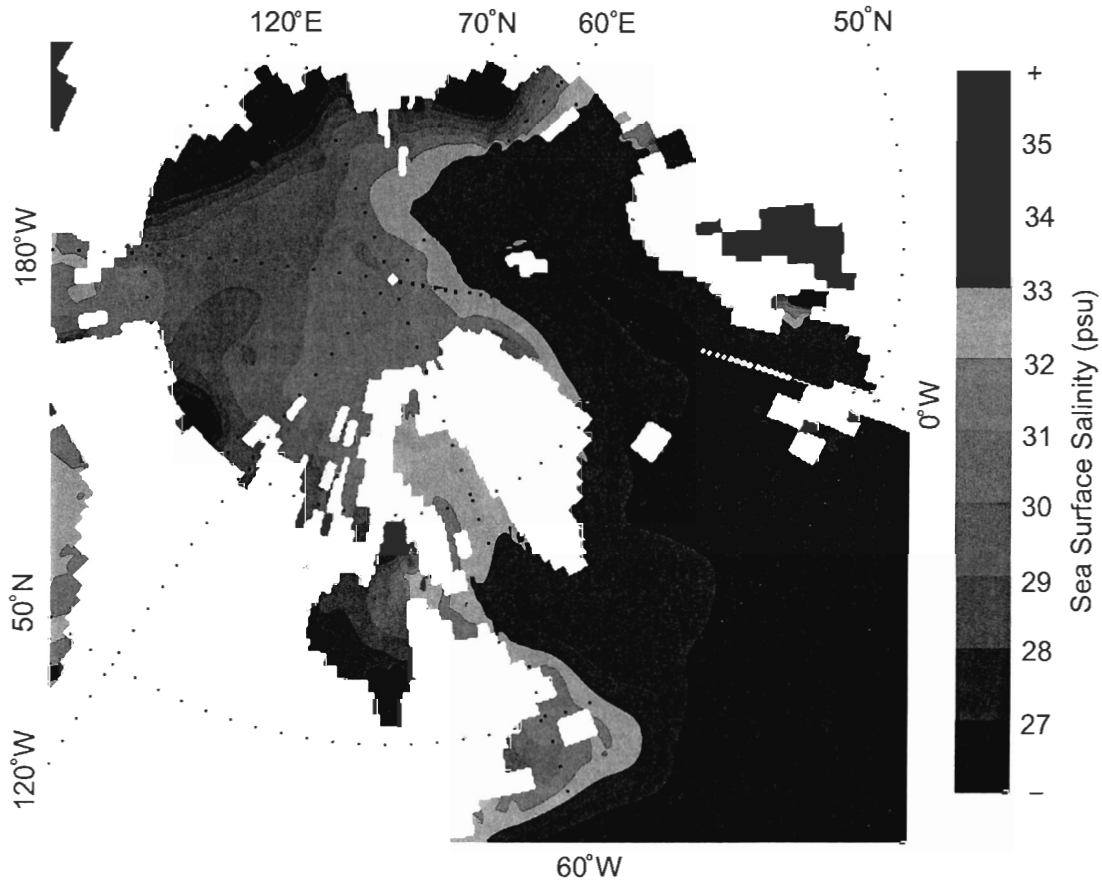

Figure 2: Mean sea surface salinity in the Arctic and subarctic seas. Data taken from the multiannual climatology of Steele et al. (2001, PHC version 2).

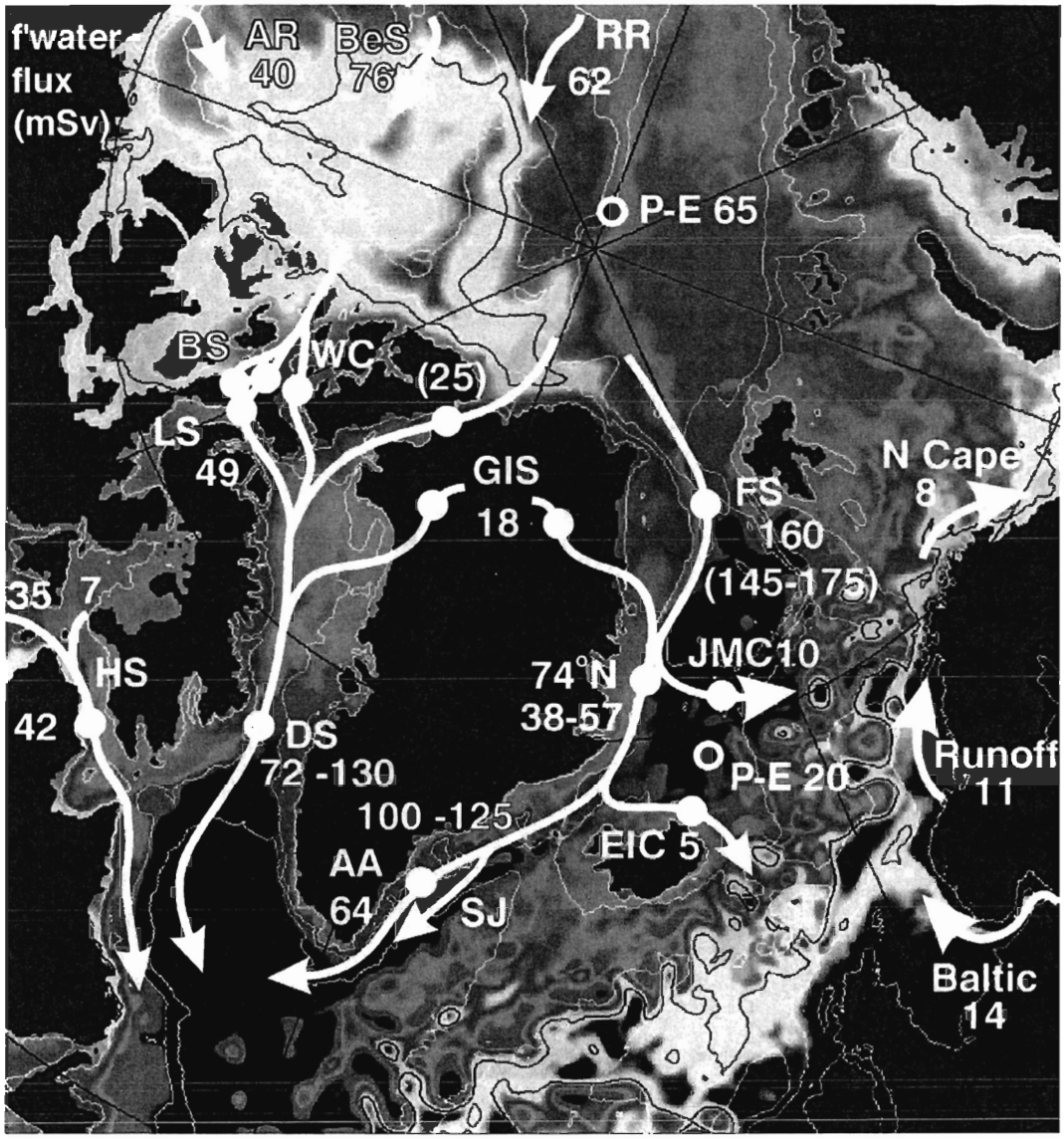

Figure 3: Pathway of freshwater from the Arctic seas to the subarctic seas (reproduced from Dickson et al. 2007). Fluxes of freshwater are represented by white arrows and in units of mSv ($1\,\mathrm{mSv} = 10^3\,\mathrm{m}^3\,\mathrm{s}^{-1}$). The background shows the sea surface deviation from the geoid, with warm (cold) colors associated with high (low) elevations. Surface geostrophic flow is to the left of gradients in elevation. All acronyms are described in Fig. 1 except AR (North American Rivers), RR (Eurasian Rivers), $P - E$ (precipitation minus evaporation), BS (Barrow Strait), WC (Wellington Channel), LS (Landcaster Sound), DS (Davis Strait), GIS (Greenland Ice Sheet), EIC (East Icelandic Current), FS (Fram Strait), and JMC (Jan Mayen Current).

waters, and (2) as a faucet that delivers a certain flux of freshwater to the nordic and subarctic seas located downstream (e.g., Fig. 3). The first of these concepts, the freshwater reservoir, is best illustrated by calculating the thickness of liquid freshwater over the Arctic and subarctic seas. This is accomplished by first defining the local concentration in liquid freshwater as:

$$c_{\mathrm{fw}} = \frac{S_0 - S}{S_0}, \tag{1}$$

where $S_0 \geq S$ is a constant salinity reference. With this relation, freshwater is assumed to be mixed within seawater of salinity S_0 in a proportion given by c_{fw}. The freshwater thickness of a water column is obtained by integrating Eq. 1 from the sea surface down to a depth z that could not be reached by river waters, precipitation, or ice melt, so that $S(z) = S_0$ (e.g., McPhee et al., 2009; Proshutinsky et al., 2009, note that z varies from one location to another):

$$T_{\mathrm{fw}} = \int_z^0 c_{\mathrm{fw}} \, \mathrm{d}z'. \tag{2}$$

The resulting freshwater thickness in the Arctic and subarctic areas is shown in Fig. 4. The figure is constructed from climatological salinity data (Steele et al., 2001) and thus represents the locations where freshwater is found on a time-averaged sense. It is seen that freshwater is mainly stored in the Beaufort Sea (see map on Fig. 1), a large basin characterized by a clockwise circulation (the Beaufort Gyre; see Proshutinsky et al., 2009).

Another region of significant freshwater storage is Hudson Bay (see Figs. 4 and 1). Hudson Bay is a shallow inland sea located in northeastern Canada between 50 and 65°N. Even though it is below the Arctic Circle, Hudson Bay is often considered part of the Arctic seas because of its anomalous cold climate (Maxwell, 1986) and because of its location upstream of an important subarctic sea (the Labrador Sea).

In summary, the Arctic seas are conceptualized as a reservoir where freshwater is stored, and also as a faucet that maintains a southward flux of freshwater. The storage is particularly evident in the Beaufort Sea and Hudson Bay areas, while the southward flux oc-

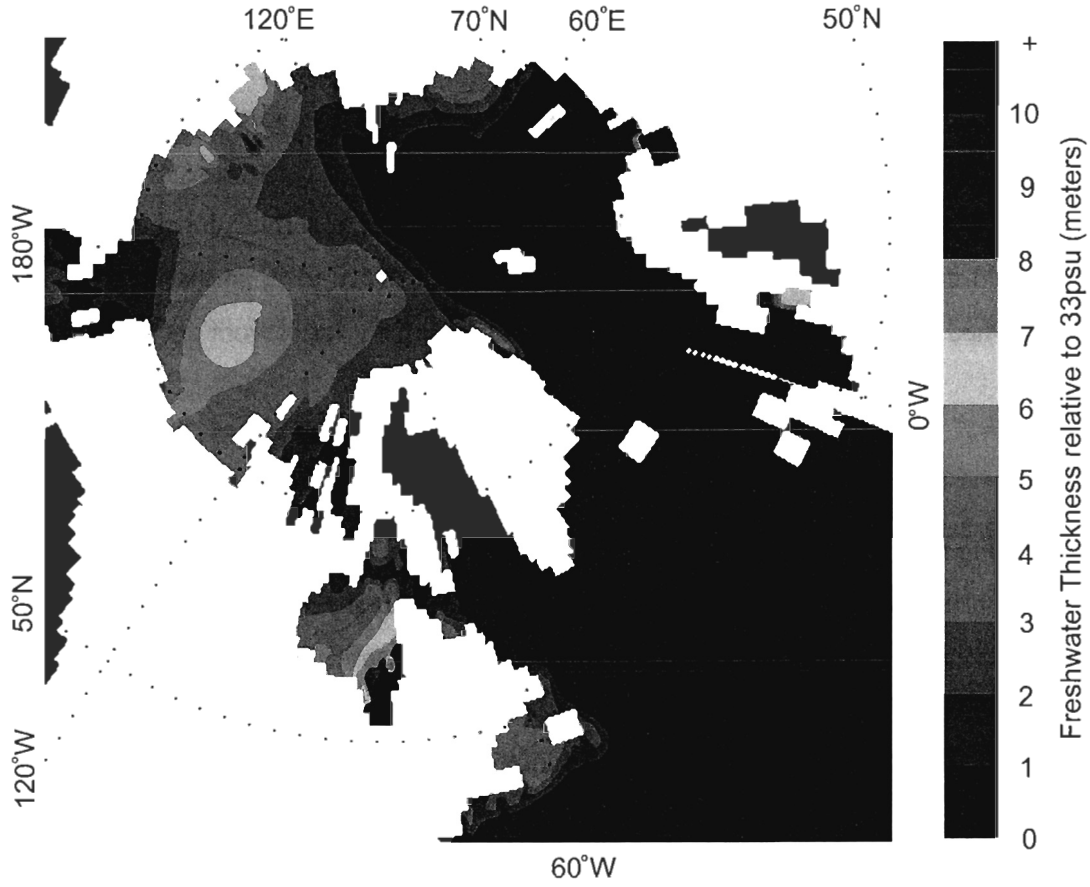

Figure 4: Mean thickness of liquid freshwater within the Arctic and subarctic seas (see Eqs. 1 and 2). Data taken from the multiannual climatology of Steele et al. (2001, PHC version 2).

curs on the eastern side of Greenland and on the western side of Baffin Bay/Labrador Sea. These observations summarize the key features of the time-averaged Arctic freshwater budget, and the deviations from this mean state will now be introduced in the next section.

Variability of the Freshwaters and its Scientific Implications

The previous section described key features of the mean state in the Arctic seas, in particular its storage of freshwater, and the mean freshwater fluxes toward the nordic and subarctic seas. These parameters are not fixed in time in reality, and constantly fluctuate around their mean value. Such variability is in many cases poorly understood (see Melling et al., 2008), first because of the difficulty of adequately sampling these systems, and also because of the inherent complexity of time-varying systems. This leads us to the central question of the thesis:

What are the controls and impacts of the variability in the Arctic freshwaters?

The goal of the thesis is thus to better understand the controls and impacts of the seasonal and interannual variability of the Arctic freshwaters, or more specifically those of Hudson Bay as it will be discussed in the next section. This investigation has several scientific implications. First, the variability in the freshwater storage and outflow from the Arctic seas is particularly relevant in the context of the large-scale Meridional Overturning Circulation (MOC) and its role in the global climate. The pathways of Arctic freshwater cross areas where deep convection normally occurs during the winter (e.g., Dickson et al., 2008), these convective sites being found notably in the Greenland and Labrador seas (Marshall and Schott, 1999). Anomalous high inputs of freshwater can increase the stratification and inhibit the wintertime convection and formation of dense waters (e.g., Lazier, 1980). Depending on the timing and magnitude of the freshwater anomaly over the convective sites, the MOC can be affected in important ways, with potential impacts for the climate of the Northern Hemisphere (Rahmstorf et al., 2005; Stouffer et al., 2006; Huisman et al., 2009).

Another issue that involves the whole Arctic region are the changes in climate that are induced by global warming. Although these changes occur on long timescales (30 years and longer), they are clearly visible in observational records, and the Arctic region is amongst the most severely affected regions on the planet (Bernstein et al., 2007). The warming atmosphere yields a reduced ice cover, so that a larger fraction of the seas is free to exchange freshwater with the atmosphere through evaporation and precipitation. The gradual release of solid freshwater (snow and ice) through melt/thaw also contributes to enhanced exchanges of freshwater between the atmosphere and the surface. This results in an increasing variability of the air–surface exchanges, i.e. the acceleration of the hydrologic cycle. Although such large-scale shift is difficult to assess with limited observations, there are recent evidences that the increased variability in precipitation is detectable in river runoff records around the Arctic seas (Déry et al., 2009).

Apart from its role in modulating the air–sea fluxes, the ice growth/melt cycle modifies in a profound way the ocean density field and its vertical stratification by brine rejection or melt-induced freshening (e.g., Prinsenberg, 1987). Through this seasonal cycle in stratification, the sea ice is likely to modulate the turbulent exchanges between the nutrient-rich deep layers and the surface layers where light is available, with consequences upon the primary production (e.g., Sibert et al., 2010). The sea ice cover can also play an important role in the seasonal modulation of the ocean flow within Arctic seas. Where it is thick and strong enough to resist the wind forcing, the ice cover acts as an insulator that inhibits the transfer of momentum from the winds to the ocean. A motionless ice cover can also act as a rough surface against which the ocean currents are damped (e.g., Prinsenberg, 1988a). The advection of the different water masses can be substantially different during the ice-covered period because of these processes.

Perhaps of even greater importance is the variability in the river runoff, the main source of freshwater in the Arctic budget (Dickson et al., 2007). Rivers first have a strong seasonal signal caused by the annual melt of snow over the continent. For instance, this freshet

causes the river runoff of Hudson Bay to increase by a factor of four between March and June (Fig. 23, this thesis). River runoff also has a substantial (±10%) interannual variability (Shiklomanov et al., 2000) that is related in some cases to the main mode of atmospheric variability north of 20°N (the Arctic Oscillation, Déry and Wood, 2004). On top of this natural variability, hydroelectric developments in some of the Arctic seas (e.g., Prinsenberg, 1980) lead to higher runoff during the winter and lower runoff during the spring and summer seasons.

Understanding the fate of these highly variable river waters within the Arctic seas seems of particular ecological importance. As for the annual ice melt, river runoff is a source of buoyancy that modifies the stability of the water column and the vertical exchanges of properties. Rivers are sometimes also sources of pollutants, notably mercury in the vicinity of hydroelectric developments (e.g., Mailman et al., 2006), and radioactive materials from the Russian rivers to the Kara Sea (Lind et al., 2006). Although the pathway of these substances is often complex, an assessment of their role at the ecological level would benefit from the knowledge of the dispersion and residence time of the river waters within the seas.

It was seen in this section that Arctic seas are subject to substantial variability in their freshwater content and inputs. This variability occurs on a continuum of timescales, in particular at the seasonal timescale through the sea ice growth/melt cycle and annual river freshet, and at interannual timescales typical of the large-scale atmospheric variability. This variability in the freshwaters of the Arctic seas was also seen to have broad implications, both at the global and regional scales. The next section will introduce one particular Arctic basin, Hudson Bay, where some of the issues mentioned will be examined in details.

The Case of Hudson Bay

The previous sections provided a general overview on the freshwaters of the Arctic seas. A comprehensive examination of these issues in all Arctic seas is obviously beyond the scope of this work, and so the present study focuses upon one Arctic sea in particular, Hudson Bay.

The present section shows that this specific basin includes the necessary components of an Arctic sea, so that its study in particular is useful for the understanding of the Arctic seas in general.

Hudson Bay is a large ($\sim 900\times900\,\mathrm{km}^2$), shallow ($\sim 100\,\mathrm{m}$), semi-enclosed sea located in northeastern Canada (Fig. 1; NOAA, 2006). Despite being located below the Arctic Circle, Maxwell (1986) notes that "in comparison with most other lands around the globe at the same latitude in the Northern Hemisphere, those in the vicinity of Hudson Bay and James Bay are abnormally cold". The cold climate over the basin results in the annual formation of a complete ice cover around December, this ice cover remaining in place until the early summer when it completely disappears (Hochheim and Barber, 2010). The thickness of the ice cover is only known from measurements nearshore and qualitative estimates from satellite images that range between one and two meters during the peak of winter (Markham, 1986; Prinsenberg, 1988b), comparable to the current mean ice thickness in the Arctic Ocean (1.75 m, Kwok and Rothrock, 2009).

Another component of the freshwater balance of the basin is the net precipitation minus evaporation rate. This rate is particularly difficult to estimate from the limited observations but the literature suggests values around $290\,\mathrm{kg\,m^{-2}\,y^{-1}} \approx 220\,\mathrm{km^3\,y^{-1}}$ at 60°N (Gill, 1982, his Fig. 2.5). This is much lower than, e.g., the annual freshwater input from the river runoff estimated to be $635\,\mathrm{km^3\,y^{-1}}$ on average in Hudson and James bays. We note that this value is a substantial (12%) fraction of the total pan-Arctic runoff (Lammers et al., 2001). The river runoff of Hudson Bay is spatially distributed within the basin, the main sources being the Thelon River, Nelson River, and a group of large rivers in James Bay (Fig. 24 of this thesis; see also Déry et al., 2005).

Hudson Bay also exchanges freshwater with its surrounding basins, but such exchanges are difficult to estimate from the limited knowledge of ocean flow and conditions (see Prinsenberg, 1984, 1986a,b, 1987; Ingram and Prinsenberg, 1998; Granskog et al., 2007, 2009; Lapoussière et al., 2009). Nearly all data are collected during the ice-free period (August–

October) and very few instruments were successfully moored over one or more years. Nevertheless, the data suggest that Hudson Bay has limited inflows of freshwater. Following the analysis of Straneo and Saucier (2008a), the flux of freshwater coming from the Arctic Archipelago is about 88 $km^3\ y^{-1}$ relative to 33 psu, which is much smaller than, e.g., the river runoff (635 $km^3\ y^{-1}$; see also section 2.3 for a discussion on the appropriate reference salinity for Hudson Bay). Similarly, transects across Hudson Strait (this channel providing the connection with the Atlantic Ocean) suggest that little freshwater enters there since the salinities on the inflowing/northern side of the channel are relatively high ($S \geq 33$ psu, see Straneo and Saucier, 2008a). This suggests that Hudson Bay imports little freshwater from the surrounding basins, and exports its net inputs from river runoff and net precipitation.

From the information gathered in this section, Hudson Bay includes the main components involved in the freshwater balance of an Arctic sea. First, it has a seasonal ice cover whose thickness is comparable to that in the Arctic Ocean. Second, Hudson Bay receives a substantial fraction of the pan-Arctic river runoff. Finally, the atmosphere and the surrounding basins contribute to smaller but significant inputs of freshwater. The next section will present which of these components are investigated within the body of the thesis.

Chapters and Objectives of the Thesis

The goal of this thesis is to better understand the controls and impacts of the variability in Hudson Bay's freshwaters. This central goal is addressed by considering in the first two chapters the seasonal variability of the system, and by examining its interannual variability in the third chapter. More precisely, the objective of the three chapters is to:

C.1 Examine the impacts of the seasonal sea ice cover upon the circulation of the waters.

C.2 Investigate the seasonal processes controlling the fate of the river waters.

C.3 Examine the controls behind the interannual variability in storage and export of freshwater.

The following paragraphs describe in more details these objectives, and the reader is referred to the chapters themselves for further reading.

Chapter 1: Impacts of the seasonal sea ice cover upon the circulation of the waters. The circulation of the waters in high latitude seas often shows a significant seasonality. Such seasonality may occur through several processes: (1) lower inputs of buoyancy (e.g. river runoff) during winter lead to a weaker buoyancy-driven flow, (2) a motionless ice cover reduces the transfer of momentum from the winds to the ocean, and (3) a motionless ice cover acts as a frictional surface that damps the ocean flow and spins it down. The objective of the first chapter is to specifically investigate process (3) by examining its effect upon the barotropic tidal currents (that have the advantage of being largely independent of changes in buoyancy inputs and wind forcing). The study builds on the previous work of Godin (1986) and Prinsenberg (1988a) by making use of several new records from year-long mooring deployments and a 3–D sea ice-ocean coupled primitive equations model of Hudson Bay.

Chapter 2: Seasonal processes controlling the fate of the river waters. Hudson Bay is characterized by a large annual river input representing the addition of an 80 cm layer of freshwater if distributed over the whole area of the bay. Moreover, a substantial fraction of this annual runoff is concentrated over a few months during the freshet period. Our understanding of the impacts of these river waters at the scale of the bay is however limited as it mostly originates from intantaneous samplings conducted during the ice-free period (Granskog et al., 2007, 2009). The objective of this chapter is to examine the relative importance of the river waters within the annual budget of the bay, and to investigate what processes control their seasonal dispersion and residence time within the basin. To circumvent the difficulty of obtaining year-long measurements, the chapter makes use of the results from a realistic 3–D sea ice-ocean coupled model.

Chapter 3: Controls behind the interannual variability in storage and export of freshwater. Arctic seas often have significant interannual variability in their atmospheric, cryospheric, and hydrologic forcing. It is a priori not simple to determine how these forcings relate to the

variability in the ocean freshwater storage and export, and through what processes. Following the results from previous studies (Déry et al., 2005; Proshutinsky et al., 2009; St-Laurent et al., 2010), the objective of this chapter is to specifically examine the role of the variable rivers and variable winds in the storage and export of freshwater. For this purpose, a conceptual model of an Arctic sea is designed. The storage of freshwater within the model is controlled by Ekman pumping, and the export of freshwater integrates the effect of the cryospheric, hydrologic, and atmospheric forcing. The simulated freshwater storage and export are compared to both historical and previously unpublished year-long observations from Hudson Bay.

These three chapters address the questions I considered the most important or urgent for the understanding of the freshwater balance of Hudson Bay. Obviously, all aspects of this freshwater balance could not be covered within the body of the thesis, and a number of open questions remain. Moreover, the results obtained in the study suggest interesting tracks for future research on Hudson Bay in particular and for the Arctic seas in general. These topics (and others) will be discussed together in the General Conclusion section.

∴

À propos des eaux douces des mers arctiques

Les mers arctiques sont un ensemble de bassins situés au nord du Cercle arctique (66°N, voir Fig. 1 et IHO, 1953). Ces mers sont caractérisées par dex eaux relativement peu salées (Fig. 2) et sont parfois décrites collectivement comme un estuaire de l'océan Atlantique (Britannica, 1984) en référence à la zone saumâtre située en aval d'une rivière et en amont des eaux océaniques très salées.

Un certain nombre de sources d'eau douce contribuent à la faible salinité des mers arctiques : les eaux provenant du Pacifique via le détroit de Bering (Melling et al., 2008,

les eaux du Pacifique étant généralement moins salées que celles de l'Atlantique), un bilan précipitation moins évaporation qui est positif (Dickson et al., 2007), et un apport des rivières relativement grand aussi bien du côté de l'Eurasie que du côté américain (Lammers et al., 2001). L'influence des rivières est clairement visible dans les régions côtières (Fig. 2).

Sur de longues échelles temporelles, le bilan des eaux douces arctiques doit être près d'un équilibre où les sources d'eau douces sont compensées par un export net d'eau douce. L'export se produit des côtés ouest et est du Groenland (flèches blanches, Fig. 3) et traverse notamment les mers nordiques (mers du Groenland et de Norvège) et les mers subarctiques (mers d'Irminger, d'Islande et du Labrador ; voir Fig. 1). La signature de cet export d'eau douce arctique est visible sur les cartes de salinité de surface (Fig. 2), particulièrement du côté est du Groenland et du côté ouest de la mer du Labrador. Cette dernière mer est l'hôte du courant du Labrador (Fig. 1), un courant froid et peu salé s'étendant jusqu'au sud de la Nouvelle-Angleterre (Chapman and Beardsley, 1989).

Les mers arctiques apparaissent donc conceptuellement comme (1) une région comprenant une grande quantité d'eaux douces, et (2) un robinet qui produit un flux d'eau douce en direction des mers nordiques et subarctiques situées en aval (e.g., Fig. 3). Le premier de ces concepts, le réservoir d'eau douce, est bien illustré par le calcul de l'épaisseur d'eau douce liquide des mers arctiques et subarctiques. Ce calcul s'effectue en définissant tout d'abord la concentration locale en eau douce liquide (Eq. 1), où $S_0 \geq S$ est une valeur constante de salinité, dite salinité de référence. Dans cette définition, l'eau douce est mélangée avec de l'eau de mer de salinité S_0 en une proportion donnée par c_{fw}. L'épaisseur d'eau douce d'une colonne d'eau est obtenue en intégrant l'Eq. 1 de la surface de l'eau jusqu'à une profondeur z qui n'a pu être atteinte par les eaux des rivières, des précipitations, ou par les eaux de fonte glacielle, de façon à ce que $S(z) = S_0$ (Eq. 2, e.g. McPhee et al., 2009; Proshutinsky et al., 2009, notez aussi que z varie d'un endroit à l'autre).

L'épaisseur d'eau douce qui en résulte est montrée pour les mers arctiques et subarctiques à la Fig. 4. La figure est assemblée à partir de données climatologiques de salinité

(Steele et al., 2001) et représente donc les régions où l'eau douce se trouve en moyenne. Il est apparent que l'eau douce est principalement stockée dans la mer de Beaufort (voir la carte, Fig. 1), un large bassin caractérisé par une circulation dans le sens des aiguilles d'une montre (la gyre de Beaufort; voir Proshutinsky et al., 2009).

Une autre région où le stockage d'eau douce est important est la baie d'Hudson (voir Figs. 4 et 1). La baie d'Hudson est une mer intérieure peu salée située au nord-est du Canada entre 50 and 65°N. Bien qu'elle soit située au sud du Cercle arctique, la baie d'Hudson est souvent considérée comme une mer arctique étant donné sont climat anormalement rigoureux (Maxwell, 1986) et sa position en amont d'un bassin subarctique important (la mer du Labrador).

En résumé, les mers arctiques sont représentées conceptuellement comme un réservoir où l'eau douce est stockée, et comme un robinet maintenant un flux d'eau douce vers le sud. Le stockage est particulièrement évident dans la mer de Beaufort et dans la baie d'Hudson, alors que le flux d'eau douce vers le sud est visible du côté est du Groenland et du côté ouest de la baie de Baffin ou de la mer du Labrador. Ces observations résument les éléments clefs du bilan moyen des eaux douces arctiques, et l'existence de déviations par rapport à cet état moyen sera discutée dans la prochaine section.

Variabilité des eaux douces et ses implications scientifiques

La section précédente a décrit les éléments clefs de l'état moyen des mers arctiques, en particulier le stockage de l'eau douce, et la présence d'un flux moyen dirigé vers les mers nordiques et subarctiques. Ces paramètres ne sont toutefois pas fixes dans le temps, et fluctuent constamment autour de leur valeur moyenne. Cette variabilité temporelle est encore largement inconnue (voir Melling et al., 2008), tout d'abord à cause de la difficulté d'échantillonner de façon adéquate ces systèmes, et aussi à cause de la complexité inhérente aux systèmes non-stationnaires (variables dans le temps). Cela nous mène à la question centrale de la thèse :

Quels sont les impacts de la variabilité des eaux douces arctiques, et quels processus la contrôlent ?

Le but de cette thèse est donc de mieux comprendre ce qui contrôle la variabilité saisonnière et interannuelle des eaux douces arctiques, et quels sont ses impacts. Cette recherche a plusieurs portées scientifiques. Tout d'abord, la variabilité du stockage et de l'export d'eau douce des mers arctiques est particulièrement intéressant dans le contexte de la circulation méridionale atlantique (Meridional Overturning Circulation, MOC) et son rôle dans le climat global. Le parcours des eaux douces arctiques traverse des régions où une convection profonde se produit normalement durant l'hiver (e.g., Dickson et al., 2008), ces sites convectifs étant notamment présents dans les mers du Groenland et du Labrador (Marshall and Schott, 1999). Des apports anormalement élévés d'eau douce peuvent accroître la stratification de ces régions et inhiber la convection hivernale et la formation d'eau dense (e.g., Lazier, 1980). Dépendant du synchronisme et de l'amplitude de l'anomalie en eau douce au dessus des sites convectifs, la MOC peut être affectée de façon importante, avec des impacts potentiellement importants pour le climat de l'Hémisphère Nord (Rahmstorf et al., 2005; Stouffer et al., 2006; Huisman et al., 2009).

Une autre question qui implique l'ensemble des mers arctiques est le changement climatique induit par le réchauffement global. Malgré que ces changements s'effectuent sur de longues échelles temporelles (30 ans et plus), ils sont clairement visibles dans les enregistrements expérimentaux, et l'Arctique est appelée à être une des régions les plus touchées par le réchauffement (Bernstein et al., 2007). Un tel réchauffement mène à une couverture glacielle réduite, signifiant qu'une proportion plus grande des mers est libre d'effectuer des échanges d'eau douce avec l'atmosphère (via l'évaporation et les précipitations). La libération graduelle des eaux douces autrefois stockées sous phase solide (neige et glace) contribue aussi à des échanges accrus entre l'atmosphère et la surface terrestre. Ces changements résultent en une variabilité accrue des échanges air–surface, c'est-à-dire en l'accélération du cycle hydrologique. Bien que ce genre de changement à grande échelle soit difficile à ob-

server avec un nombre limité d'instruments, des observations récentes montrent que la variabilité croissante des précipitations est détectable dans les jauges de débit des rivières tout autour de l'Arctique (Déry et al., 2009).

Outre son rôle dans la modulation des échanges air–océan, le cycle de croissance et de fonte glacielle modifie de façon profonde le champ de densité et sa stratification verticale à travers le rejet de sel lors de la croissance ou le rejet d'eau douce lors de la fonte (e.g., Prinsenberg, 1987). De par cette modulation saisonnière de la stratification, la glace de mer est susceptible d'aussi moduler les échanges turbulents entre les couches profondes riches en nutriments et les couches plus superficielles où la lumière est disponible, ceci ayant des conséquences sur la production primaire (e.g., Sibert et al., 2010). La couverture glacielle peut aussi jouer un rôle important dans la modulation saisonnière de la circulation océanique au sein des mers arctiques. Là où elle est épaisse et suffisamment rigide pour résister à la traction du vent, la couverture glacielle agit tel un isolant qui inhibe le transfert de momentum des vents à l'océan. Une couverture glacielle immobile peut aussi agir telle une surface rugueuse contre laquelle les courants océaniques sont amortis (e.g., Prinsenberg, 1988a). L'advection des différentes masses d'eau s'en trouve alors substantiellement modifiée pendant la période hivernale.

Peut-être d'encore plus grande importance est la variabilité de l'apport des rivières, ces rivières représentant la principale source d'eau douce dans l'Arctique (Dickson et al., 2007). Les rivières comportent tout d'abord un fort signal saisonnier causé par la fonte annuelle de la neige au dessus des continents. Par exemple, cette période de fonte s'accompagne d'un débit des rivières qui quadruple de mars à juin dans la baie d'Hudson (Fig. 23). Le débit des rivières comporte aussi une variabilité interannuelle substantielle ($\pm 10\%$) (Shiklomanov et al., 2000) qui est liée dans certains cas au principal mode de variabilité atmosphérique au nord du 20e parallèle (l'oscillation arctique, Déry and Wood, 2004). Outre cette variabilité naturelle, des développements hydroélectriques dans certaines mers arctiques (e.g., Prinsenberg, 1980) mènent à des débits plus élevés pendant l'hiver et des débits moins élevés au printemps et à

l'été.

La compréhension du parcours et du destin des eaux des rivières arctiques semble être d'une importance particulière pour l'écologie de ces systèmes. De façon analogue à la fonte annuelle des glaces, l'apport des rivières représente une source de flottabilité qui modifie la stabilité de la colonne d'eau et l'échange vertical des propriétés. Les rivières sont aussi parfois sources de polluants, notamment du mercure à proximité des développements hydroélectriques (e.g., Mailman et al., 2006), et aussi de substances radioactives dans le cas des rivières russes se jettant dans la mer de Kara (Lind et al., 2006). Bien que le cheminement exact de ces substances soit souvent complexe (notamment à cause de leur interaction avec les organismes marins), toute étude de la portée de ces substances au niveau écologique bénéficierait de la connaissance de leur dispersion et de leur temps de résidence dans les mers arctiques.

Il a été vu dans cette section que les mers arctiques sont sujettes à une variabilité temporelle substantielle dans leurs apports et leur contenu en eau douce. Cette variabilité apparait sur un continuum d'échelles temporelles, en particulier à l'échelle saisonnière de par le cycle de production/fonte glacielle, et aux échelles interannuelles typiques de la variabilité atmosphérique de grande échelle spatiale. Il a aussi été vu que cette variabilité des eaux douces arctiques a plusieurs implications, aussi bien aux échelles régionale que globale. La prochaine section introduiera une mer arctique en particulier, la baie d'Hudson, où certains éléments de la problématique décrite ci-haut seront examinés en détails.

Le cas de la baie d'Hudson

Les sections précédentes ont procuré un aperçu général des eaux douces des mers arctiques et des questions scientifiques s'y rapportant. Un examen approfondi de ces questions dans l'ensemble des mers arctiques est bien évidemment au delà des objectifs du présent travail, et c'est pourquoi cette étude se concentre plutôt sur une mer arctique en particulier, la

baie d'Hudson. La section présente montre que ce bassin inclut les composantes nécessaires d'une mer arctique, et donc que l'étude de la baie d'Hudson en particulier représente une avancée pour la compréhension des mers arctiques en général.

La baie d'Hudson est une large ($\sim 900 \times 900\,km^2$) mer, peu profonde ($\sim 100\,m$), partiellement refermée, et située au nord-est du Canada (Fig. 1 ; NOAA, 2006). Bien qu'elle soit située au sud du Cercle arctique, Maxwell (1986) note que « in comparison with most other lands around the globe at the same latitude in the Northern Hemisphere, those in the vicinity of Hudson Bay and James Bay are abnormally cold ». Le climat froid au dessus du bassin résulte chaque année en la formation d'une couverture glacielle complète en décembre, cette couverture demeurant en place jusqu'à l'été où elle disparait complètement (Hochheim and Barber, 2010). L'épaisseur de la couverture de glace n'est connue que de quelques mesures effectuées près des côtes, et d'estimations qualitatives (e.g. le type/catégorie de la glace) obtenues d'images satellitaires ; des épaisseurs variant entre un et deux mètres sont rapportées au plus fort de l'hiver (Markham, 1986; Prinsenberg, 1988b), comparable à l'épaisseur moyenne actuelle dans l'océan arctique (1.75 m, Kwok and Rothrock, 2009).

Une autre composante du bilan des eaux douces du basin est celle des précipitations nettes (précipitation moins évaporation). Les précipitations nettes sont difficiles à évaluer avec le peu de mesures disponibles, mais la littérature suggère des valeurs autour de $290\,kg\,m^{-2}\,y^{-1} \approx 220\,km^3\,y^{-1}$ à 60°N (Gill, 1982, sa Fig. 2.5). Cette valeur est beaucoup plus faible que, par exemple, l'apport annuel des rivières qui est estimé à $635\,km^3\,y^{-1}$ en moyenne dans les baies d'Hudson et de James. On note aussi que cet apport des rivières représente une proportion substantielle (12%) de l'apport total des rivières arctiques (Lammers et al., 2001). Les rivières de la baie d'Hudson sont spatialement distribuées sur le bassin, les principales sources étant les rivières Thelon, Nelson, et un groupe de rivières situées dans la baie James (Fig. 24 de cette thèse ; voir aussi Déry et al., 2005).

La baie d'Hudson échange aussi de l'eau douce avec les bassins avoisinants, mais ces échanges sont difficilement quantifiables à partir des connaissances limitées des conditions

océaniques et de leur circulation (voir Prinsenberg, 1984, 1986a,b, 1987; Ingram and Prinsenberg, 1998; Granskog et al., 2007, 2009; Lapoussière et al., 2009). Pratiquement toutes les données sont recueillies pendant la période libre de glace (août à octobre) et très peu d'instruments sont demeurés mouillés et fonctionnels sur des périodes d'une année ou plus. Malgré ces difficultés, les observations suggèrent que la baie d'Hudson reçoit peu d'eau douce des bassins voisins. Suivant l'analyse de Straneo and Saucier (2008a), le flux d'eau douce provenant de l'archipel canadien est environ 88 $km^3\ y^{-1}$ relatif à 33 psu, ce qui est beaucoup plus faible que, e.g., l'apport dû aux rivières (635 $km^3\ y^{-1}$; voir aussi la section 2.3 pour une discussion sur le choix de la salinité de référence). De façon similaire, des sections latérales dans le détroit d'Hudson (ce détroit permettant le lien avec l'océan Atlantique) suggèrent que bien peu d'eau douce y entre étant donné que les salinités du côté nord (où l'eau entre) sont relativement élevées ($S \geq 33$ psu, voir Straneo and Saucier, 2008a). Ces observations suggèrent que la baie d'Hudson importe bien peu d'eau douce des bassins avoisinants, et exporte principalement des eaux douces provenant des rivières et des précipitations.

Des informations rassemblées dans cette section, il est évident que la baie d'Hudson comporte les principales composantes impliquées dans le bilan des eaux douces d'une mer arctique. Tout d'abord, la baie a une couverture glacielle dont l'épaisseur est comparable à celle de l'océan arctique. Puis, la baie d'Hudson reçoit une proportion substantielle de l'apport total des rivières arctiques. Finalement, l'atmosphère et les bassins avoisinants contribuent à des apports d'eau douce faibles mais néanmoins significatifs. La section suivante présentera lesquelles de ces composantes feront l'object d'une étude approfondie dans le cadre de cette thèse.

Chapitres et objectifs de la thèse

Le but de cette thèse est de mieux comprendre ce qui contrôle la variabilité des eaux douces de la baie d'Hudson et quels sont les impacts de cette variabilité. Les deux premiers

chapitres de la thèse considèrent la variabilité saisonnière du système, alors que le troisième porte sur la variabilité interannuelle du système. Plus spécifiquement, l'objectif de chacun des trois chapitres est de :

C.1 Examiner les impacts du cycle glaciel saisonnier sur la circulation des eaux.

C.2 Étudier les processus saisonniers déterminant le parcours et le devenir des eaux des rivières.

C.3 Examiner les processus contrôlant la variabilité interannuelle du stockage et de l'export de l'eau douce.

Les paragraphes qui suivent décrivent ces objectifs, et le lecteur est référé aux chapitres eux mêmes pour plus de détails.

Chapitre 1 : Impacts du cycle glaciel saisonnier sur la circulation des eaux. La circulation des eaux aux hautes latitudes montre souvent une certaine saisonnalité. Cette saisonnalité peut être liée à différents processus : (1) une diminution des apports en flottabilité durant l'hiver (e.g. débit des rivières) qui engendre un ralentissement de l'écoulement estuarien, (2) une couverture de glace immobile réduit le transfert de momentum des vents jusqu'à l'océan, et (3) une couverture de glace immobile agit comme une surface rugueuse qui amortit l'écoulement océanique et la décélère. L'objectif du premier chapitre est spécifiquement d'étudier le processus (3) en examinant son effet sur les courants de marée barotrope (qui ont l'avantage d'être largement indépendants des apports de flottabilité et des vents). Ce chapitre dépasse les études précédentes de Godin (1986) et Prinsenberg (1988a) en faisant l'usage de nombreux enregistrements provenant de mouillages déployés sur plusieurs années, et en utilisant un modèle 3–D couplé océan–glace de mer pour la baie d'Hudson.

Chapitre 2 : Processus saisonniers déterminant le parcours et le devenir des eaux des rivières. La baie d'Hudson est caractérisée par un important apport des rivières, cet apport représentant l'ajout annuel d'une couche d'eau douce de 80 cm lorsque distribué sur la superficie du bassin. Plus encore, cet apport est concentré pendant les quelques mois du printemps où a lieu la fonte des neiges sur le continent. Notre compréhension des impacts à l'échelle

de la baie de ces eaux des rivières est toutefois limitée car nos connaissances originent la plupart du temps d'échantillonnages instantanés effectués pendant la période libre de glace (Granskog et al., 2007, 2009). L'objectif de ce chapitre est d'examiner l'importance relative des eaux des rivières dans le bilan annuel des eaux douces de la baie, et de rechercher quels processus contrôlent leur dispersion saisonnière et leur temps de résidence dans le bassin. Afin de coutourner la difficulté associée à l'obtention de mesures in situ, le chapitre fait usage des résultats d'un modèle réaliste (3–D couplé océan–glace de mer).

Chapitre 3 : Processus déterminant la variabilité interannuelle du stockage et de l'export des eaux douces. Les mers arctiques comportent souvent une variabilité interannuelle significative dans leurs forçages atmosphériques, cryosphériques, et hydrologiques. Il est a priori difficile de déterminer comment ces forçages sont liés à la variabilité du stockage et de l'export des eaux douces, et par quels processus. Suivant les résultats d'études précédentes (Déry et al., 2005; Proshutinsky et al., 2009; St-Laurent et al., 2010), l'objectif de ce chapitre est d'examiner spécifiquement le rôle de la variabilité des rivières et des vents dans le stockage et l'export d'eau douce. À cette fin, un modèle conceptuel d'une mer arctique est développé. Le stockage d'eau douce dans ce modèle est contrôlé par le pompage d'Ekman, et l'export d'eau douce intègre les effects du forçage cryosphérique, hydrologique, et atmosphérique. Le stockage et l'export simulés sont comparés à des données historiques et à d'autres observations présentées pour la première fois.

Ces trois chapitres portent sur les questions que j'ai considérées comme les plus importantes ou pressantes pour la compréhension du bilan des eaux douces dans la baie d'Hudson. Évidemment, tous les aspects de ce bilan n'ont pu être couverts dans la thèse, et un nombre de questions demeurent ouvertes. De plus, les résultats obtenus dans la thèse suggèrent d'intéressantes pistes pour des études subséquentes sur la baie d'Hudson en particulier et sur les mers arctiques en général. Ces éléments (et bien d'autres) seront discutés en commun dans la section Conclusion Générale.

ARTICLE I

ON THE MODIFICATION OF TIDES IN A SEASONALLY ICE-COVERED SEA

1.1 Abstract

New observations from eight moorings located in Foxe Basin, Hudson Strait, and Hudson Bay, are used to study the seasonal variability of the M_2 tide. Significant seasonal variations of the M_2 surface elevation are found in all these regions and at all seasons. The largest variations occur during winter while both elevation increase (Hudson Strait) and decrease (Hudson Bay, Foxe Basin) are observed. These variations are found recurrent at the stations where multiyear observations are available. Observations from a velocity profiler are consistent with a seasonal damping of the tides because of friction under ice. Numerical simulations with a sea ice-ocean coupled model and realistic forcing qualitatively reproduce most of the features of the observed variability. The simulations show that the winter M_2 variations are essentially caused by the under-ice friction, albeit with strong regional differences. Under-ice friction mostly occurs in a limited region (Foxe Basin) and can account for both increased and decreased M_2 elevations during winter.

De nouvelles observations provenant de huit mouillages situés dans le bassin de Foxe, le détroit d'Hudson, et la baie d'Hudson, sont utilisés pour l'étude de la variabilité saisonnière de la marée M_2. Des variations saisonnières significatives dans l'amplitude de M_2 sont observées dans toutes ces régions et en toutes saisons. Les variations les plus grandes se produisent pendant l'hiver alors que des augmentations (détroit d'Hudson) et des diminutions (baie d'Hudson, bassin de Foxe) de l'amplitude sont observées. Ces variations sont montrées récurrentes aux stations où sont disponibles des relevés couvrant plusieurs années. Des observations provenant d'un courantomètre couvrant la colonne d'eau sont cohérents avec un amortissement saisonnier des marées causé par la friction à l'interface glace–océan. Des sim-

ulations numériques avec un modèle couplé océan–glace de mer et des forçages réalistes reproduisent de façon qualitative la plupart des caractéristiques de la variabilité observée. Ces simulations montrent que les variations hivernales de M_2 sont principalement causées par la friction contre la glace, avec toutefois de fortes différences spatiales. La friction contre la glace se produit surtout dans une région limitée (basse de Foxe) et elle explique tout aussi bien l'augmentation que la diminution des amplitudes de M_2 pendant l'hiver.

1.2 Introduction

Seasonal changes in the characteristics of Arctic tidal waves have been reported as early as 1917 (Zubov, 1943). The changes often consist in a decrease of tidal elevations during winter (Zubov, 1943; Godin and Barber, 1980; Murty, 1985; Johnson and Kowalik, 1986). The lower elevations suggest a damping mechanism that dissipates tidal energy during winter. A potential damping mechanism is the friction produced at the interface between the ice and the ocean. For instance, Sverdrup (1927) described the near-surface shear layer formed by tidal currents underneath the ice.

Under-ice friction is particularly expected in the marginal seas that are characterized by significant tides and ice cover. The horizontal stress at the ice-ocean interface is often parameterized as the stress over the sea floor (a quadratic stress). Sea ice is seldom motionless so the stress is proportional to the relative velocity between ice and water (e.g., Pease et al., 1983). High levels of under-ice friction are expected during high ice concentration periods, i.e. when the ice cover is complete. The ice plates are then confined by shorelines and their mobility is significantly hampered. The relative velocity between the ice and the tidal current increases and the stress exerted over the tidal stream becomes significant.

Recent studies have shown that the interaction between ice and tides may play a significant role in the climate of ice-covered seas. The model study from Polyakov and Martin (2000) showed that tidal mixing helps in transporting heat to the sea surface and is important

in the establishment and maintenance of a recurrent polynya in the Okhotsk Sea (see also observations from Martin et al. 2004). In a similar way, the parameterization of tides in the Arctic Ocean Model Intercomparison Project (AOMIP) led to a more realistic ventilation of ocean heat through atmosphere-ocean exchanges in tidal leads (Holloway and Proshutinsky, 2007). Heil et al. (2008) also studied the drift and deformation of sea ice in the Weddell Sea using an array of drifting ice buoys. The sea ice velocity variance over the continental shelf was found to be dominated at semidiurnal frequencies by tides rather than inertial response. The variability of the sea-ice deformation was dominated by sub-daily processes (tides and inertial response) and low-frequency atmospheric changes played a secondary role.

While the importance of tides in the climate of ice-covered seas is investigated, the effect of ice upon tides remains elusive. Existing studies either show observed tidal variations alone (e.g., Prinsenberg and Hamilton, 2005) or model results without comparison with seasonal observations (Kagan et al., 2008). The precise role of the ice-ocean stress in the observed tidal variations is thus unclear. The Hudson Bay System (HBS), a shallow inland sea located in northern Canada (see Fig. 5), is an appropriate region to examine this process. The sea ice cover in HBS has a concentration c that seasonally fluctuates from $c \cong 0$ (generally ice-free conditions, around September) to $0.95 < c < 1$ (complete ice cover, around March). Significant seasonal variability of tides was reported in HBS by Godin (1986) and Prinsenberg (1988a) who both suggested that the changes are related to the ice cover.

In this work, we re-examine the seasonal variations of the principal tidal wave (M_2) in the HBS using new observations and results from a sea ice-ocean coupled 3–D numerical model. The new observations extend the work from Godin (1986) and Prinsenberg (1988a) by providing year-long coverage in Foxe Basin, Hudson Strait, and Hudson Bay. Section 1.3 describes the instruments and the numerical model used throughout the study. Section 1.4 shows the results from the observations. Significant seasonal changes in M_2 elevations are found throughout the Hudson Bay System. The numerical model is used in section 1.5 to examine the relationship between the under-ice friction and the seasonal variability of the

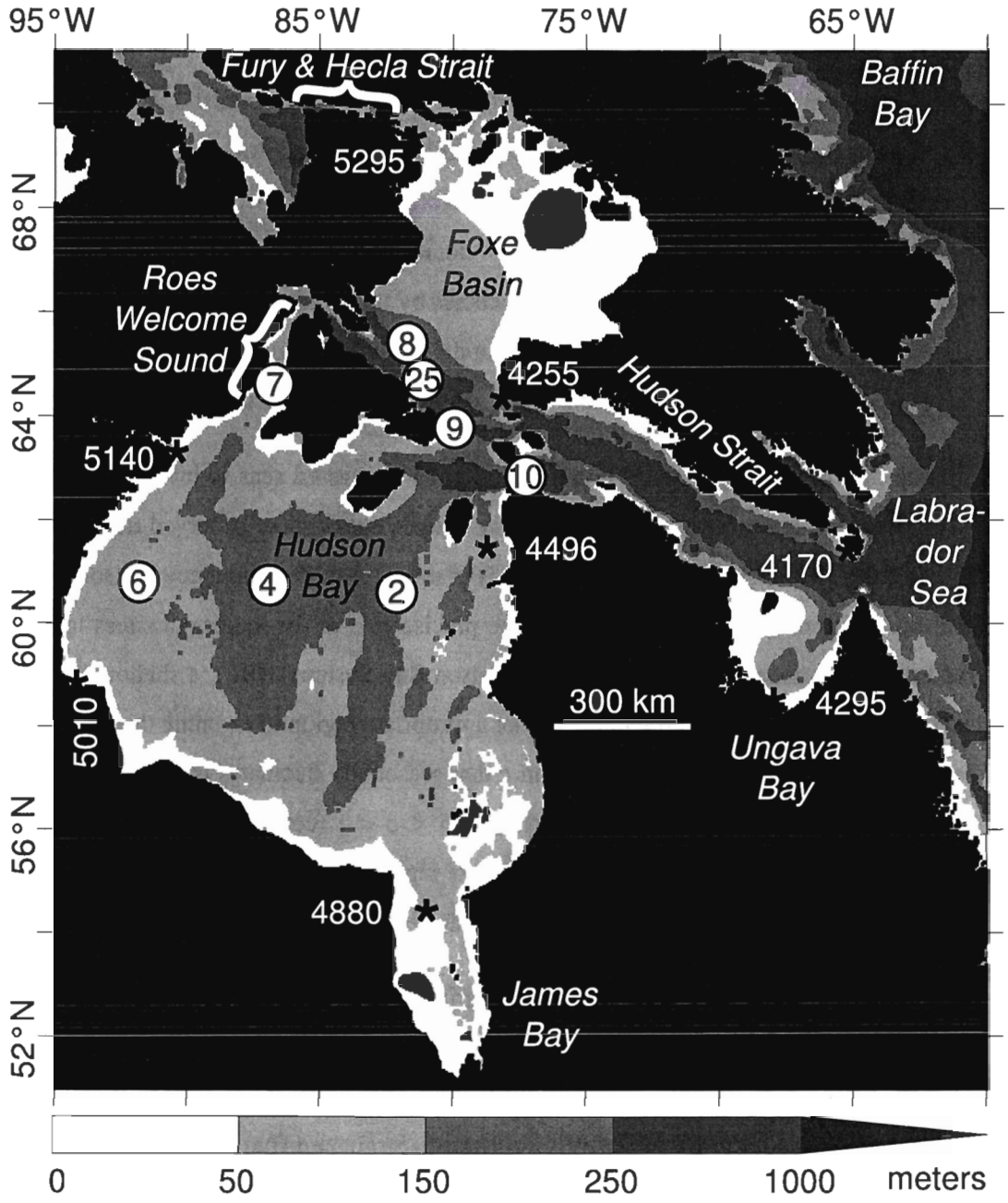

Figure 5: Map of the Hudson Bay System (HBS: Hudson Bay, Hudson Strait, Foxe Basin, James Bay, and Ungava Bay) with neighboring Labrador Sea and Baffin Bay. The stations used for the seasonal analyses are indicated by circled numbers. The stations used in Table 2 are indicated as black stars.

M_2 tide. It is found that the winter variations of the M_2 tide are essentially caused by the under-ice friction, albeit with strong regional differences. Finally, these results are discussed in section 1.6.

1.3 Method

1.3.1 Observations

Observed data (Saucier et al., 2004b) are from CTDs (Conductivity, Temperature and Depth measuring instruments) moored at eight different stations (see Fig. 5). Four stations are located in Hudson Bay, two are in Hudson Strait, and two are in southern Foxe Basin. All stations were occupied with CTDs for at least one year during August 2003–August 2006 (see Table 1 for the duration of the timeseries and the depth of the instruments). Pressure recorded every 30 min is used to study the seasonal modifications in the M_2 tide. We restrict our analyses to the M_2 wave since it dominates the tidal records and the currents in general (e.g., Prinsenberg, 1987).

The pressure record from each mooring is segmented into slightly overlapping monthly timeseries (32 days) for sequential harmonic analyses (Foreman, 1978; Mofjeld, 1986; Pawlowicz et al., 2002). This produces values for M_2 $\rho_s g\eta$ surface pressure and phase. The symbol ρ_s represents sea surface density and $g = 9.8$ m s^{-2}. The symbol η is the sea surface elevation above the mean sea level ζ. The sea surface elevation η and the mean sea level ζ include the submerged fraction of sea ice (see Mellor and Kantha, 1989, Fig. 1).

From the observations, the M_2 $\rho_s g\eta$ pressures typically deviate by 3×10^{-2} dbars from the annual mean. Such a large pressure deviation can hardly be related to changes in sea surface density (ρ_s). From observations at 25 m depth, and the model by Saucier et al. (2004a), monthly-averaged densities change by at most 2 kg m^{-3} over a year. For a tidal elevation with fixed amplitude $\eta = 1$ m, the resulting surface wave pressure change is

Table 1: Location, period and depth of the pressure records used in the study[a].

Station	2003	2004	2005	Depth (m)	H (m)
2[b]		X	X	148	155
4[c]	X	X	X	35	205
6	X			63	108
7	X			100	103
8	X			440	443
9	X			149	152
10	X			374	377
25		X		363	366

[a]All timeseries begin in August of the indicated year and last one year. H is the depth of the water column.

[b]The 2004 timeseries is used in Fig. 7.

[c]The 2003 timeseries is used in Fig. 7.

$|\Delta(\rho_s g\eta)| = 2 \times 10^{-3}$ dbars, an order of magnitude smaller than the observed $\rho_s g\eta$ deviation. Thus, observed M_2 $\rho_s g\eta$ pressure amplitudes may be converted to η amplitudes without significant alteration. This is performed using a constant density value of $\rho_s = 1024\,\mathrm{kg\,m^{-3}}$ determined from available observations and model results (e.g., Mofjeld, 1986).

The pressure records used in this study were mostly obtained from CTDs located a few meters above sea floor, making them only slightly sensitive to a tilt of the mooring line. The shallowest instrument was located 35 m below surface at station 4 in 2003 (Table 1). Records from this station are also available for years 2004 and 2005. The instruments in 2004 and 2005 were much deeper (7 m above sea floor) and the M_2 harmonics from 2004 and 2005 are consistent with those obtained from the shallow instrument in 2003. In any case, the software used for the harmonic analyses provides confidence intervals (level 95%) according to the spectrum of the residual, i.e. the energy that could not be related to tides (Pawlowicz et al., 2002). The intervals thus provide the error associated with the ambient noise.

One station in Hudson Strait was eliminated because of the poor quality of the pressure record. The mooring had only one CTD located close to the surface (at 30 m depth). Investigations have shown that the particularly strong currents found there caused a significant and irregular tilt of the mooring line (e.g., Straneo and Saucier, 2008b). Also, the seasonal variations of the phase of M_2 at station 25 are not available. Comparison between instrument records revealed that the internal clock of this particular CTD cumulated a lag of 10 hours over the year, which resulted in a gradual and artificial change in the phase of the wave over the months. Such lag was not observed in the records from the other instruments.

The measurements from a velocity profiler are also available for this study. This ADCP (Acoustic Doppler Current Profiler) was moored in an upward-looking position at station 7 from August 2003 to August 2004. The currents were recorded with a vertical separation of 2 m and a sampling frequency of 30 min. Harmonic analyses are performed over these velocity records to provide the seasonal variations of the M_2 velocity profile in the meridional direction. This corresponds to the amplitude of the horizontal M_2 currents in (approximately)

the along-strait direction.

1.3.2 Numerical Simulations

The results from a numerical model (Saucier et al., 2004a) are used to further investigate the M_2 variations. The model solves the 3–D hydrostatic primitive equations over the whole HBS domain (Foxe Basin, Hudson Bay/Strait, James and Ungava Bays, see Fig. 5). The horizontal resolution is 10 km and bathymetry is reproduced using 36 z-levels and partial cells at the bottom (e.g., Adcroft et al., 1997). The ocean model is coupled to a dynamic and thermodynamic two-layer sea ice model (Semtner, 1976; Hunke and Dukowicz, 1997), and a single layer snow model. Landfast ice is not included in the model. According to Markham (1986), landfast ice is important in only two locations, east of the Belcher Islands, and in northern Foxe Basin. The simulated ice velocities (Fig. 12a) are particularly small in these regions which is consistent with the behavior of landfast ice. The absence of landfast ice in the model should thus not represent an important limitation.

The simulation is conducted under realistic atmospheric, hydrologic, and oceanic forcing for the August 2003–August 2004 period. These forcing, initial salinity and temperature, momentum and scalar diffusion, and comparison with observations are discussed in Saucier et al. (2004a). Tides are introduced by prescribing the sea elevation at open boundaries according to nine tidal constituents: M_2, S_2, N_2, K_2, O_1, K_1, P_1, M_4, and MS_4. These constituents are held constant throughout the simulation and astronomical forcing over HBS is neglected (see Freeman and Murty, 1976). The free surface is treated using a semi-implicit time discretization and a 5 min timestep. Modeled harmonics are computed as with the observations but this time using modeled water levels sampled at the model timestep.

Table 2 shows a comparison between the simulated M_2 wave (Fig. 6) and observations. The largest relative errors are found in Roes Welcome Sound and in James Bay, and sensitivity experiments have shown that these errors can be attributed to the poorly constrained

bathymetry of the basin. Significant variations in depths are visible when comparing common bathymetric databases and the nautical charts from the Canadian Hydrographic Service. The amplitude and phase in specific locations (Roes Welcome Sound, James Bay, and western Hudson Strait) were found particularly sensitive to changes in bathymetry, perhaps because of significant wave interference. The results from this study are obtained using Etopo2'v2 (NOAA, 2006) and the nautical charts from the Canadian Hydrographic Service.

The ocean currents and sea ice interact through a stress at the ice-ocean interface:

$$\tau_{\text{ice}} = \rho_0 C_{\text{DIO}} \|\mathbf{v}_{\text{water}} - \mathbf{v}_{\text{ice}}\| (\mathbf{v}_{\text{water}} - \mathbf{v}_{\text{ice}}) \tag{1.1}$$

where $\rho_0(\mathbf{x}_h)$ is time and depth-averaged seawater density, $\mathbf{x}_h$ is the position in the horizontal (h) plane, C_{DIO} is the ice-ocean drag coefficient valid at five meters below ice ($z = -5$ m), $\mathbf{v}_{\text{water}}(\mathbf{x}_h, t)$ is the horizontal ocean velocity at $z = -5$ m, and $\mathbf{v}_{\text{ice}}(\mathbf{x}_h, t)$ is sea ice velocity. Empirically-derived ice-ocean quadratic drag coefficients are often calculated using ocean velocity at one meter below sea ice, and their magnitude is found in the range $1.32 \times 10^{-3} < C_{\text{DIO}} < 26.8 \times 10^{-3}$ (Langleben, 1982; Pease et al., 1983; Madsen and Bruno, 1986). There is a considerable spread in these values as they were estimated in highly different ice conditions. For instance, Steiner (2001) suggests an empirical relation between ice thickness and the drag coefficient.

A series of experiments was conducted to determine the appropriate ice-ocean drag coefficient in the range $1 \times 10^{-3} < C_{\text{DIO}} < 4 \times 10^{-3}$. The value 2×10^{-3} (applied at $z = -5$ m) produced satisfactory agreement between observed and modeled M_2 surface elevations over the year. This value is close to that used by Hibler (1979) for the Arctic ice (5.5×10^{-3}). The spatial and temporal distributions of the friction under ice were found qualitatively similar in all our simulations. The main difference was that the simulations using the highest drag coefficients produced M_2 seasonal variations that exceeded the natural range shown by observations.

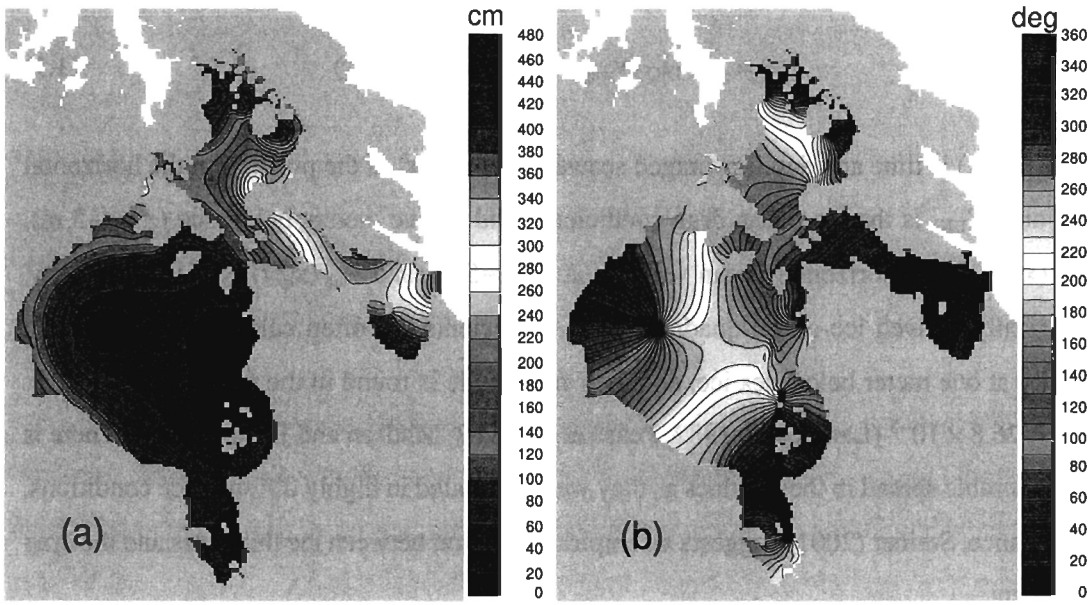

Figure 6: (a) Amplitude and (b) phase (relative to Greenwich) of the M_2 surface tidal wave during September 2003 (ice-free period) in the control simulation.

Table 2: Comparison between observed (o) and modeled (m) values for the M_2 surface elevation amplitude A and phase ϕ relative to Greenwich. No observations are available for the phase at station 25 (see text).

Station	A_o (m)	ϕ_o (deg)	$A_m - A_o$ (m)	$\phi_m - \phi_o$ (deg)
4170	2.3	349	0.22	8
4255	2.1	112	−0.08	−7
4295	4.1	14	0.35	8
4496	0.4	95	−0.04	−24
4880	1.0	4	−0.38	2
5010	1.5	26	0.19	10
5140	1.4	276	0.14	−9
5295	0.7	0	−0.04	1
2	0.26	171	−0.07	1
4	0.18	243	0.02	0
6	0.74	335	0.04	3
7	1.78	258	0.47	−10
8	1.40	160	−0.02	−6
9	1.08	116	0.03	−16
10	1.31	59	0.37	3
25	1.30	na	−0.09	na

1.4 Results from Observations

The observed monthly variations of the M_2 surface elevation, referenced to the mean value in August, are shown for the four stations of Hudson Bay in Fig. 7a. Significant elevation decrease is seen at station 7 from August to October. The decrease is also seen at stations 6 and 2, although it is not significant at the 95% level. Following this late summer decrease, amplitudes rise abruptly in December. The December rise is significant for stations 6 and 2 while station 7 shows a similar but non significant change. Winter (January to March) is characterized by decreasing amplitudes that are significant at all stations. During spring (April to July), amplitudes gradually rise back to their August value. The M_2 variability at these stations is similar to that from Godin (1986) and Prinsenberg (1988a).

Figure 7b shows the monthly variations of the M_2 surface elevation in Hudson Strait and Foxe Basin. The late summer/early autumn amplitude decrease is found again in Hudson Strait and Foxe Basin, and is significant at all stations. The December abrupt amplitude rise found in Hudson Bay can be compared to a similar rise occurring over January in Hudson Strait and Foxe Basin. During winter, stations 8 and 25 show a significant amplitude decrease also followed by a gradual increase back up to their August value. Recall that stations 8 and 25 are located in southern Foxe Basin, and stations 9 and 10 in western Hudson Strait (see Fig. 5). Stations 9 and 10 show a significant amplitude increase during winter and spring (January–May), with levels above those found in August.

The phase of the tidal wave also fluctuates over the year. Figure 8a shows these fluctuations for the stations inside Hudson Bay. A significant seasonal cycle is seen at all stations except station 4. The phase is advanced (high and low tides occur earlier) and the largest deviations are found during March and April. This deviation is particularly large at station 2 as the M_2 tide is earlier by 30 min ($-14°$). Figure 8b shows the fluctuations of the wave in Hudson Strait and Foxe Basin. The deviations are much smaller than in Hudson Bay and do not exceed $\pm 2°$. A significant seasonal cycle occurs at all stations with maximum deviations

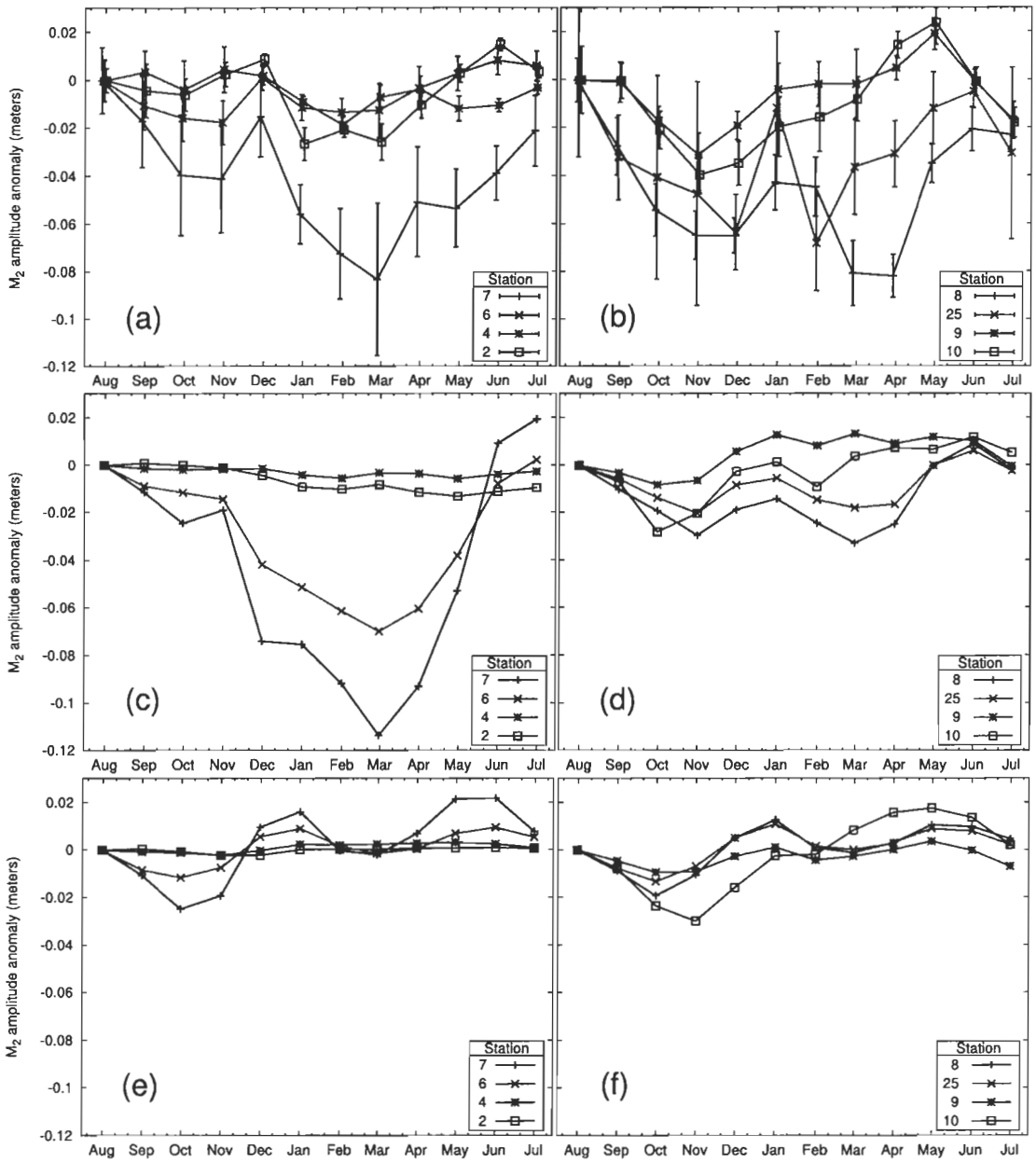

Figure 7: Monthly elevation of the surface M_2 tidal wave from (a,b) observations, (c,d) the control simulation, and (e,f) the experiment without ice-ocean stress. All values are referenced to those in August. Bars represent 95% confidence intervals (see Pawlowicz et al., 2002).

also around March and April. The phase is advanced at station 9 (mouth of Hudson Bay) but it is retarded in Foxe Basin and western Hudson Strait (stations 8 and 10, respectively). The phase at station 25 is not available (see section 1.3).

Multiyear timeseries are available at two stations and similar seasonal variations are observed over the years. Figure 9 shows the two longest timeseries available (3 years at station 4, and 2 years at station 2). A minimum is found over February–March of each year with small but significant interannual variations. The most noticeable anomaly is seen in June 2004. The figure also shows the variations of the phase at these stations. The particularly large deviation at station 2 is observed during the two sampled years.

The wave amplitudes that were shown in Figs. 7 and 9a represent the divergence $\nabla \cdot \overline{\mathbf{v}}$ of the depth-averaged current $\overline{\mathbf{v}}$. These values only reflect the vertical integration of all the changes in the tidal velocity profile. The velocity profile was measured at station 7 over the Aug. 2003–Aug. 2004 period, and Fig. 10a shows the meridional (i.e. approximately along-strait) amplitude of the M_2 velocities. The seasonal variations mainly occur in the first 30 m below the surface and the largest deviation from summertime values (Aug.–Sep.) occurs during the Feb.–March period. Note the increasing velocities at 80 m as the surface velocities decrease. These results are consistent with those from Fig. 7a and support the hypothesis of a seasonal modulation of tides caused by under-ice friction.

The new observations revealed three previously unknown features of the M_2 seasonal variability. First, significant variations occur all over the year and not only during winter. Then, the variability in Hudson Strait is qualitatively different from the one in Hudson Bay and Foxe Basin. Finally, the M_2 seasonal variations were found to be reproducible and similar over the years. The nature of this complex M_2 variability will be examined in the next section (section 1.5) with the help of numerical experiments.

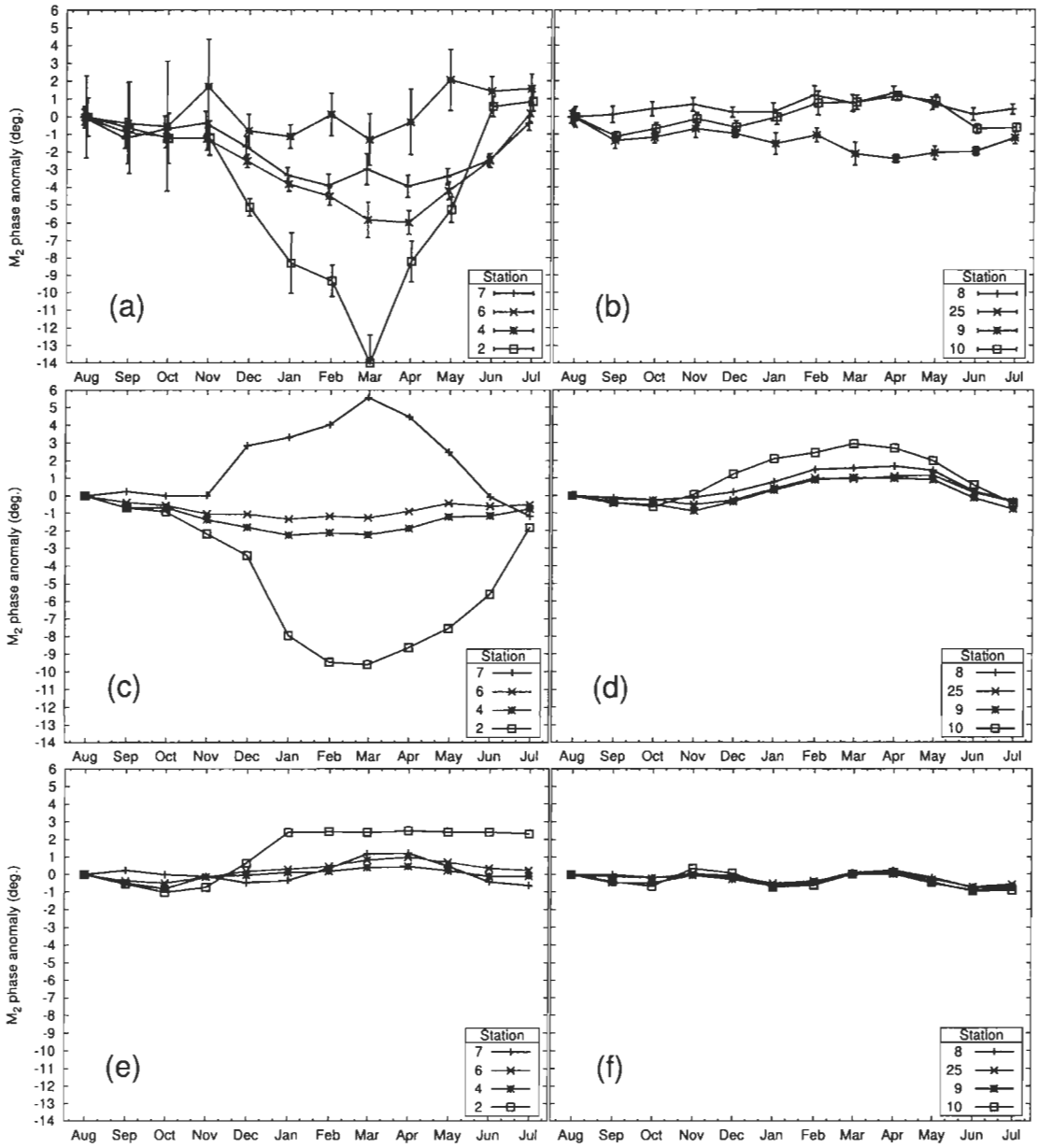

Figure 8: Monthly phase of the surface M_2 tidal wave from (a,b) observations, (c,d) the control simulation, and (e,f) the experiment without ice-ocean stress. All values are referenced to those in August. No observations are available for the phase at station 25 (see text). Bars represent 95% confidence intervals (see Pawlowicz et al., 2002).

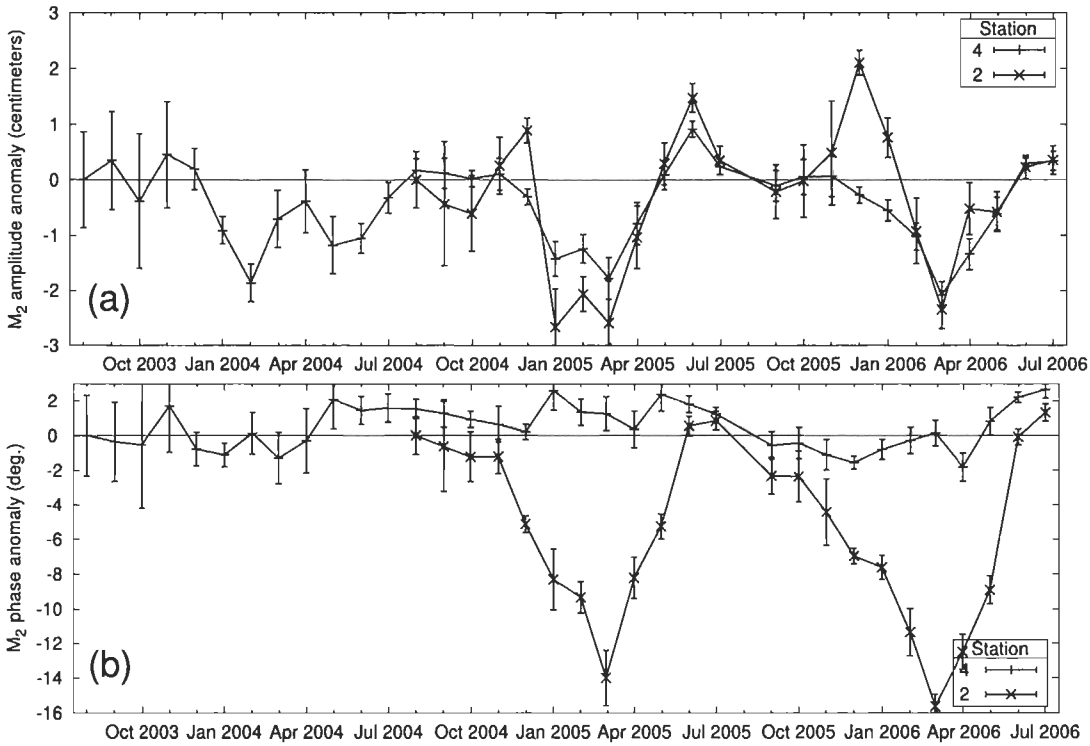

Figure 9: Multiyear timeseries of (a) amplitude and (b) phase of the M_2 surface wave from observations. The values at station 4 (2) are referenced to those in August 2003 (2004). Bars represent 95% confidence intervals (see Pawlowicz et al., 2002).

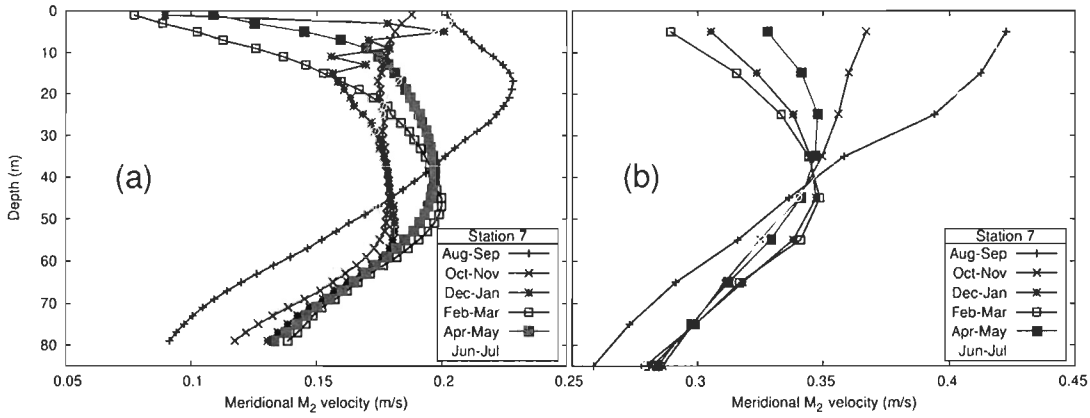

Figure 10: Meridional M_2 velocity profile at station 7 from (a) observations and (b) the control simulation for the 2003–2004 period.

1.5 Results from Numerical Experiments

The complex M_2 variability depicted in Figs. 7a,b and 8a,b is now examined using a numerical model. The model is able to simulate complete seasonal cycles of tidal amplitude and phase, and qualitatively reproduce most of the features of the observed variability. We first present a comparison between the modeled and observed variability. Then, we conduct an experiment where the ice-ocean stress is removed, in order to determine its role in the seasonal variations. The remote effect of the ice-ocean stress upon tides is presented. Finally, some effects of the tides upon the sea ice cover are introduced.

1.5.1 Comparison with Observations

Figures 7c,d and 8c,d show modeled results that correspond to the same period (Aug. 2003–Aug. 2004) and locations as the observations shown above. The model reproduces well the temporal variability of the variations, including summer decrease, the December abrupt rise in amplitude, largest deviations in amplitude and phase occurring in March, the relatively large phase deviation at station 2, and the general return to summertime values in July. However, the model overestimates or underestimates the variations at some stations, and does not reproduce the phase advance at stations 7 and 9. Investigations have shown that these errors can be related to the uncertain bathymetry in some locations (see section 1.3).

Regarding the effect of the ice-ocean friction upon the tidal velocity profiles, Fig. 10 shows a comparison between observed and modeled results at station 7. The modeled velocities show a constant barotropic overestimation of approximately 15 cm s^{-1}, an error already visible in Table 2 and that can be related to errors in bathymetry (see section 1.3). Apart from this constant barotropic offset, it can be seen that the model satisfactorily represents the seasonal variations, including thickness of the surface boundary layer, magnitude of the seasonal deviations in the upper velocities, and timing of the seasonal changes (minimum velocities over Feb.–March).

1.5.2 The Role of the Ice-Ocean Friction in the Modification of Tides

The modeled results presented so far (Table 2, Figs. 7c,d, 8c,d, and 10b) were obtained from a simulation using realistic conditions and this simulation will be called the control simulation hereafter. The presumed influence of under-ice friction upon the M_2 variability will now be discussed using the results of a second simulation with the same conditions as in the control, except that the ice-ocean friction is removed. Thus the dynamics remain the same in the ice-free situation but the tides are no longer damped by friction underneath the ice.

The comparison between the control (Fig. 7c,d) and the no-ice-ocean stress simulation (Fig. 7e,f) shows that the late summer decrease (first noticed in observations, Fig. 7a,b) is not modified by removing the ice-ocean stress. However, the M_2 variations during winter are greatly diminished by removing the ice-ocean stress. The stress causes a winter elevation decrease in Hudson Bay and Foxe Basin, and a small increase in western Hudson Strait (station 9). A similar comparison for the phase of the control (Fig. 8c,d) and the no-ice-ocean stress simulation (Fig. 8e,f) shows that the seasonal phase variations essentially vanish when the ice-ocean stress is removed.

Significant variance remains after the removal of the ice-ocean stress (Fig. 7e,f). The comparison of these curves with those observed (Fig. 7a,b) suggests that the remaining oscillations also occur in reality (but are partly obscured by the ice-ocean friction). For instance, a decrease is visible from July to November at stations 7, 6, 8, 25, 9 and 10, and an abrupt increase is visible in Dec.–Jan. at stations 7, 6, 8 and 25. The model seems to qualitatively reproduce these oscillations but their cause remains unknown.

1.5.3 Local and Remote Effects of the Ice-Ocean Stress upon Tides

The results from section 1.5.2 have shown that the effect of the ice-ocean friction is generally important for the phase or the amplitude of the M_2 wave. However, significant regional differences are noticeable in both observed and modeled seasonal variations. In this section, we examine these regional differences using the results from the numerical model.

Figure 11 shows the modification of the wave during the month when the ice cover is maximum (March). The amplitude of the wave increases in some locations and such increase is also visible in the observations from stations 9 and 10. The model predicts a significant decrease in eastern Hudson Bay and James Bay (consistent with the observations from Godin 1986) but the decrease in western Hudson Bay is known from Fig. 7a,c to be excessive. The modification of the phase is particularly important in northeastern Hudson Bay, a prediction that is consistent with the observations from station 2.

These changes were shown in section 1.5.2 to be essentially caused by the friction under ice. However, we do not know if this friction acts all over the system or if it is concentrated in specific locations. To answer this question, the rate at which the ice-ocean friction removes the barotropic energy at a given location is quantified for the month of March 2004 using Eq. 1.2:

$$D_{\text{ice}} = \overline{\mathbf{v}} \cdot \tau_{\text{ice}} c \tag{1.2}$$

In this equation, $\overline{\mathbf{v}}(\mathbf{x}_{\text{h}}, t)$ is the depth-averaged horizontal (h) ocean velocity, τ_{ice} is described in Eq. 1.1, and $0 < c < 1$ is the local ice concentration. The result from this computation, averaged over 708 h (approximately one month), is shown in Fig. 12b. The magnitudes vary largely because of the cubic relation with water velocity, i.e. $D_{\text{ice}} \propto \overline{\mathbf{v}} \cdot \|\mathbf{v}_{\text{water}} - \mathbf{v}_{\text{ice}}\| (\mathbf{v}_{\text{water}} - \mathbf{v}_{\text{ice}})$. The dissipation is concentrated along coasts, over shallow regions such as James Bay and eastern Foxe Basin, and where the amplitude of the wave is large (see Fig. 6a). The domain-integrated rate of dissipation averaged over March 2004 is 40 GW, which represents 18% of the dissipation that occurs over the sea floor during the same period

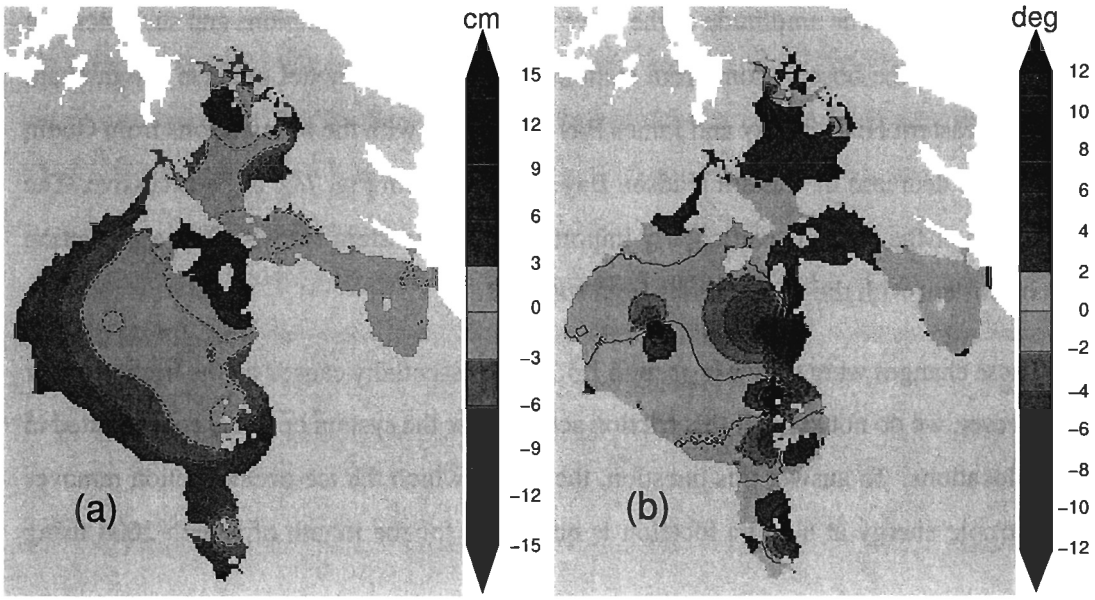

Figure 11: (a) Amplitude anomaly $A_{\text{March}} - A_{\text{Sept}}$ and (b) phase anomaly $\phi_{\text{March}} - \phi_{\text{Sept}}$ for the M_2 surface tidal wave in the control simulation. September is a generally ice-free period and March is the month of maximum ice cover.

(220 GW).

These results show that the changes in Fig. 11 are caused by friction that mostly occurs in Foxe Basin. The effects of the friction are however visible in remote locations (far from Foxe Basin) since friction leads to a modification of the interference pattern over the whole system. For instance, the large phase deviation at station 2 is, according to the model, caused by the shoreward displacement of the nearby amphidromic point during winter (the point is visible in northeastern Hudson Bay, Fig. 6b). This particular amphidromic point becomes degenerate (e.g., Pugh, 1987, p. 261) during winter because of friction.

1.5.4 The Effects of the Tides upon the Ice Cover

The previous sections focused on the effects of the ice-ocean friction upon the M_2 wave. We will conclude this study by showing some effects of the tides upon the ice cover according to the control simulation. Figure 12a shows the ellipses of tidal ice drift for the M_2 wave during the month of maximum ice cover (March 2004). It is found that significant ice movements are induced by the tides. The ice velocities are approximately 30 cm s^{-1} in Hudson Strait and Foxe Basin but attain 1 m s^{-1} in southeastern Foxe Basin (the M_2 tidal range is above 4 m in these locations). Lower velocities (below 15 cm s^{-1}) are found in the other regions. The ice ellipses are similar to those of the M_2 barotropic tide (not shown) except that the ice velocities are generally lower. Notably, the ratio between the barotropic M_2 velocities and the ice velocities exceeds 3 in northern Foxe Basin, James Bay, and southeastern Hudson Bay.

The low ice velocities in southeastern Hudson Bay and northern Foxe Basin are consistent with the recurrent presence of landfast ice in these areas (Markham, 1986) but further work would be required to understand this uneven response to tides, and the effect of tides upon ice mechanics. For instance, tidally-induced movements of ice may contribute to the redistribution (ridging) and deformation of the ice cover. The modeled internal ice stress

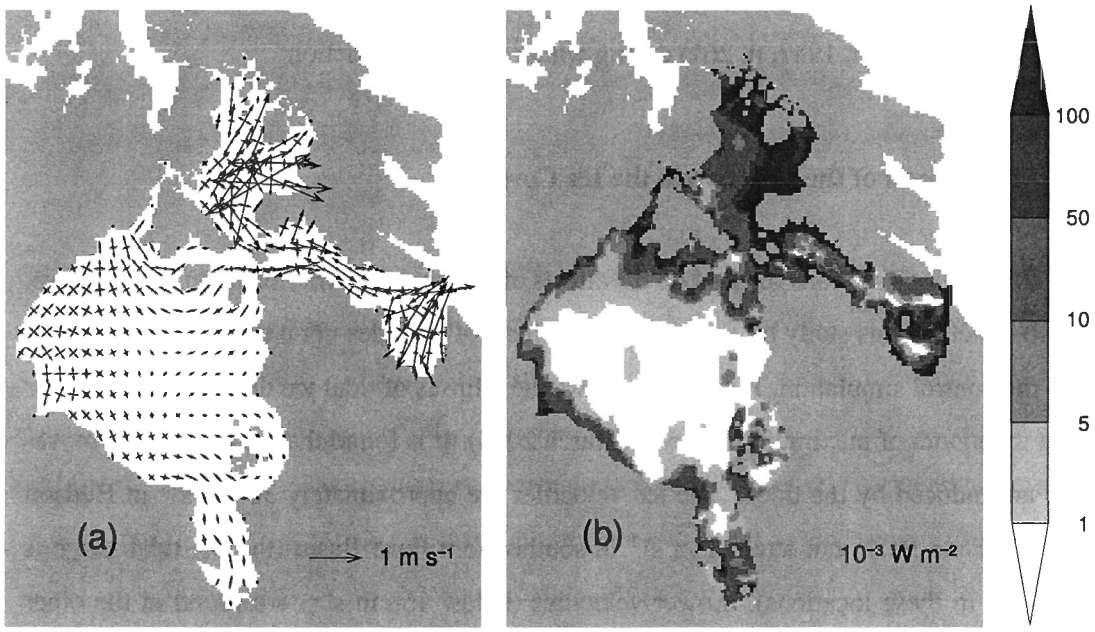

Figure 12: (a) Ellipses of tidal ice drift for the M_2 wave and (b) under-ice barotropic energy dissipation rate during the month of March 2004 (maximum ice cover) in the control simulation.

components σ_{11} and σ_{22} (σ is the internal ice stress tensor, see Hunke and Dukowicz 1997) essentially oscillate at a semidiurnal rate, and Fig. 13 provides the peak-to-peak amplitude of the internal ice stress $\sqrt{\sigma_{11}^2 + \sigma_{22}^2}$ oscillation at M_2 frequency, along with the thickness of the ice cover during March 2004. It is seen that the tidally-induced ice stress is most important in Foxe Basin, with values of the same order of magnitude as semidiurnal fluctuations observed in the Barents Sea (25 to 50 kPa) (Tucker and Perovich, 1992).

1.6 Discussion

The seasonal variability of the M_2 elevation was examined using new observations from Hudson Bay, Hudson Strait, and Foxe Basin. It was shown for the first time that significant seasonal M_2 variability occurs throughout the system and at all seasons. This expands the results from Godin (1986) and Prinsenberg (1988a) as their studies were limited to Hudson Bay and James Bay. Another new result is the presence of variations in the tidal wave during the ice-free period. Although these variations were qualitatively captured by the model, their cause remains unknown.

The largest fluctuations occur during winter and are qualitatively different amongst regions. The M_2 elevation in Hudson Bay and Foxe Basin decreases from December to March, but the elevation in Hudson Strait increases. Such increase was also observed in the Bering Sea by Mofjeld (1986) but the cause of these variations could not be determined. Our numerical experiments confirm that the winter modifications of the M_2 elevation in HBS are essentially caused by the under-ice stress, as suspected by Godin (1986). These experiments also show that the friction is mostly active in a limited region (Foxe Basin) and modifies the position of the amphidromic points in remote locations (station 2).

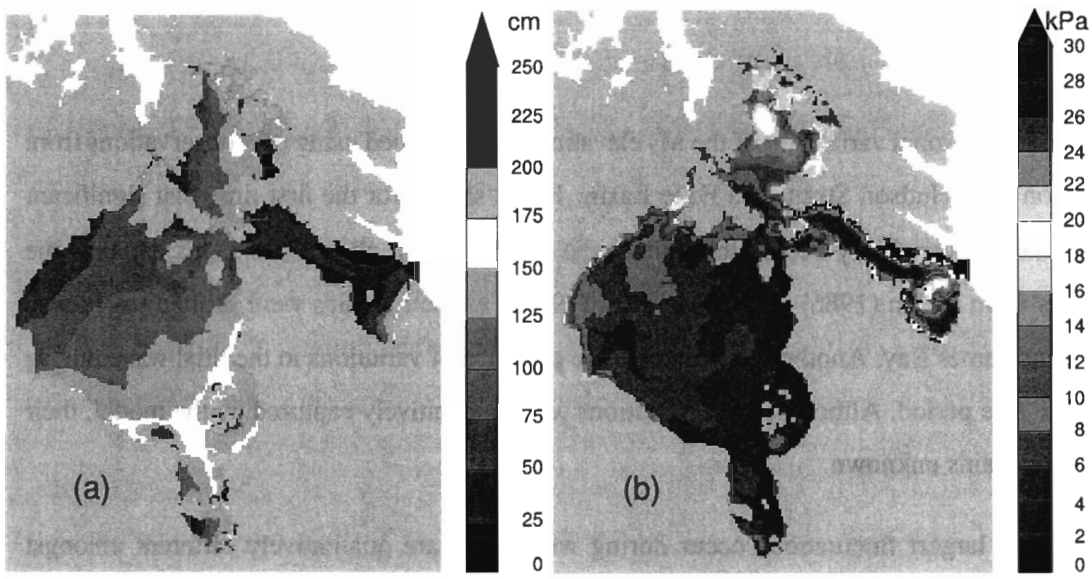

Figure 13: (a) Average thickness of sea ice during March 2004 from the control simulation. (b) Peak-to-peak amplitude of the internal ice stress $\sqrt{\sigma_{11}^2 + \sigma_{22}^2}$ oscillation at the M_2 frequency during March 2004 (control simulation).

1.7 Conclusions

Significant seasonal changes in M_2 elevations are found in all the regions of the Hudson Bay System, and at all seasons. The largest changes occur during winter while both elevation increase (Hudson Strait) and decrease (Hudson Bay, Foxe Basin) are observed. These variations are found recurrent at the stations where multiyear observations are available. Numerical simulations show that the winter M_2 variations are essentially caused by the under-ice friction. This friction mostly occurs in a limited region (Foxe Basin) and can account for both the increased and decreased elevations during winter.

1.8 Acknowledgements

The authors would like to thank the Department of Fisheries and Oceans, the captains and crews of the CCGS Pierre Radisson and Des Groseillers, technicians Sylvain Cantin, Roger Pigeon, Rémi Desmarais and Simon Senneville. The authors would also like to thank J. Caveen and F. Roy for technical support. We gratefully thank Fiamma Straneo and two anonymous reviewers for helpful comments and suggestions which led to the improvement of this paper. We thank the Natural Sciences and Engineering Research Council of Canada, and the Canadian Foundation for Climate and Atmospheric Sciences. This is a contribution to the Canadian CLIVAR and ArcticNet programs.

ARTICLE II

WHAT IS THE FATE OF THE RIVER WATERS OF HUDSON BAY?

2.1 Abstract

We examine the freshwater balance of Hudson Bay, a shallow Arctic sea that holds a large volume of freshwater and annually receives 12% of the pan-Arctic river runoff. The annual freshwater balance is essentially between the river input and a large outflow toward the Labrador shelf. The volume of freshwater involved in the seasonal ice growth/melt cycle is found to be relatively large, but the cycle has a fairly small net effect over the annual budget as the ice cover mostly recycles freshwater locally. River waters are seasonally exchanged from the nearshore region to the interior of the basin, and the volumes exchanged are substantial (of the same order of magnitude as the annual river input). This lateral exchange is mostly caused by Ekman transport, and its magnitude and variability are controlled by the curl of the stress at the surface of the basin. The transport of the river waters to the interior leads to its storage over extended periods of time (several years). It takes an average time of 3.0 years to flush the river input from a given year, meaning that the outflow is a complex mixture of the runoff from the three preceding years.

Nous étudions le bilan des eaux douces de la baie d'Hudson, une mer arctique peu profonde avec un grand volume d'eau douce et recevant annuellement 12% de l'apport total des rivières arctiques. Le bilan annuel des eaux douces exprime principalement un équilibre entre l'apport des rivières et un grand export d'eau douce vers le plateau du Labrador. Le volume d'eau douce impliqué dans le cycle glaciel saisonnier est relativement important, mais il est trouvé que ce cycle a un impact annuel net assez faible puisqu'il implique surtout l'eau douce d'origine locale. Les eaux des rivières sont échangées saisonnièrement de la région côtière à la région intérieure du bassin, et les volumes échangés sont substantiels (du même ordre

de grandeur que l'apport annuel des rivières). Cet échange latéral est principalement causé par le transport d'Ekman, son amplitude et sa variabilité étant contrôlés par le rotationnel de la contrainte exercée à la surface des eaux du bassin. Le transport des eaux des rivières vers l'intérieur du bassin mène à leur stockage sur de longues périodes de temps (plusieurs années). Un temps moyen de 3.0 années est nécessaire pour expulser l'apport des rivières d'une année donnée, cela signifiant que l'export d'eau douce est un mélange complexe du débit des rivières des trois années précédentes.

2.2 Introduction

Polar regions are characterized by a highly seasonal insolation as a consequence of seasonal Sun–Earth geometry. This seasonal insolation leads to air temperatures above and below the freezing point of water, causing its storage in the form of snow and ice during winter, and its release to liquid during the spring. The release occurs as an increased river discharge to the ocean, and by the melting of the sea ice cover (Crabs et al., 2000; Rothrock et al., 2000). It is often assumed that this annual input of freshwater to the ocean is closely balanced by sinks and outward fluxes (e.g. evaporation), so that the ocean is in a steady state (e.g., Yamamoto-Kawai et al., 2008). While this assumption is reasonable at long timescales, the polar seas can accumulate part of their annual freshwater input over some periods of time. For instance, Peterson et al. (2006) show how the Arctic Ocean stored and accumulated freshwater over several years, before releasing it to the subarctic seas downstream (the Labrador Shelf/Sea, Irminger and Icelandic basins), and giving rise to what has been called the Great Salinity Anomaly (Dickson et al., 1988). The Arctic Ocean stores most of its freshwater in the Beaufort Sea, and recent studies relate the variability in storage to the atmospheric regime above the Arctic (Proshutinsky et al., 2002, 2009).

Another Arctic basin that holds a large volume of freshwater is Hudson Bay, an inland shallow sea located upstream of the Labrador Shelf and Current (7500 km^3 relative to 34.8;

Fig. 14). The mean river discharge in Hudson Bay is 635 $km^3 y^{-1}$, or 12% of the total pan-Arctic runoff (Lammers et al., 2001). This value represents the annual addition of an 80 cm layer of freshwater if distributed over the whole area of the bay. Satellite observations also show the formation of a complete ice cover around December and its complete disappearance by early summer (Hochheim and Barber, 2010). The thickness of the ice cover is only known from measurements nearshore and qualitative estimates from satellite images that range between one and two meters during the peak of winter (Markham, 1986; Prinsenberg, 1988b). The precipitation P and evaporation E rates over the basin are also difficult to estimate from the limited observations, and the literature provides conflicting estimates. Nevertheless the values suggested for $P-E$ remain smaller than the annual runoff or ice melt by a factor of two or more (see Straneo and Saucier 2008a for a review of Hudson Bay's freshwater budget).

A recent observational study highlights how the outflow from Hudson Strait (the channel linking Hudson Bay to the Labrador Sea) is a significant contributor to the freshwater flux over the Labrador Shelf, both by conveying the freshwater from Hudson Bay and by recycling part of the Baffin Current (Straneo and Saucier 2008b, see also Straneo, this issue). The variability and magnitude of this fresh outflow is only weakly related to local wind forcing, and the importance of an upstream control (i.e. from Hudson Bay) is suggested by these authors (see also Sutherland et al., this issue). Such upstream-to-downstream relationship was examined by Myers et al. (1990) who calculated lagged-correlations between salinities from the Labrador Shelf and interannual river discharge or ice volume from Hudson Bay. They obtained a significant inverse correlation between the runoff and the salinity by assuming a point-wise runoff and a travel time of nine months before reaching the shelf. A more sophisticated river water tracking algorithm by Déry et al. (2005) recently illustrated how the salinity minimum recorded at the shelf would be in fact a combination of the runoff from three different years owing to the spatially-distributed runoff inside the large basin.

Although the studies from Myers et al. (1990) and Déry et al. (2005) differ regarding the time required to reach the Labrador Shelf, they both assume freshwater to be advected as

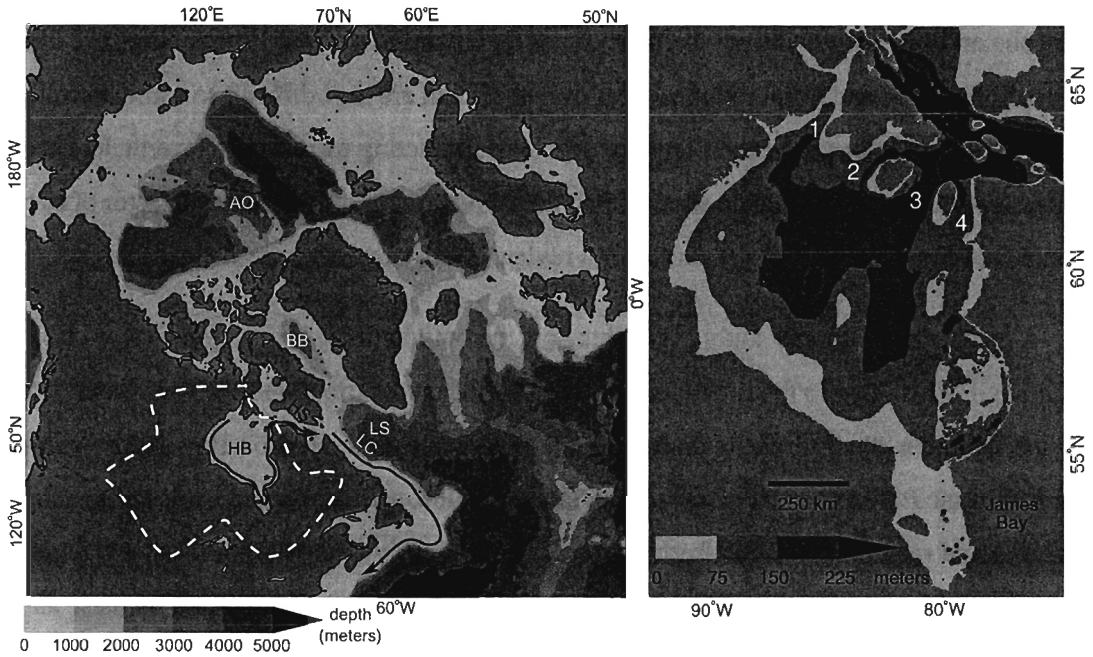

Figure 14: (left) Hudson Bay (HB) within the Arctic region. The drainage basin of HB is shown by the white dashed line. Also shown are the basins surrounding HB: Hudson Strait (HS), Labrador Sea (LS), Baffin Bay (BB), and Arctic Ocean (AO). The surface currents of HB and the Labrador Current (LC) are schematized by the magenta and black arrows respectively. (right) Bathymetry of Hudson and James Bays, with the four channels of Hudson Bay being labeled 1–4.

in a pipeline: the outflow downstream is solely determined by the freshwater input upstream (scenario 1). This will not be the case if processes within Hudson Bay act to accumulate and release freshwater on interannual timescales, as was shown by Peterson et al. (2006) for the Arctic Ocean (scenario 2). This question on the storage/release of freshwater from the Arctic seas becomes particularly relevant in the context of recent studies of the large-scale ocean circulation. An increasing body of literature highlights the sensitivity of this circulation to the amount of freshwater released to the subarctic seas, in particular the Labrador Sea (Rahmstorf et al., 2005; Stouffer et al., 2006; Huisman et al., 2009).

The fate of Hudson Bay's freshwaters is also an issue at the regional scale. In the first scenario defined above, the river waters are confined to a pipe (the boundary current), while in scenario 2 the river waters accumulate over some time and are likely to interact with the off-shore region. For instance, the plume of the Mackenzie River in the Beaufort Sea sometimes stretches 400 km off the shelf (Macdonald et al., 1999). Such interactions with the offshore region matters for the climate of the bay, its ecosystem, and its biogeochemical conditions. Riverine freshwater increases the stability of the water column and thus exerts a control on the mixing and formation of the bay's waters. The stability also impacts the primary production, the basic component of the food web, which relies on vertical exchanges with nutrient-rich deep waters (e.g. Sibert et al., this issue). Finally, the spatial re-distribution of the riverine tracers is likely to be different according to the scenario. These tracers include colored dissolved organic matter (CDOM, Granskog et al. 2007), that absorb the light necessary for the primary production, and also mercury, a contaminant found in very high concentrations in marine mammals, and a concern for the health of the northern residents (Hare et al., 2008).

The objective of this study is to determine the kinematics, or fate, of the river waters of Hudson Bay. More specifically, we investigate the following aspects: to what extent do the river waters spread to the interior region of the basin? Are they stored over periods of time? How long does it take before they are flushed? Which processes control this storage/release of river water from the interior? Answering these questions will help us determine the role of the

river waters at the regional scale, and the potential impact of this Arctic sea on the subarctic basins depending on its capability to store/release freshwater. The study is structured in the following manner. In section 2.3 we describe the method used to examine the fate of the river waters. The following section (2.4.1) presents the annual freshwater and volume budgets for the system. The role of sea ice in the freshwater budget is specifically discussed in section 2.4.2. Section 2.4.3 qualitatively illustrates the cross-shore advection of the river waters during the summer, and this transport is then quantitatively shown to play a crucial role in the freshwater budget of the interior region (section 2.4.4). The main process controlling the magnitude and variability of the lateral exchanges is identified in section 2.4.5. The last section (2.4.6) illustrates the storage of the freshwater in the interior region over years, and its impact upon the residence time of the river waters. The implications of the results, as well as the limitations of the study, are discussed in section 2.5. The conclusions of the study follow in section 2.6.

2.3 Method

For this study we make use of a regional 3–D numerical model that covers Hudson Bay, James Bay, Hudson Strait, and Foxe Basin. The ocean model (Backhaus, 1983, 1985) solves the primitive equations with a resolution of 10 km on the horizontal and 10 m on the vertical. It is coupled to a dynamic and thermodynamic two-layer sea ice model (Semtner, 1976; Hunke and Dukowicz, 1997) and a single layer snow model. The simulations are initialized from a composite of historic salinity-temperature profiles (see Saucier et al. 2004a) and conducted under realistic forcing from tides, ocean boundaries, river runoff, and atmosphere. Tides are introduced by prescribing the sea elevation at the open boundaries according to Matsumoto et al. (2000). Temperature and salinity at these boundaries are set according to historic profiles acquired at the mouth of Hudson Strait (Canadian Marine Environmental Data Service) and in Fury and Hecla Strait (Barber, 1965; Sadler, 1982). Daily river runoff is obtained from provincial institutions of Québec, Ontario, Manitoba, and from HYDAT (HY-

drometric DATabase, Environment Canada). Three-hourly winds and precipitation are taken from the high-resolution (15 km), data-assimilating, operational model used for weather forecast in Canada (GEM, Global Environmental Model, Côté et al., 1998).

Further description of the model and extensive comparison with observations are available in the work of Saucier et al. (2004a). We nevertheless present here a comparison with observations recently acquired during the ArcticNet and Merica cruises. We specifically show the salinity field since it largely controls the density of the waters (thus the pressure field and its gradient) and the local concentration of freshwater. The top panel of Fig. 15 shows the surface salinity in late summer for the model (year 2003) and observations (year 2005, see Lapoussière et al. 2009). Although the years are different, the main features of the salinity field are preserved over years and apparent in both observations and model results, notably the relatively fresh boundary region and the saltier interior region. We also note that the location of the isohalines and their spacing (gradient) are similar in a) and b). The bottom part of Fig. 15 shows a salinity transect along 61°N from the Merica cruises (Saucier et al., 2004b) and for the same year as in the simulation. Again the model reproduces the key features of the salinity field, including the wedge of freshwater in the eastern part and the saltier interior. The model is slightly too stratified around 30 m (a frequent problem with statistical closure schemes, Martin 1985) and slightly underestimates the salinity of the mixed bottom layer (the model gives values around 32.9 psu). Nevertheless this comparison confirms that the model is able to reproduce the main dynamical processes governing the freshwater balance of the basin.

The model results presented in this study are obtained using the following strategy. The model is first spun-up from rest using repeatedly the forcing for the period August 2003 to August 2004 (we did not consider spinning the model using interannually-varying forcing since only four years of continuous data were available.) The spin-up process ends once we obtain a stable seasonal cycle for the salinity and temperature fields. Trends in these fields rapidly disappear within five years of spin-up, and all transient oscillations have disappeared

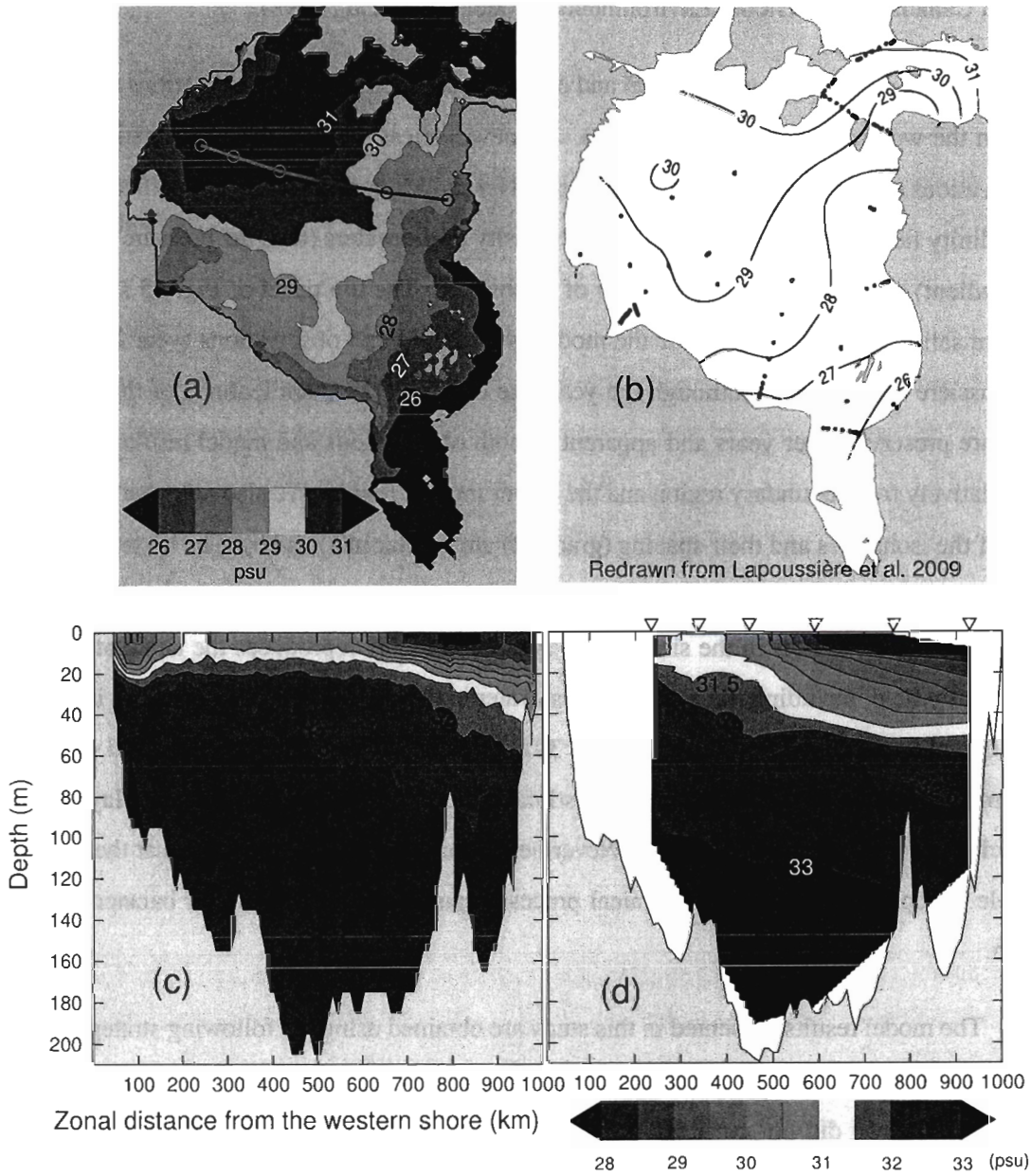

Figure 15: (top) Surface salinity in September according to a) the simulation (year 2003), and b) observations (year 2005, from Lapoussière et al. 2009). The magenta line in a) gives the location of the six stations of d). (bottom) Salinity along 61°N in August 2003 according to c) the simulation, and d) observations from six stations (∇ symbols).

after 20 years. It is this stable seasonal cycle that is used for all the calculations and figures. The simulations are conducted using the same model configuration as in the study of Saucier et al. (2004a) except for several minor enhancements. First, the atmospheric and hydrologic forcing was extended to cover the period of the simulation. Then, the air-ocean drag coefficient was updated according to Zedler et al. (2009, Table A2, right column). The air-ice drag coefficient is 1.2×10^{-3} as suggested by Hibler (1979). Finally, the model was modified for the use of salty sea ice (7 psu, e.g. Prinsenberg 1984) instead of pure fresh sea ice. It is found that these modifications have only a small effect on the simulated seasonal cycle, but they are nevertheless included for completeness.

Sections 2.4.3 and 2.4.6 present results from experiments involving a numerical tracer. The tracer corresponds to a passive concentration field (i.e. it does not intervene in the dynamics) that is advected and diffused in the same way as temperature or salinity. It is used to mimic the behavior of the river freshwaters, and it is thus injected into the system at the same rate and locations as the river waters. Once inside the basin the tracer spreads and mixes with the surrounding waters, and its concentration decreases accordingly. For instance, a concentration of one in a given location corresponds to pure river water, and a concentration of zero is an absence of river water.

During the winter, some freshwater from the top of the water column gets transformed into sea ice. This means that some of the river waters is involved into the annual growth of the sea ice cover. To estimate how much river water gets transformed into sea ice, we first define Γ as the local ice growth/melt rate (in $\mathrm{m\,s^{-1}}$), and then multiply Γ by a ratio that gives the contribution of river waters to the local ice growth/melt:

$$\Gamma \frac{c_{\mathrm{riv}}}{c_{\mathrm{fw}}}. \tag{2.1}$$

The contribution of river waters to ice growth/melt is thus proportional to its local abundance. Note that $c_{\mathrm{riv}} \leq c_{\mathrm{fw}}$ at all times. During the ice growth period ($\Gamma > 0$), c_{riv} is the concentration of the river tracer in the first (surface) model level, and c_{fw} is the freshwater concentration

(defined from salinity, see Eq. 2.2) in the same level. During the ice melt period ($\Gamma < 0$), c_{riv} is the local thickness of solid river tracer (i.e., the ice formed from river waters), and c_{fw} is the local ice thickness. The solid river tracer is advected using the ice model velocities. With this procedure we can track the river tracer during the whole year, taking into account its movement, spread, and changes of phase.

The word freshwater is used throughout this study and it becomes necessary at this point to clarify its meaning. We conceptualize one cubic meter of seawater as a mixture of salty ocean water (of fixed salinity $S_0 = 33\,\mathrm{psu}$) and of freshwater ($S = 0\,\mathrm{psu}$). The local freshwater concentration, $0 \leq c_{\mathrm{fw}} \leq 1$, is thus defined as:

$$c_{\mathrm{fw}} = \begin{cases} (S_0 - S)/S_0 & \text{if } S \leq S_0, \\ 0 & \text{otherwise.} \end{cases} \tag{2.2}$$

The reference salinity S_0 corresponds to the salinity of the bottom layer that is isolated from the fresh buoyant waters (see Fig. 15c). Note that the model calculations are independent of the c_{fw} definition since the model dynamics are written in term of absolute densities. The choice of S_0 only impacts the freshwater budget that is computed a posteriori from the model salinities and velocities.

Previous studies used similar values for the salinity reference of Hudson Bay (32.8 psu for Prinsenberg 1984; 33.1 psu for Granskog et al. 2007). The use of a higher reference salinity, such as $S_0 = 34.8\,\mathrm{psu}$, would only scale (roughly double) the freshwater content of the basin and the freshwater fluxes at its mouth. Since both inflowing and outflowing fluxes would be scaled, the higher reference value would represent a larger volume of freshwater transiting through the basin, with no net effect on its budget. The definition of freshwater above is also appropriate for the sea ice, with the exception that water is denser than ice, so that a density ratio is taken into account during the calculations.

2.4 Results

2.4.1 The Baseline: the Annual Freshwater Budget

The freshwater budget of a coastal basin describes how the various processes balance each other so that the freshwater content of the basin is maintained on long timescales. Table 3 shows this budget calculated from the annual mean of the simulation starting in August 2003 and ending in August 2004 (see section 2.3 for a description of the method). The top part of the table describes a balance between the riverine and atmospheric inputs of freshwater, the effect from ice growth and ice melt, and the net lateral exchange of freshwater at the mouth of the system. As will be discussed in the next section (2.4.2), the growth and melt of ice nearly cancel each other, leaving a simplified balance between the river input, the net precipitation, and a fresh flow exiting the basin (Net Flow).

The flow at the mouth of Hudson Bay is further detailed in the lower part of Table 3. The freshwater and volume fluxes are shown for the four channels bounding Hudson Bay in the north, these channels being numbered from west to east (see map in Fig. 14). Relatively small amounts of freshwater enter Hudson Bay through the west (negative fluxes), so that the bulk of the exchange is a large freshwater flux leaving Hudson Bay through the easternmost channel. The magnitude of this freshwater outflow ($802\,km^3\ y^{-1}$) is consistent with measurements made downstream of Hudson Bay ($760–880\,km^3\ y^{-1}$, or 24–28 mSv, Straneo and Saucier 2008b, Table 2). The volume fluxes describe a similar pattern with inflow in the west and outflow in the east. The net volume flux nearly equates the river inflow since all other sources of volume in the budget (e.g. P and E) are parameterized as diffusive fluxes (like in many general circulation models), which means that they do not modify the volume of the basin. In all cases the volume contribution from $P - E$ is negligible compared to the changes associated with the volume fluxes at the mouth of the bay.

Important features of the system are revealed by this budget. First, the basin tends to

Table 3: Annual budget (Aug. 2003 to Aug. 2004) for the freshwater (FW) and volume (Vol.) of Hudson Bay, in $km^3\,y^{-1}$ relative to $S_0 = 33$ psu. The top table lists the sources and sinks of freshwater, and the lower table details the fluxes through the four channels (Ch. 1–4, see Fig. 14) making the mouth of Hudson Bay (positive fluxes are outward). Note that the river runoff for this year is slightly lower than the long-term mean ($635\,km^3\,y^{-1}$, Lammers et al., 2001). $P - E$ stands for precipitation minus evaporation rate.

Riv.	+	$P-E$	−	Growth	+	Melt	=	Net Flux	+	Residual
607	+	222	−	729	+	649	=	743	+	6

	Net Flux	=	Ch. 1	+	Ch. 2	+	Ch. 3	+	Ch. 4	+	Residual
FW	743	=	−16	+	−57	+	14	+	802	+	—
Vol.	607	=	−556	+	−2026	+	−3474	+	6615	+	48

be isolated from its surroundings in the sense that only a small amount of freshwater enters through its mouth, so that the freshwater leaving is essentially from local sources (rivers and net precipitation). Next, the net effect of ice on the annual budget is much smaller than the riverine and atmospheric inputs. The latter is about one third of the river input, so that the approximate balance is between river waters acting as the main source of freshwater, and the outflow of liquid freshwater in the easternmost channel acting as the main sink of freshwater. It must be said though that this balance reflects conditions averaged over the basin, and the conditions in certain locations might differ significantly from the average. This will be specifically discussed for the case of the ice cycle in the next section.

2.4.2 The Role of Sea Ice Growth and Melt

Sea ice modifies the freshwater content of a basin by removing freshwater from the water column during ice growth (ice is much fresher than seawater), and by releasing it back during ice melt. Polynyas occur throughout Hudson Bay and these areas can continuously produce winter sea ice in one region, then export this ice to another area. This can initiate bottom water formation, through densification, and increased export of freshwater (Barber and Massom, 2007). The strength and duration of the growth and melt periods are highly seasonal given the large seasonal variations in the atmospheric conditions found over the Arctic and sub-Arctic seas. For instance, Hudson Bay is known to oscillate between a state of complete ice cover and a state in which it is completely ice-free. The volumes of freshwater involved in this cycle, once the density differences between ice and water are taken into account, are as important as the annual river input (Table 3).

Despite the large volume of freshwater involved in this cycle, its net effect on the annual freshwater budget of Hudson Bay is rather small. This is apparent in Table 3, the annual ice growth differing from the annual ice melt by only $80\,km^3\ y^{-1}$, which amounts to a net ice export. The table reflects basin-averaged values though, and at the local scale the ice cycle will still play a role in the freshwater balance if there is a large mismatch between

the local ice growth and the local ice melt. We quantified this imbalance by calculating at each point of the bay the volume of ice grown that exceeded the local ice melt. The sum over the whole bay of this local imbalance is 190 km^3, which should be compared to the annual ice production of 729 km^3 (Table 3). From these numbers we conclude that the bulk of the annual ice production (about 75%) is associated with a balanced uptake/release of local freshwater, and thus no net effect. The remaining 25% corresponds to enhanced ice formation in northwestern Hudson Bay polynya and enhanced ice melt in southeastern Hudson Bay (in response to a southeastward ice drift, see Markham 1986; Saucier et al. 2004a).

Other evidences show that the sea ice cycle has a limited impact on how much freshwater is released from the basin. Figure 16 shows the volume of solid, liquid, and total freshwater over the year. From May to September the total freshwater content (red curve) increases as expected from the seasonality of the river runoff that peaks during these months (see Déry et al., 2005, Fig. 4). We also note that the most rapid variations in total freshwater content occur between the months of October and December, when the basin is virtually ice-free. It suggests that growth and melt of sea ice have a smaller effect on the total freshwater content of the system than the processes acting during the autumn.

The results presented in this section and in Table 3 support the idea that the seasonal cycle of ice growth and ice melt has a net effect that is smaller than the annual river input, and smaller than the annual net precipitation. In the next sections we turn our attention toward the river waters (the next largest term in the freshwater budget) and their potential role in the balance of the interior of the bay.

2.4.3 The Fate of the River Waters

The previous sections illustrated the importance of the river input in the domain-averaged freshwater budget. In this section we will focus upon these river waters by examining how they spread within the system, and possibly affect the areas outside the nearshore region. Nu-

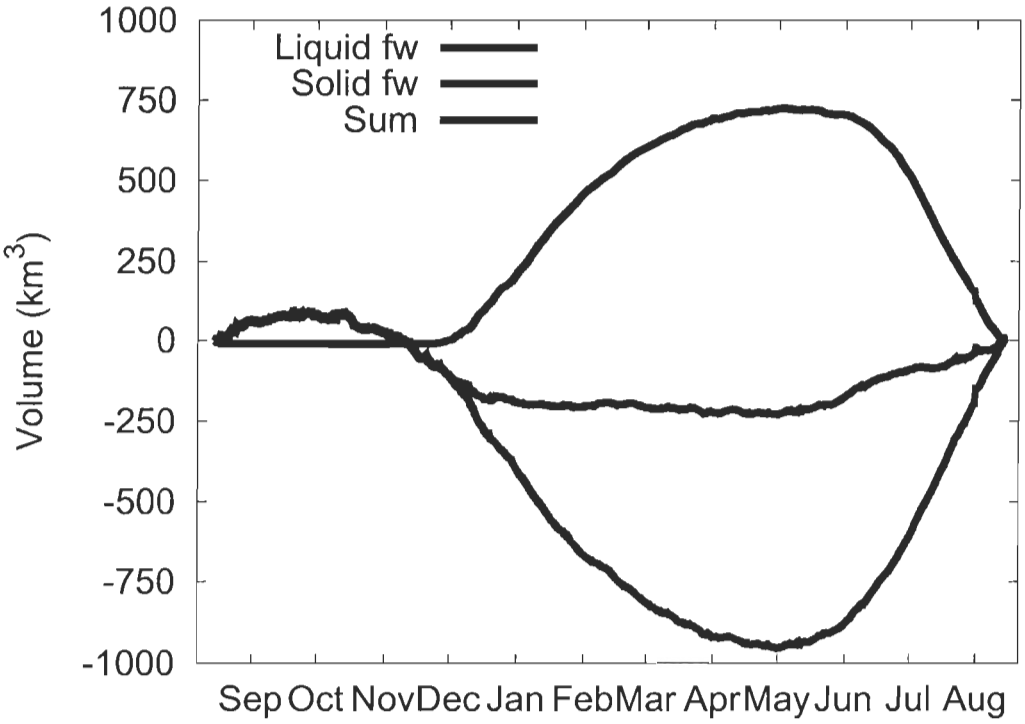

Figure 16: Volume of freshwater (fw) in Hudson Bay over the year, referenced to its initial value.

merous experiments in idealized conditions (Garvine, 1999) show that the waters from large rivers at mid or high-latitudes are deflected by the rotation of the earth. They tend to hug the shorelines and remain trapped within a distance from the shore that scales with an internal Rossby radius, on the order of 10 km in Hudson Bay. The longitudinal extent of the plume formed by the river waters depends on several parameters but can reach great distance. For instance, the fresh Labrador current is thought to be the large-scale equivalent of a river plume, extending from 60°N down to the mid-Atlantic Bight (Chapman and Beardsley, 1989).

In order to track the river waters we tag these with a passive tracer, the tracer being injected at precisely the locations and rate of the river input of Hudson Bay. This is analogous to a field experiment where one would continuously dye all the waters leaving the river outlets. The concentration of the dye, or tracer, then represents the fraction occupied by the river waters inside one cubic meter of seawater.

Figure 17a shows the surface concentration of the river tracer once its concentration has reached steadiness. The concentration is shown for the summer period when observations of the surface salinity are available for comparison (see section 2.3 for a description of the data). The figure shows that the highest concentrations are effectively found near the shorelines, and that the deflection is clearly toward the right for the Thelon River (northwestern Hudson Bay) and the plume out of James Bay. The tracer field evolves over time by moving in a counterclockwise sense and leaving through Hudson Strait, as expected from the known currents of the basin (Prinsenberg, 1986a). What is less expected is that the river waters seem to be only loosely trapped to the coastlines, leaking toward the interior of the basin at scales of 100 km rather than 10 km.

A closer examination of the seaward transport reveals that it is due to advection by cross-shore velocities simulated by the model (horizontal diffusion of the tracer by the subgrid scale mixing parameterization plays a negligible role). The existence of such seaward transport is supported by a certain number of observations. Granskog et al. (2009) calculated the distribution of riverine freshwater in southwestern Hudson Bay according to $\delta^{18}O$ mea-

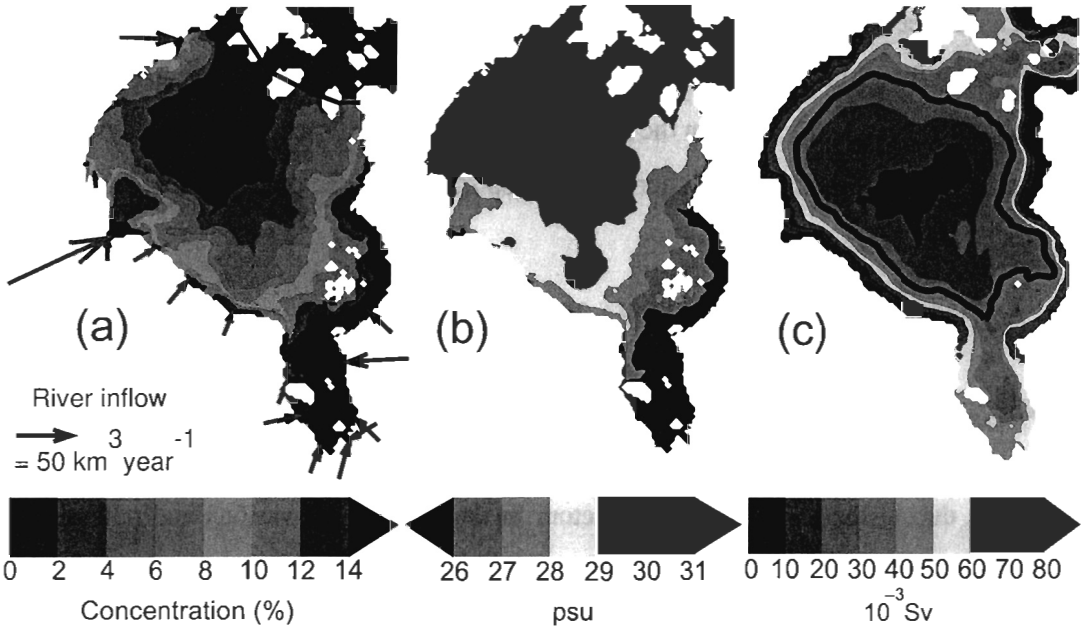

Figure 17: a) Horizontal distribution of the river tracer in the upper 10 m during the summer. The black lines delineate the extent of the tracer experiment. The arrows show the location and mean discharge of the rivers in Hudson Bay. b) Simulated sea surface salinity for the same period. c) Streamfunction for the mean surface currents of the basin.

surements in late summer 2005. Their results clearly show concentrations decreasing seaward on scales of 100 km rather than 10 km. Further evidence is given in Fig 17b, where the simulated surface salinity is shown for the same period as the tracer concentration from Fig. 17a. Striking similarities are visible between the salinity of the water and the tracer concentration, which suggests that river waters are to a large degree responsible for the freshness of the waters offshore during the summer period. This model result is consistent with the observed salinity charts (see section 2.3, and also the charts from Prinsenberg 1986b) that show similar features during the summer. Finally, Macdonald et al. (1999) report similar observations for the plume of the Mackenzie River in the Beaufort Sea. In the next section we will investigate the meaning and importance of this shoreward transport of the river waters in Hudson Bay.

2.4.4 Exchanges between the Boundary and Interior Regions

The previous sections have shown the river input to be the main source of freshwater in the annual budget of Hudson Bay, and that these river waters spread over part of the interior of the basin during the summer. Such a detour in the interior has various and potentially important implications. First, relatively large exchanges between the boundary and interior regions would mean that the river waters influence the density field of the interior of the basin. It also means that the river waters have a non-trivial pathway, with a potentially long residence time.

To investigate the exchanges between the boundary and interior regions we begin by identifying these two distinct areas: the boundary holds a narrow, swift flow that follows the shorelines, while the interior has a broad, slow flow following a closed circuit (e.g., Pedlosky, 1996, p. 2). Thus the two regions are naturally identified from the mean streamlines, or more specifically those of the surface currents (first model level, 0–10 m, see Li et al. 2006) since we focus upon the buoyant freshwater. The mean streamlines (Fig. 17c) depict a counter-clockwise flow around Hudson Bay, with the waters leaving Hudson Bay through the easternmost channel, and then heading toward the east along the southern shore of Hudson

Strait. The magnitude of the currents is proportional to the gradient of the streamfunction, and so the flow is relatively strong in the nearshore region and rather quiescent in the central region. The streamline highlighted in black marks the frontier between the boundary (open streamlines) and interior (closed streamlines) regions. Note that having a streamline as the frontier does not mean the interior is isolated from the boundary: seasonal advection, and eddy exchange of scalars, can act across the mean streamline.

We now examine the contribution of lateral fluxes (i.e. the boundary/interior exchanges) in the freshwater budget of the interior. This budget is shown in Fig. 18a,b, where V stands for the total (solid plus liquid) freshwater content. The volume V undergoes large seasonal variations, decreasing by 225 km^3 during the autumn, and increasing during early winter and during summer. It is also seen in Fig. 18b that the variations in V (dV/dt, red curve in b) cannot be explained by the divergence of ice and by net precipitation, so that lateral exchanges play a significant role. In particular, the increase in V during the summer is what is expected from the observed and simulated summer surface salinity charts (see section 2.4.3).

These results illustrate key features of the freshwater balance of the system. We have shown that the volume of freshwater in the interior region has large seasonal variations which cannot be solely explained by local processes (net precipitation). This means that lateral fluxes complement the local processes by transporting freshwater in and out of the interior region. Our simulation suggests that the volume of freshwater involved in these exchanges is comparable in magnitude to the annual river input.

2.4.5 What Regulates the Freshwater Stored in the Interior?

The large interior region of Hudson Bay was seen in the previous section to act as a reservoir that receives freshwater over some periods of the year, and releases it back to the boundary region during the autumn. Two processes are likely to contribute to such a cross-shore transport of freshwater: 1) Ekman transport in the fresh surface layer (e.g., Lentz,

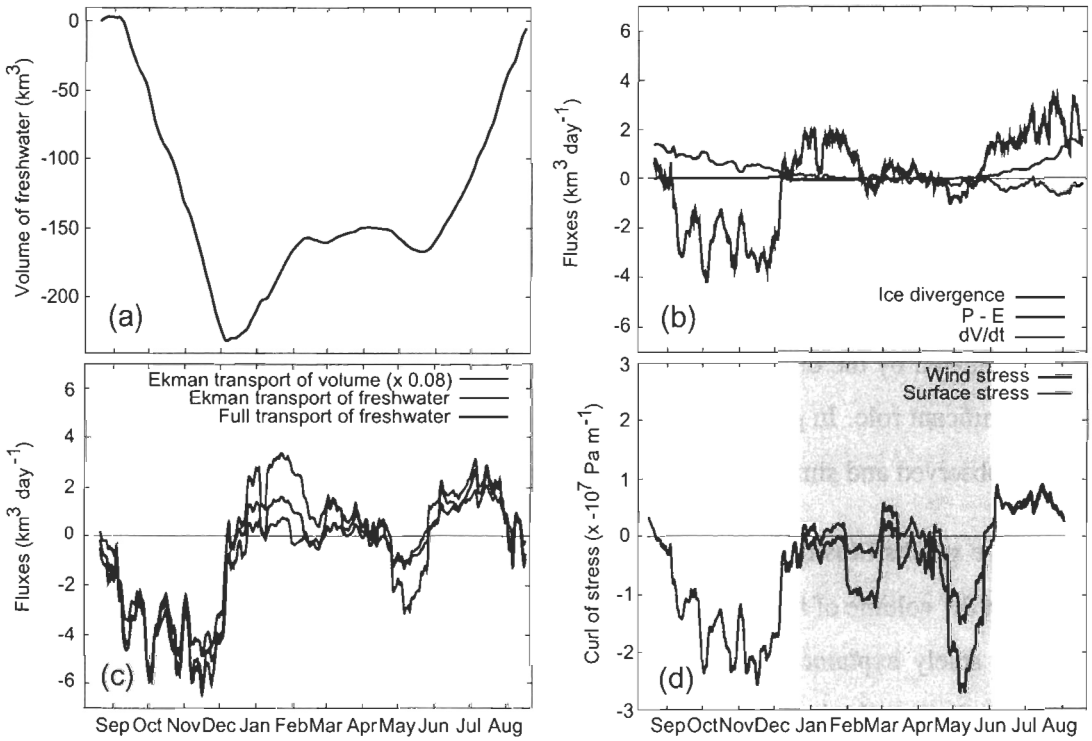

Figure 18: a) Volume V of freshwater (solid + liquid) within the interior region, referenced to its initial value. b) Contribution from ice fluxes and net precipitation to the variations dV/dt. c) Lateral exchange due to the true velocities and to the Ekman velocities. d) Seasonal cycle for the curl of the wind stress and the curl of the stress at the surface of the ocean. The period when the ice cover is above 85% is highlighted.

2004), and 2) eddies formed through baroclinic instability of the boundary current (e.g., Spall, 2004). The latter is associated with boundary flows that are wide relative to the Rossby radius and then tend to amplify perturbations into wavelike and eddy structures (Stern, 1975). The resulting eddies carry waters from one side of the boundary front to the other and thus contribute to an across-shore transport of properties. Note that lateral fluxes caused by the subgrid scale mixing parameterization are negligible in comparison with the other fluxes and thus are disregarded.

In general eddies can be found over a broad spectrum of timescales and so a priori there is no simple or obvious way to determine the relative importance of mean, eddy, and Ekman fluxes of freshwater. As a first attempt we will assume the Rossby numbers to be small, so that the flow can be decomposed into geostrophic and Ekman components (e.g., Müller, 2006, section 15.2). The latter is defined by the dynamical balance:

$$f\mathbf{e}_3 \times \mathbf{u}_{\mathrm{ek}} = \frac{\partial}{\partial z} A_3 \frac{\partial}{\partial z} \mathbf{u}_{\mathrm{ek}} \tag{2.3}$$

where f is the Coriolis parameter in the f-plane approximation, $\mathbf{e}_3$ the unit vector pointing upward, $\mathbf{u}_{\mathrm{ek}}$ the Ekman velocity as a function of horizontal position and time, $\partial/\partial z$ is the vertical derivative, and A_3 is the model vertical turbulent viscosity being also a function of position and time. Ekman velocities are computed at each grid point and timestep, with $A_3 \partial \mathbf{u}_{\mathrm{ek}}/\partial z$ set to the surface stress, and a no-slip condition at the bottom. Note that $\partial \mathbf{u}_{\mathrm{geos}}/\partial z$ is assumed negligible within the Ekman layers. The surface stress is defined as a smooth function of the wind stress (ice-free period) and of the ice-ocean stress (ice-covered period, see Mellor and Kantha 1989). Once the Ekman velocities are obtained, the corresponding freshwater fluxes are calculated using the salinity reference S_0.

Figure 18c shows the comparison between the lateral exchange of freshwater caused by the true model velocities (red curve), and the lateral exchange of freshwater due to Ekman velocities (green curve). The two timeseries are very close one to another, meaning that Ekman velocities are in a large part responsible for the exchanges of freshwater between the

interior and boundary regions. The interior region releases freshwater to the boundary region during the autumn (negative fluxes), and then receives freshwater from the boundary region in early winter and during the summer. These results essentially reflect the variations in the freshwater content of the interior region that were seen previously (Fig. 18b, red curve).

The important role played by the Ekman velocities for the regulation of the freshwater present in the interior means that the stress applied at the surface of the basin exerts a significant control over these exchanges. Such a relation between the stress field τ_s and the actual freshwater exchange due to Ekman velocities can be a priori complex. However a close examination of the surface stress field yields a fairly close correlation between its curl averaged over the interior ($\nabla \times \tau_s$, blue curve in Fig. 18d), and the actual Ekman exchange of volume and freshwater (blue and green curves, Fig. 18c). Most of the variations in the curl are reflected in the Ekman exchange, which suggests a dynamical relation between the two. This relation is directly obtained by computing the divergence $\nabla\cdot$ of the Ekman volume transport $\mathbf{M}_s = -\mathbf{e}_3 \times \tau_s / (f\rho_0)$ (Ekman, 1905):

$$\nabla \cdot \mathbf{M}_s = \frac{1}{f\rho_0} (\nabla \times \tau_s)_3 , \tag{2.4}$$

where ρ_0 is a density reference in the Boussinesq approximation, and the subscript $_3$ refers to the vertical component of $\nabla \times \tau_s$.

The relation can be summarized in the following way. The Ekman exchange shown in Fig. 18c is the resultant of the fluxes across the frontier separating the interior from the boundary region (a closed contour integral for the normal component of the flux). From the divergence theorem, this contour integral is equal to the area integral of the divergence $\nabla \cdot \mathbf{M}_s$ in the interior region. It means that a counter-clockwise tendency in the wind stress (positive curl, $\nabla \times \tau_s > 0$) forces the surface waters to leave the interior region (divergence, $\nabla \cdot \mathbf{M}_s > 0$). A clockwise tendency in the wind stress (negative curl, $\nabla \times \tau_s < 0$) forces the surface waters to enter the interior region (convergence, $\nabla \cdot \mathbf{M}_s < 0$). These concepts are illustrated in Fig. 19. Note that the horizontal scale of the wind stress field is comparable with the size of

the domain.

It is worth noting that Eq. 2.4 relates the curl of the stress at the surface of the sea to the Ekman volume transport. However it is the Ekman transport of freshwater that is the quantity of interest here, and it could differ appreciably from the volume transport depending on the cross-shore salinity gradients. Figure 18c shows that in fact the volume and freshwater transports share the same seasonal evolution. The salinity field only causes a slight amplification or damping of the seasonality in some periods. In other words, variations in the cross-shore flux of freshwater (a product of velocity and freshwater concentration) are more closely related to the velocities than to the salinity.

Another dynamical consideration is that the Ekman transport is driven by the stress at the top of the water column, which differs from the wind stress in winter. During this period, the ice cover acts as an intermediary that transfers part of the wind stress to the ocean (sea ice tends to be driven by winds, and damped by its contact with the ocean and by ice-ice interaction; Martinson and Wamser 1990; Steele et al. 1997. This is most likely the case in the interior region since the currents are so weak, see Fig. 17c, and Markham 1986). It raises the question of whether sea ice plays a role in the seasonality of the Ekman exchange. Figure 18d shows that the curl of the surface and wind stresses are identical during the ice-free period (as expected), and similar during the ice-thick period (Jan.–June). Therefore the sea ice in the interior of Hudson Bay is mostly mobile (in agreement with Markham 1986) and allows, to a large extent, the transmission of the wind stress to the water column. We conclude that the sea ice plays a small role in the seasonality of the exchange between the interior and boundary regions.

In summary, we have provided in this section evidence of the important role played by the atmospheric stress in the seasonal re-distribution of the freshwater within the basin. This stress gives rise to Ekman transports of freshwater, the freshwater being either accumulated in the interior (convergence) or released (divergence) according to the clockwise or anticlockwise tendency of the atmospheric stress. In the next section we will see the impact of such

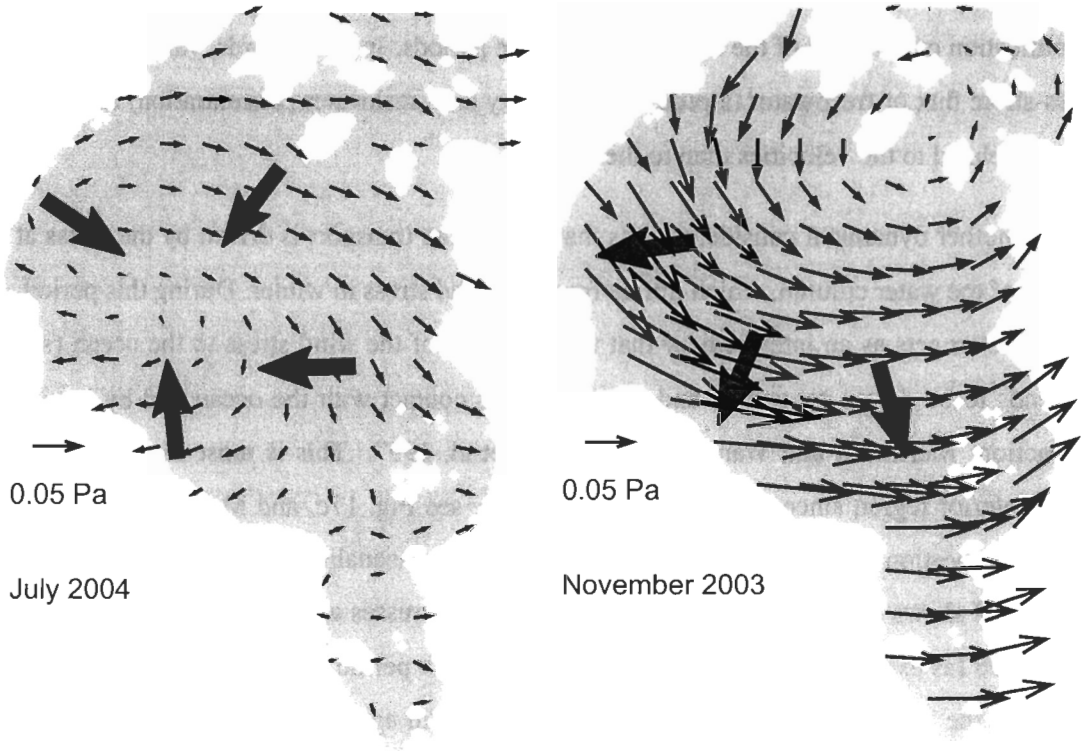

Figure 19: Stress (black arrows) at the ocean surface for two contrasting periods. Ekman transport (red arrows) is directed toward the right of the stress.

freshwater reservoir on the annual river input and its residence time.

2.4.6 The Residence Time of the River Waters

In a basin without an interior region (e.g. a channel), the outflow is a function of the river runoff, the distance from the rivers to the mouth of the bay, and the advective velocity that determines the time required to travel this distance. With an interior reservoir, the river waters can be diverted from their straight course along the boundary, and the longer pathway results in a longer period of time spent inside the bay. These ideas are illustrated in an experiment that again makes use of a tracer being injected at the mouth of the rivers (see section 2.3 for a detailed description). The injection of the tracer starts in April 2004 (beginning of the 2004 freshet) and lasts for one year (i.e. until the beginning of the 2005 freshet). The time required for the dyed waters to leave the basin (once the injection is complete) is called their residence time. Some of the dyed waters leave the system faster than others and so the values reported here correspond to the average time for the whole volume of tracer injected. Also note that, although this tracer experiment spans over 10 years (2003–2013), it is the same winds and river forcing that is applied each year (see section 2.3).

The red curve of Fig. 20 shows the volume of dyed river water within the basin during the injection period and after, normalized by the annual river input. The volume of dyed river water increases rapidly during the injection period (ending in April 2005) and gradually decreases afterward as an exponential function of time. About 15% of the river waters have left the basin when the injection period comes to an end (i.e. one year after the beginning of the experiment). The green and blue curves also represent the amount of dyed river water, but within the boundary and interior regions instead of the whole bay. Initially there is no river waters within the interior region since the river inflow occurs in the boundary region. The volume of river water within the interior (blue curve) increases during the early winter and summer of each year, while release occurs during the autumn. This is consistent with the seasonal exchange of freshwater identified in the previous sections (Fig. 18c), and it

shows that freshwater of riverine origin effectively contributes to the seasonal exchange of freshwater.

The exchange between the interior and the boundary is illustrated in Fig. 21. Note that the only way for the interior region to gain or lose river water is through exchanges with the boundary region. The volume of river water within the interior increases up to the summer of 2006 (reaching one quarter of the annual river input), and decreases afterward. At this point the interior region has become a net source of river water for the boundary region. This flux from the interior to the boundary region increases until mid-2008, when the slope of the blue and green curves become equal, meaning that the bay is now releasing equal amounts from the interior and boundary regions. The influence of the interior region on the rate of flushing of the whole bay is illustrated by the light and dark gray lines in Fig. 21. Prior to 2008 the bay linearly releases river water that mostly come from the boundary (light gray line). After 2008 the influence of the interior becomes significant (blue and green curves share the same slope) and the rate of release slows considerably (dark gray curve). The light gray line corresponds to the case of no interior and a short residence time (linear regression gives 2.2 years). The excursion in the interior represents a longer pathway and produces a longer timescale of 3.0 years (obtained with an exponential regression to the dark gray curve).

The estimate of 3.0 years means that Hudson Bay approximately stores the river input from the three preceding years, and that the river water leaving the basin is a complex mixture of the runoff from these years. The relatively long residence time is, in part, due to some of the largest rivers being located far upstream (e.g. Thelon and Nelson rivers) and having a long distance to travel before leaving the basin. But the results also show clearly the impact of the storage in the interior, that lengthens the average residence time from 2.2 years to 3.0 years.

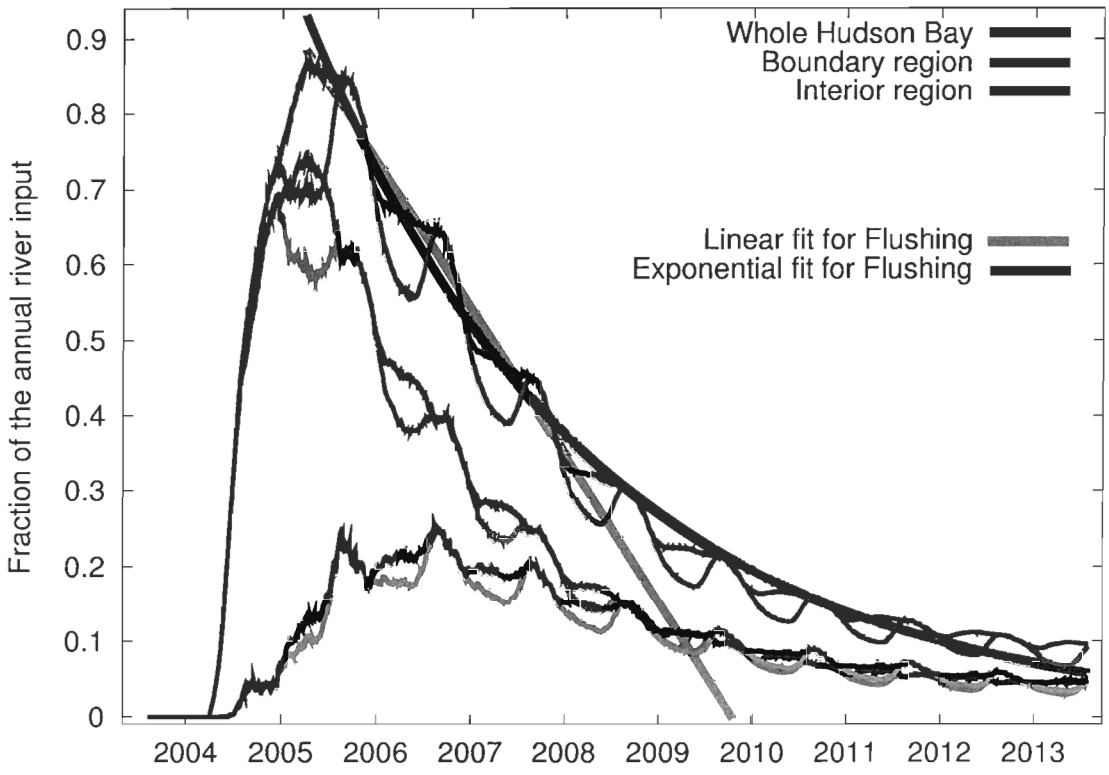

Figure 20: Gradual release of the river waters of 2004 (April 2004 to April 2005). For each region, the dark curve represents the total (solid + liquid) content of riverine water, and the light curve is its liquid content alone. The gray curves show two different fits for the flushing of the river waters (linearly or exponentially decreasing).

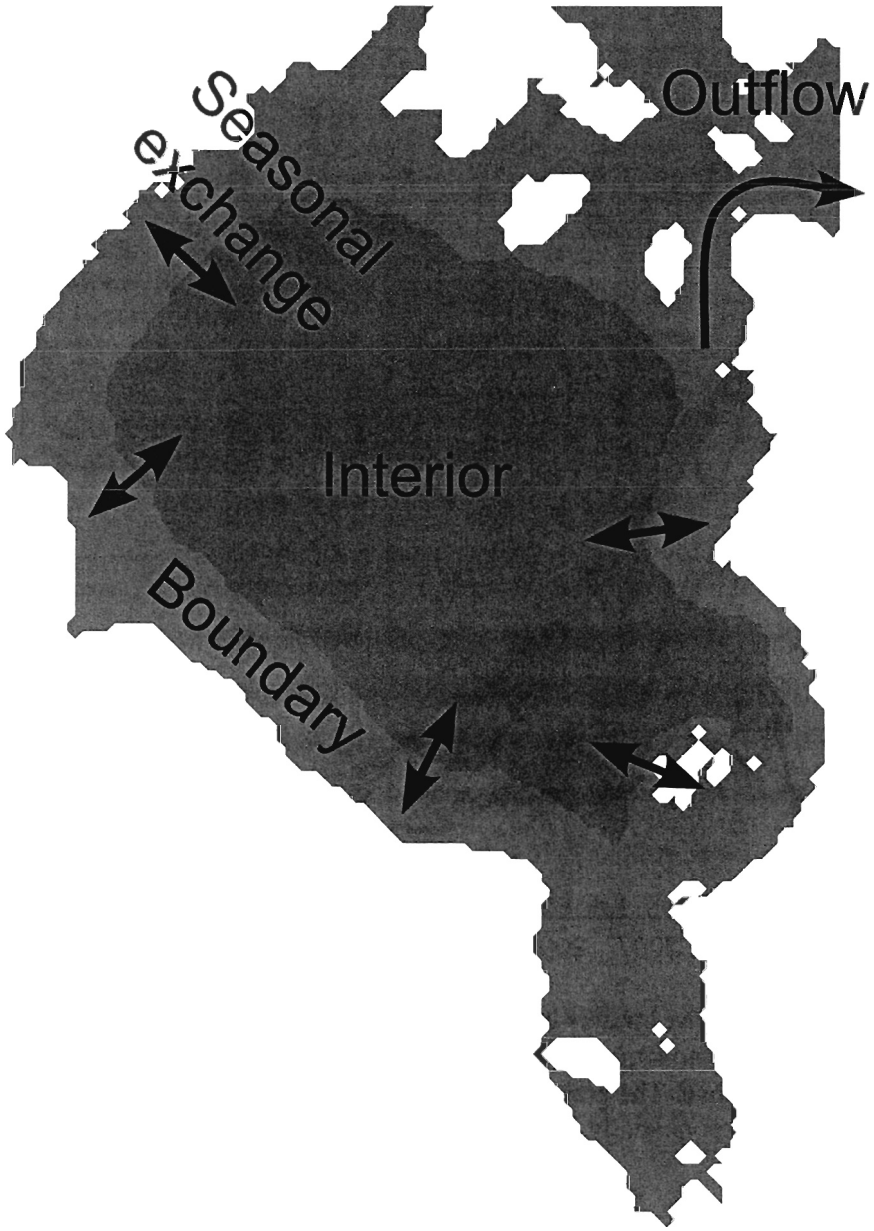

Figure 21: Schematic for the fluxes of river water after the injection period (i.e. there is no longer a source of river waters). The interior region exchanges river waters only with the boundary region.

2.5 Discussion

The objective of this study was to examine the pathway, or kinematics, of the river waters of Hudson Bay. The study necessitated a certain number of simplifications, one of them being that we examined in detail the components of the freshwater balance over a finite period of time (August 2003–August 2004). It raises the question of whether these components and processes have the same importance during other years. We speculate that it is the case, given the large seasonality of the insolation at these high latitudes that leads to particularly marked seasonal cycles and, in comparison, small interannual variability. For instance, the seasonality of the bay's waters and that of its hydrologic forcing in 2003–2004 are qualitatively the same, and quantitatively close, to those from the 1996–1998 period considered by Saucier et al. (2004a). We also examined the generality of our analysis regarding the curl of the wind stress by comparing them with NCEP winds (National Centers for Environmental Prediction, Kalnay et al., 1996) covering a 30-year period (1979–2008). The curl over the 30 years has a mean value similar to that from the 2003–2004 forcing, and seasonal periods of strongly cyclonic/lightly anticyclonic conditions similar to those described in section 2.4.5 (see also Sutherland et al., this issue, on the role of the curl during other years). For these reasons, we believe the results obtained here with the forcing from 2003–2004 are most likely generally applicable.

We initially envisioned two scenarios for the fate of the freshwaters of Hudson Bay. In scenario 1, the outflow is a function of the river runoff, the distance to the mouth of the bay, and the advective velocity. This corresponds to the study from Déry et al. (2005), who illustrated how the spatially-distributed runoff in the wide bay leads to an outflow over the Labrador Shelf made of river waters from the three preceding years. This basic conclusion is recovered here with a residence time of 2.2 years for the case neglecting the storage in the interior. Taking into account the interior reservoir means that one quarter of the annual river input is diverted and stored, and that the residence time lengthens to 3.0 years. The interior reservoir can simultaneously store/release the freshwater input from different years, and the

seasonal exchange that results (Fig. 18c, red curve) is large enough to substantially modulate the actual flow of freshwater leaving Hudson Bay. In this sense, Hudson Bay complies to the second scenario from section 2.2.

The scenario 2 was also encountered by Proshutinsky et al. (2002, 2009) who examined the basin-scale mechanisms regulating anomalies in the freshwater content of the Beaufort Sea/Gyre. The authors find that the major cause of the large freshwater content in the Beaufort Gyre is the process of Ekman pumping. This process corresponds to a convergent/divergent flux of freshwater in the upper Ekman layer, as was shown here for Hudson Bay. The seasonality of the freshwater content of the Beaufort Gyre is controlled by variations in the curl of the wind stress, which again is similar to what is found in our study. The authors expand their analysis to interannual variations and attribute the decadal variability in storage to changes in the atmospheric circulation regime. Unfortunately the long-term variability was not examined in the present study because of a lack of long-term forcing (see section 2.3), but the important role played by Ekman transport in the seasonal cycle suggests that the wind regime over Hudson Bay can be the primary control over its interannual freshwater content/outflow, exceeding the impact of interannual variations in river runoff. This hypothesis is the subject of a forthcoming article.

The capability of Hudson Bay to store river water highlights the need for interannual measurements of its outflow to constrain the potential impact of the bay on the subarctic region downstream (cf. Straneo, this issue), and more generally the global ocean circulation. The exchange with the interior of the bay also has regional implications. We speculate that the offshore excursion of river water, apart from its impact on the density field and formation of water masses, plays a significant role in the redistribution of river tracers such as mercury and colored dissolved organic matter (CDOM). Through the seasonal excursion in the interior, these substances can impact the marine life outside of the nearshore region.

2.6 Conclusions

Hudson Bay is a shallow Arctic sea that holds a large volume of freshwater and annually receives 12% of the pan-Arctic river runoff. This sea has the potential to affect the subarctic region downstream if it stores and releases large volumes of freshwater on interannual timescales. The large river input also has the potential to play important roles at the regional scale, notably for the distribution of pollutants (mercury), and by affecting the primary production that is sensitive to stratification and the absorption of light by terrigenous material. Obtaining measurements from the basin and addressing these questions has always been difficult given the remoteness of the basin and the presence of the ice cover during most of the year. The strategy in this study was to use a high-resolution, 3–D numerical model with realistic forcing for river input, winds, and precipitation. The model compares favorably with observations collected during the ArcticNet and Merica cruises.

The annual freshwater balance of the basin is essentially between the river input and a large outflow in the easternmost channel (very small volumes of freshwater enter the basin through its mouth). Despite the particularly large volume of freshwater involved in the seasonal ice growth/melt cycle, this cycle results in a fairly small net effect over the annual budget as the sea ice cover essentially recycles freshwater locally (section 2.4.2). This result is obtained for the basin-averaged budget, and is also verified in most locations over the basin.

River waters are seasonally exchanged from the nearshore region to the interior of the basin, and the volumes of freshwater involved in this exchange are substantial (of the same order of magnitude as the annual river input). The magnitude and variability of the exchange are essentially controlled by the stress exerted at the surface of the interior region. The curl of the surface and wind stresses are equal during the ice-free period and similar during the ice-covered period (Fig. 18d). It means the sea ice in the interior can move with the wind, and largely transmits the wind stress to the water column underneath.

The transport of the river water into the interior leads to their storage over extended

periods of time (several years). It takes an average time of 3.0 years to flush the river input from a given year. This estimate means that the river water leaving the basin is a complex mixture of the runoff from the three preceding years. The storage in the interior also means that oceanographic processes within the bay have the potential to substantially modulate on interannual timescales the volume of freshwater leaving toward the Labrador area. Finally, the seasonal exchange of river water is likely significant for the dispersion of river tracers that impact the marine life, and it was shown to modify the density (salinity) field in the offshore region.

2.7 Acknowledgements

This work is a contribution to the Freshwater–Marine Coupling project of the ArcticNet network of Canada. We thank NSERC and the Canada Research Chairs program for funding. FS acknowledges support from NSF OCE-0751554. We want to thank the Department of Fisheries and Oceans of Canada, their technicians, the captains and crews of the CCGS Radisson, DesGroseillers, Martha Black, and Amundsen. We thank S. Senneville for technical support. NCEP Reanalysis data were provided by the NOAA/OAR/ESRL PSD, Boulder, Colorado, USA, from their Web site at http://www.esrl.noaa.gov/psd/.

ARTICLE III

STORAGE AND EXPORT OF FRESHWATER IN ARCTIC SEAS: THE CASE OF HUDSON BAY

3.1 Abstract

The freshwater balance of Hudson Bay is simulated over the past 28 years (1979–2007) using an idealized model driven by realistic hydrologic forcing and by winds from the high-resolution North American Regional Reanalysis. The results from the simulation are found consistent with observations from the basin and with results from a realistic 3–D sea ice-ocean coupled primitive equations model. In agreement with recent observations and simulations from other Arctic seas, the storage of freshwater in the interior of Hudson Bay is controlled by the wind stress curl through Ekman pumping. The decadal evolution of this storage is substantial and well described by the Arctic Oscillation index. The storage/release capability of the system leads to a complex interannual variability in the export of freshwater, the simulated export being in good agreement with interannual observations from Hudson Strait. Sensitivity experiments show that several parameters have a significant control on the export of freshwater, notably the hydrologic and cryospheric forcing. The wind forcing is nevertheless the most important contributor to this variability.

Le bilan des eaux douces de la baie d'Hudson est simulé sur les 28 dernières années (1979–2007) à l'aide d'un modèle idéalisé piloté par des forçages hydrologiques réalistes et des vents provenant d'une réanalyse à haute résolution couvrant l'Amérique du Nord. Les résultats de la simulation sont cohérents avec des observations provenant du bassin et avec des résultats d'un modèle réaliste solvant les équations primitives pour un océan 3–D. En accord avec de récentes observations et simulations d'autres mers arctiques, le stockage de l'eau douce dans l'intérieur de la baie d'Hudson est contrôlé par le rotationnel de

la contrainte des vents à travers le pompage d'Ekman. L'évolution décennale du stockage est substantielle et bien décrite par l'indice de l'oscillation arctique. La capacité du système à stocker/exporter l'eau douce mène à une variabilité interannuelle complexe dans l'export d'eau douce, cette variable simulée étant en bon accord avec des observations pluriannuelles du détroit d'Hudson. Des expériences de sensibilité montrent que plusieurs paramètres ont une influence significative sur l'export, notamment le forçage hydrologique et cryosphérique. Le forçage des vents demeure toutefois le principal déterminant de cette variabilité.

3.2 Introduction

Arctic basins are characterized by relatively fresh surface waters and large freshwater inputs from the Eurasian and American rivers (Levitus et al., 1994; Lammers et al., 2001). An increasing body of literature documents the capability of such systems to accumulate freshwater over some periods of time, and then to release it to the subarctic seas downstream (e.g., Peterson et al., 2006). This variability in the storage is verified both in observations (Proshutinsky et al., 2009) and in comprehensive numerical simulations (Jahn et al., 2009, 2010). Most of the freshwater of the Arctic Ocean is in the Beaufort Sea, and these authors attribute the storage/release behavior of this sea to the atmospheric forcing that moves the freshwater through Ekman transport: when the wind stress curl is anticyclonic the Beaufort Gyre accumulates freshwater, and when the curl switches to a more cyclonic state, freshwater gets released and is eventually exported from the system.

A recent study (St-Laurent et al., 2010) shows from comprehensive numerical simulations that there are similarities between the Beaufort Sea and another Arctic basin, Hudson Bay. Hudson Bay is a shallow inland sea located upstream of the Labrador Shelf and holding a large volume of freshwater (7500 km^3 relative to a salinity of 34.8 psu). The atmospheric forcing over Hudson Bay periodically shifts between cyclonic and anticyclonic states, provoking either release or storage of freshwater in the interior of the basin through Ekman

transport of freshwater. Although the impact of the storage/release on the freshwater export was not specifically examined in the study, it is expected to play a significant role.

The capability of the Arctic seas to store/export substantial volumes of freshwater is particularly relevant in the context of the large-scale Meridional Overturning Circulation (MOC) and its role in the global climate. The pathway of Arctic seas' freshwater crosses areas where deep convection normally occurs during the winter (e.g., Dickson et al., 2008), these convective sites being found notably in the Greenland and Labrador seas (Marshall and Schott, 1999). Anomalous high inputs of freshwater can increase the stratification and inhibit the wintertime convection and formation of dense waters (e.g., Lazier, 1980). Depending on the timing and magnitude of the freshwater anomaly over the convective sites, the MOC can be affected in important ways, with potential impacts for the climate of the Northern Hemisphere (Rahmstorf et al., 2005; Stouffer et al., 2006; Huisman et al., 2009).

Arctic seas are also particularly affected by global warming, in particular through a reduced extent and thickness of their ice cover (Bernstein et al., 2007; Hochheim and Barber, 2010; Joly et al., 2010). The reduced ice cover is likely to lead to increased exchanges of heat and moisture between the ocean and atmosphere, and an acceleration of the hydrological cycle. One evidence of this is the Canadian Arctic river runoff that has been increasing over the last 50 years (Déry et al., 2009). To predict the consequences of these changes, it is desirable to first have an intuitive understanding of the mechanisms controlling the freshwater balance of these Arctic seas.

The goal of this study is to investigate the physical processes which influence the freshwater balance of Hudson Bay over decadal timescales, and to identify the controls of this balance. More specifically, we ask the following questions: Does Hudson Bay have large fluctuations in its freshwater content and freshwater export over decades? What controls the export of freshwater? Can fluctuations in the freshwater balance be associated with large-scale atmospheric modes such as the Arctic Oscillation? And if so, are these climate indices sufficient to predict the freshwater export from Hudson Bay? These questions are critical to

our understanding of how these Arctic seas work, what triggers the storage/export of freshwater, and how the seas evolve under global warming.

The next section (section 3.3) describes the method used to investigate these questions. A conceptual model of Hudson Bay is presented and this model is used with realistic forcing for a 28 year-long simulation of the freshwater balance. In section 3.4.1, the circulation and hydrography obtained from this simulation are described and compared to observations. This leads us to the storage and export that is shown for the whole 28 years period in section 3.4.2. Both observed and modeled freshwater exports exhibit large annual peaks, and this particular feature is investigated in section 3.4.3. Finally, the variability in the freshwater balance is compared in section 3.4.4 to indices of the large-scale atmospheric circulation to see if there are connections between the two. The study concludes with a discussion on the implications and limitations of the work (section 3.5) and a summary of the results obtained (section 3.6).

3.3 Method

3.3.1 The Conceptual Model

To investigate the freshwater balance of Hudson Bay over decadal timescales, we make use of a conceptual model of the system. It is based on the work of Straneo (2006) who studied the response of a partially-enclosed convective basin that has a laterally-uniform interior region surrounded by a boundary current. Both the interior and boundary regions have a two-layer stratification, and the boundary current includes a two-layer flow. We retain these features from the model of Straneo (2006) and apply a number of additions to specifically simulate the freshwater balance of an Arctic sea. We only provide here a summary of the model whose full description is available elsewhere (St-Laurent, 2010, Appendix A).

Fig. 22 shows the geometry of the model and the definition of the variables used (see also Table 4 for symbols). The interior region acts as a reservoir that can store or release

freshwater. The boundary region is conceptually a channel (open at both ends) where the freshwater is conveyed around the basin. The basin is assumed haline-stratified so that freshwater is confined to the upper light layer. The geometry is cylindrical with a flat bottom and a rigid lid at the surface. In the boundary region the depth of the interface varies in time and in the along-shore direction, while it only varies in time in the interior.

Following observations and modeling efforts from the Beaufort Sea (Newton et al., 2006; Proshutinsky et al., 2009) and previous numerical simulations of Hudson Bay (St-Laurent et al., 2010), I assume that the exchange of freshwater between the interior reservoir and the boundary current is dominated by the wind stress curl through Ekman pumping. The boundary current is assumed vertically-uniform at the upstream boundary (northwestern Hudson Bay) and its volume flux is prescribed proportional to the wind stress curl as suggested by dynamical arguments and observations (St-Laurent, 2010, see Appendix A). Note that the flow is free to reverse its direction according to the sign of the wind stress curl. The shear between the boundary velocities is calculated from the cross-shore slope of the interface through the thermal wind relation (e.g., Gill, 1982, his Chap. 7).

3.3.2 Forcing used in the Simulations

The conceptual model is used for a set of prognostic simulations that begin in August 1979 and end on August 2007 (28 years long, see Table 5). In each case, the prognostic calculations are initialized from the solution of the steady model equations (time-derivatives are set to zero) with forcings that were time-averaged over the 1979–2007 period. Fig. 23 shows a climatology of the various forcings used during the prognostic simulations. Precipitation, evaporation, sea ice growth and melt are assumed to act uniformly over the basin as diffusive sources/sinks of freshwater. Following the analysis of St-Laurent et al. (2010), net precipitation does not play an important role in the seasonality and it is applied as a constant (Table 4; Fig. 23). According to the same study, the sea ice cover has a fairly small net effect over the annual freshwater budget and so it is included as a sinusoidal forcing leading to a maximum

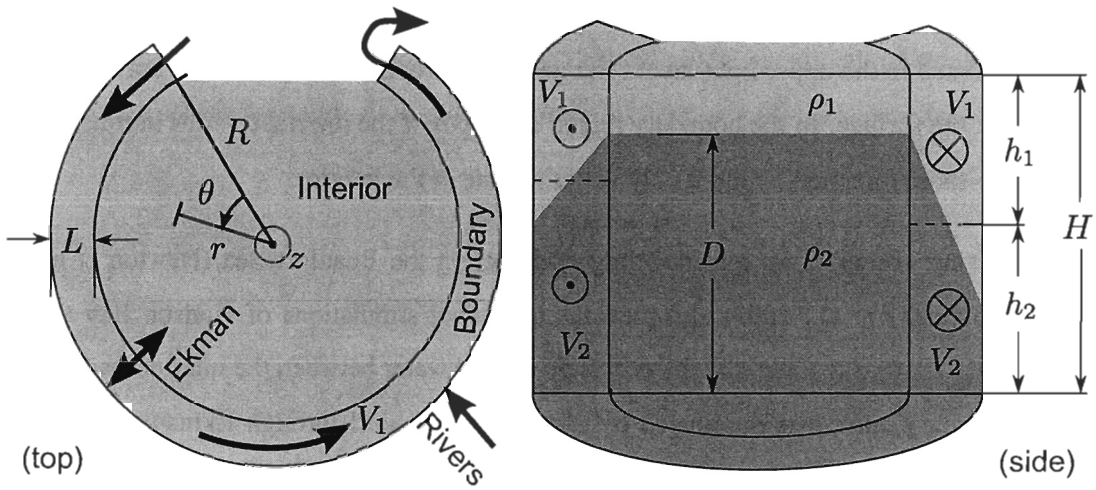

Figure 22: (a) Top and (b) side views of the conceptual model. The geometry is cylindrical with coordinates (r, θ, z) and corresponding velocities (u, v, w). See Table 4 and section 3.3 for the definition of the symbols.

Table 4: Parameters and Forcing Used in the Numerical Simulation of Hudson Bay.

Parameter	Value	Source
Mean depth H	110 m	NOAA (2006)
Coriolis parameter f	1.2×10^{-4} rad s^{-1}	NOAA (2006)
Width boundary region L	100 km	St-Laurent et al. (2010)
Radius interior region R	367 km	St-Laurent et al. (2010)
Arc interior region Θ	293°	NOAA (2006)
Net precipitation $P - E$	1 mm day^{-1}	St-Laurent et al. (2010)
Maximum ice thickness	1.3 m	St-Laurent et al. (2010)
Density bottom layer ρ_2	1026.5 kg m^{-3}	St-Laurent et al. (2010)
FW inflow $h_1 V_1 L b_1 / b_0$	3000 m^3 s^{-1}	St-Laurent et al. (2010)
Wind stress curl $\overline{\nabla \times \tau_w}$	Varies in time	Mesinger et al. (2006)
Friction coefficient ϵ	$\sqrt{\frac{5\times10^{-3} R \langle \overline{\nabla \times \tau_w} \rangle}{2\rho_0 H^2}}$	Linearized quadr. fric.
River runoff u_{riv}	Varies time-space	Saucier et al. (2004a), Déry et al. (2009)

Note: The overline denotes a domain-average, and the brackets a time-average.
See section 3.3 and Fig. 22 for further description of the symbols.

thickness on 1 May and ice-free conditions on 1 November (Fig. 23, comparable to Saucier et al. 2004a, their Fig. 11a). The dynamical role played by the ice cover during winter is neglected in this simple model, and the validity of this approximation will be discussed in section 3.5.

River runoff occurs around the perimeter of the basin and contributes to both freshwater and volume budgets of the basin. This realistic runoff varies in time and space, and it is taken from a monthly climatology (Jan.–Dec.) for each of the rivers of Hudson Bay (as described in Saucier et al., 2004a). We further introduce interannual variability in this river forcing by modulating the runoff climatology according to a timeseries (Fig. 28, upper panel) constructed from Hudson Bay's river discharge data (taken from the website described in Déry et al., 2009). Further details are available in St-Laurent 2010 (Appendix B). The flux of freshwater entering from the northwestern side of the boundary current (Fig. 24) is held constant on inflow (Table 4) and set according to the study of St-Laurent et al. (2010). Note that the constant inflow does not contribute to variations in time of the freshwater content or export.

The wind forcing is taken from the high-resolution (30 km, 3-hourly) North American Regional Reanalysis (NARR) for the the 1979–2007 period (Mesinger et al., 2006). Following the analysis of St-Laurent et al. (2010), a timeseries of the basin-averaged wind stress curl is produced from these winds and used as the atmospheric forcing of the conceptual model. A daily climatology of the curl over the 1979–2007 period is shown in Fig. 23. Curl values are lowest in the summer and highest during the fall, with frequent shifts in sign (negative values occur over 50 days in Fig. 23). We note that this seasonality is in agreement with the analysis of St-Laurent et al. (2010). Positive (negative) curl values are associated with a cyclonic (anticyclonic) boundary current and the release (storage) of freshwater in the interior reservoir through Ekman pumping.

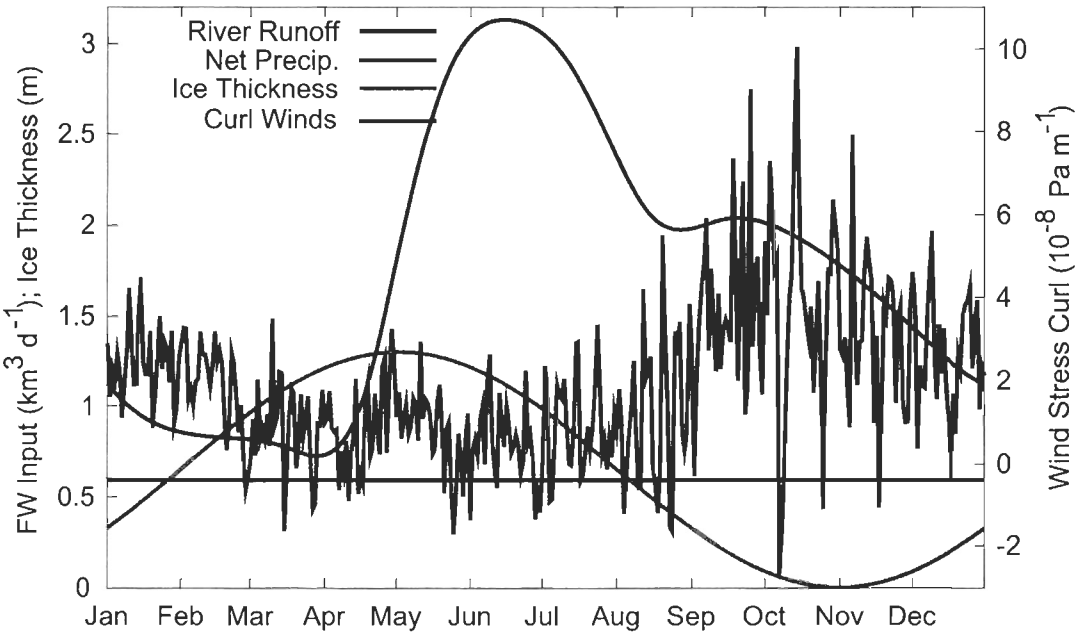

Figure 23: Climatologic seasonality of the hydrologic, cryospheric, and atmospheric forcing. Note that these curves represent climatological averages, while the conceptual model makes use of realistic, interannually-varying forcing for rivers and winds (see section 3.3.2).

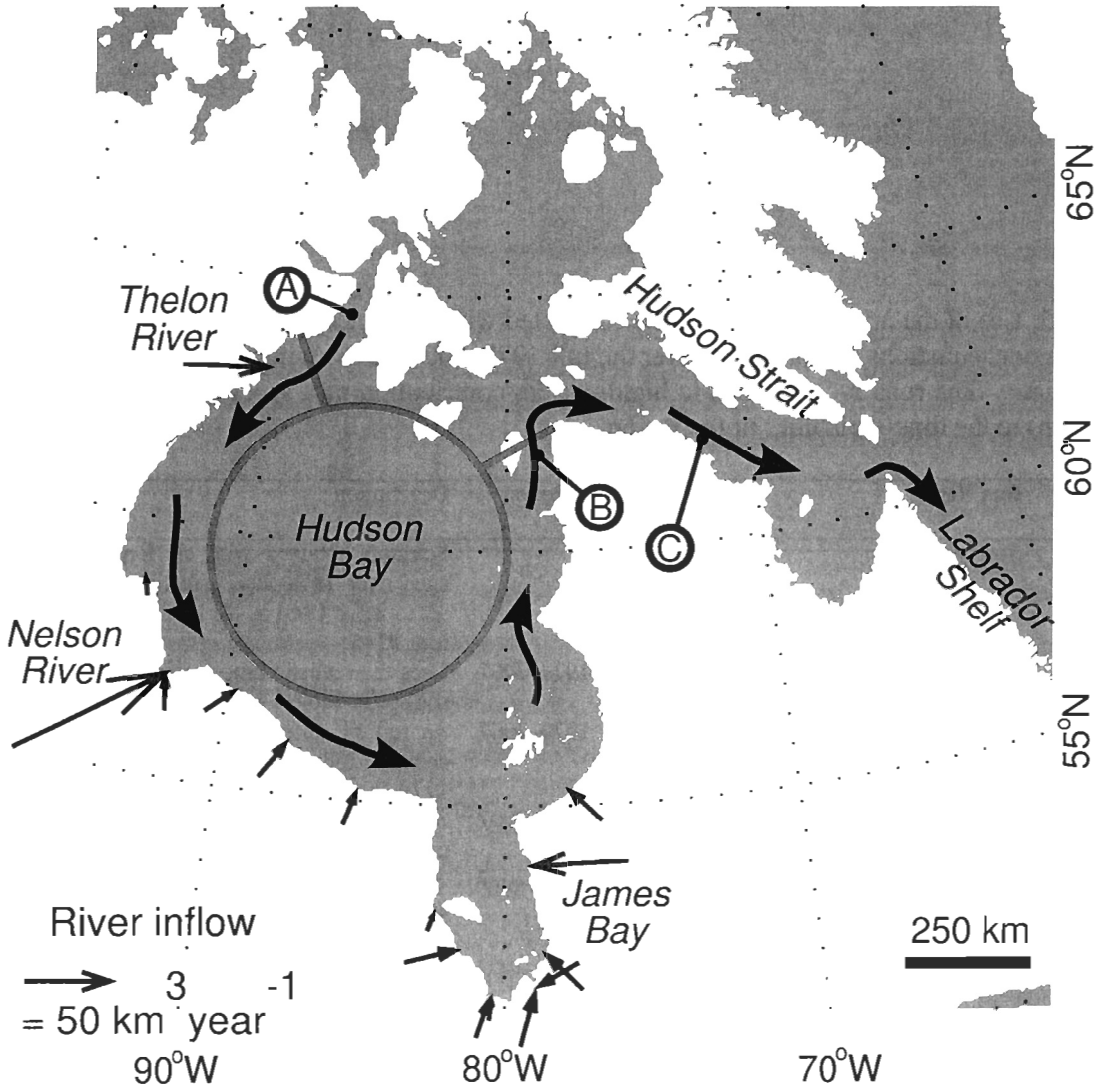

Figure 24: Map of Hudson Bay and the surrounding basins. The black arrows represent the mean surface circulation according to Prinsenberg (1986a) and St-Laurent et al. (2010). The magenta arrows indicate the location of river discharge and its mean value. The approximate divisions of the conceptual model are given by the gray lines. Circled letters show the location of the instruments used in the study.

Table 5: List of the numerical simulations conducted with the conceptual model. In runs #1–5 the model equations are integrated over the full 1979–2007 period without halt or restoring conditions. The runs 2–5 are used to highlight the contribution of a specific forcing (third column) to the time-variability of the system.

Run #	Run Name	Forcing Highlighted	Period	Description
0	Steady Solution	—	—	Solution obtained with all forcings averaged over 1979–2007 and time-derivatives set to zero. Used as the initial condition for runs #1–5.
1	Control Simulation	—	1979–2007	Uses the realistic time-varying forcings described in Table 4 and section 3.3.2.
2	Constant Winds	Rivers and Ice Cycle	1979–2007	As run #1 except that wind stress curl is constant and equal to its average value over 1979–2007.
3	Constant Winds, No Ice	Rivers	1979–2007	As run #2 except that the sea ice growth/melt cycle is absent.
4	Constant Winds & Rivers	Ice Cycle	1979–2007	As run #2 except that the discharge from each river is constant and equal to its average value over 1979–2007.
5	Constant Rivers, No Ice	Winds	1979–2007	As run #1 except that the discharge from each river is constant and equal to its average value over 1979–2007, and the sea ice growth/melt cycle is absent.

3.4 Results

3.4.1 General Features from the Model Simulation and Comparison with Observations

This section will present the main features of the system according to the conceptual model. Whenever possible, the results from the model are compared to historical or previously unpublished observations. Fig. 25 shows the time-averaged value for the depth of the pycnocline (or interface) and for the velocities within the boundary current. The pycnocline gradually deepens from upstream to downstream as the boundary current collects the freshwater from the rivers, thus increasing the thickness of the fresh (upper) layer (e.g., St-Laurent, 2010, Eq. 5.33). This increase is particularly visible at 100, 750, and 1400 km, these locations corresponding to those of the three main river discharges (Thelon River, Nelson River, and James Bay; see map on Fig. 24). The deepening of the pycnocline from western to eastern Hudson Bay is consistent with observations along transects (Prinsenberg 1986b, Fig. 9.4; St-Laurent et al. 2010, Fig. 15d) and also consistent with the observed surface salinity (Prinsenberg 1986b, Fig. 9.1; Lapoussière et al. 2009, Fig. 2a).

Waters enter Hudson Bay in both the upper and lower layers at the upstream boundary of the model (northwestern Hudson Bay; see Fig. 24) before becoming increasingly sheared going downstream. This is a consequence of the deepening of the pycnocline in the boundary current, that increases the cross-shore density gradient and the vertical shear through the thermal wind relationship (e.g. Gill 1982, Chap. 7). The upper layer thus speeds up downstream while the lower layer slows down in response to the freshwater input from the rivers. The velocity of the lower layer is negative at the downstream boundary of Hudson Bay, meaning that dense waters not only enter Hudson Bay from the western boundary but also from the eastern boundary as will be seen later.

Fig. 26 shows a comparison between modeled and observed velocities at the upstream

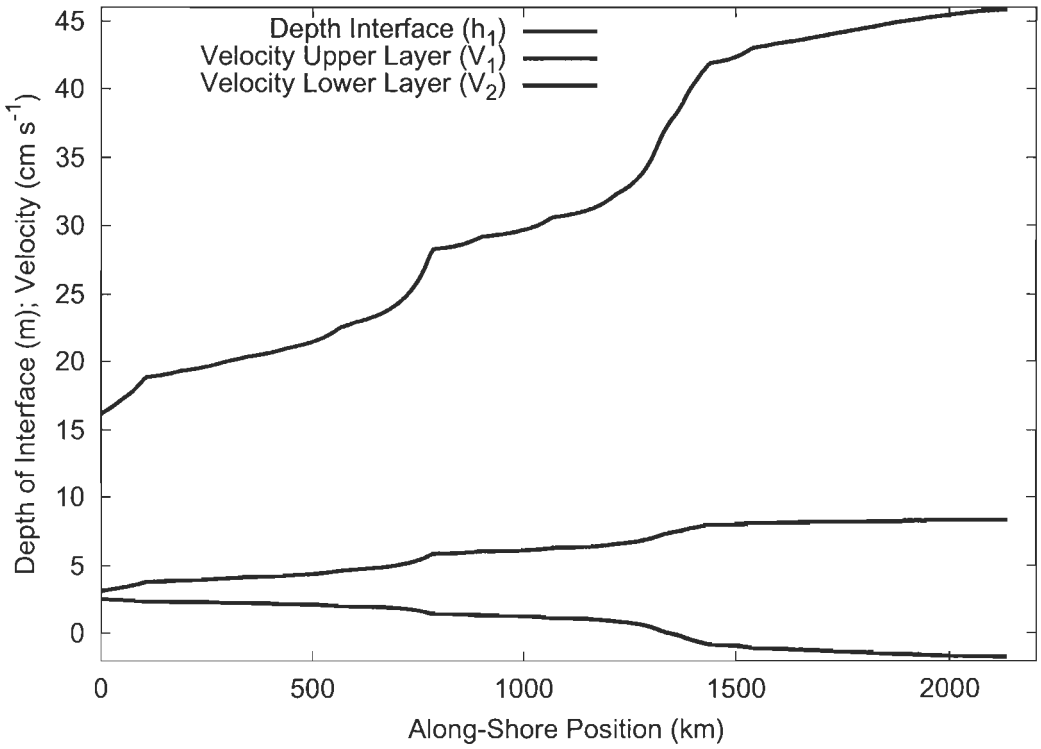

Figure 25: Depth of the interface and velocities in the boundary current, averaged over the full period (1979–2007) of the control simulation (run #1, see Table 5). The along-shore position increases in a counter-clockwise sense, starting from the upstream boundary of the model (northwestern Hudson Bay).

boundary (northwestern Hudson Bay; station A in Fig. 24). The observed along-shore velocities are vertically averaged over the thickness of the two model layers. It is seen that the magnitudes of the model velocities are consistent with those observed. Higher velocities are found during the fall in both model results and observations. The agreement is however not as good during the spring as the model velocities show a broad peak that seems to occur one month and a half later in the observations. This is interpreted as either a deficiency in the wind forcing, or more complex dynamics that is not captured by the idealized model. Nevertheless the key features of the flow are considered to be correctly reproduced, notably the low level of shear at this location of the boundary current (bottom panel, Fig. 26).

Fig. 27 shows a similar comparison with observations but this time at the downstream boundary (northeastern Hudson Bay; station B in Fig. 24). The salinity record from an instrument approximately located at the depth of the interface is used as a proxy for the seasonal movements of the interface: when the salinity increases (decreases) the interface should go upward (downward) because of the thinner (thicker) fresh layer. The seasonal cycle is qualitatively similar in both model and observations, with fresher waters found during the fall and early winter, and a broad salty period around spring. The figure also shows the comparison with velocities from two current-meters approximately located within the upper and lower model layers respectively. Again, the magnitudes of the model velocities are consistent with those observed, and some of the variations within the year are rather well captured by the idealized model. Note the presence of extended periods of flow reversal at depth, both in observed and modeled curves, representing dense water entering Hudson Bay along the coasts of Québec.

In summary, this section represents Hudson Bay as a system under a strong influence from the river runoff. River waters contribute to a general deepening of the pycnocline along the shores of the basin, in turn producing a sheared flow that includes a deep inflow at the downstream boundary. The results from the simulation are consistent with year-long observations of the system, which supports the assumptions used in the simple model. In the

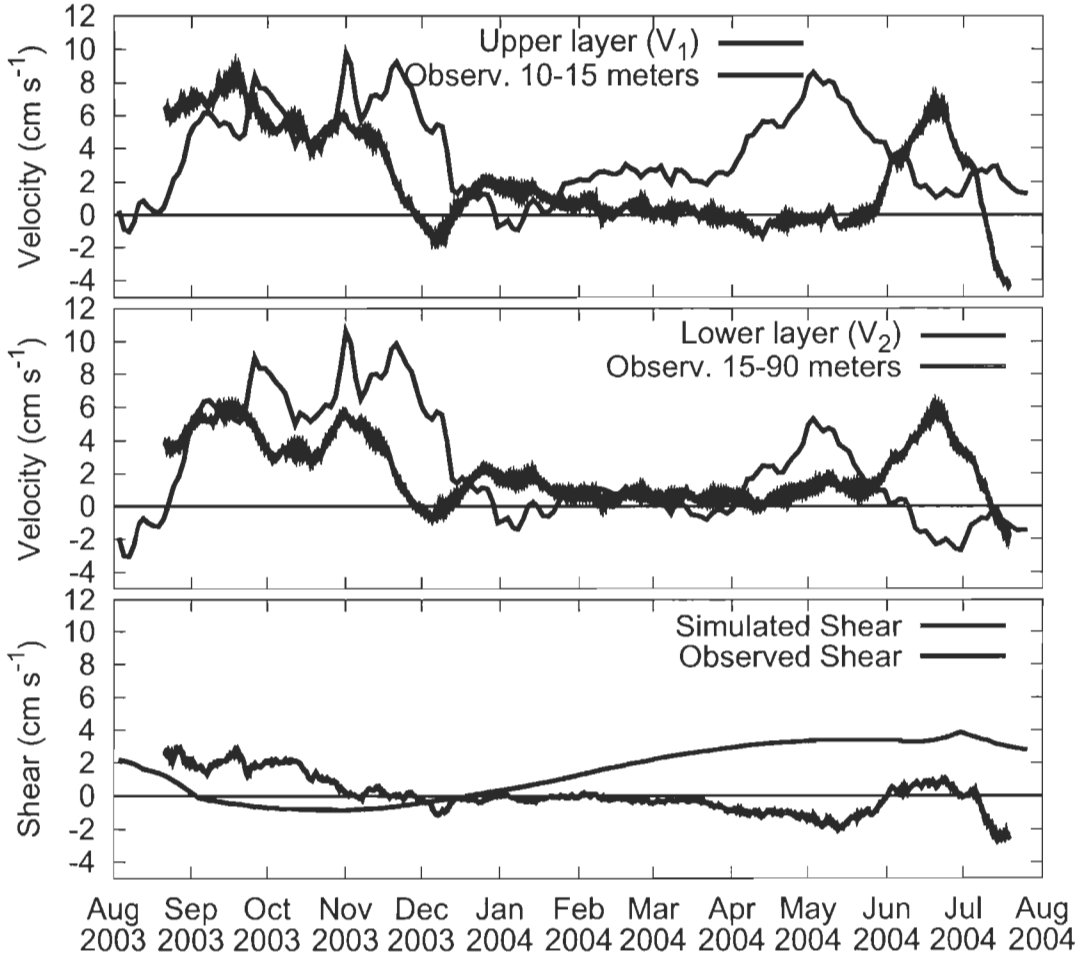

Figure 26: Comparison between observed (red curve) and modeled velocities (blue curve) upstream of the boundary current (station A in Fig. 24). The observed velocities are averaged over the depth intervals from the legend. The high-frequency oscillation visible in observations is the residual of the M_2 tidal signal. The model results are an excerpt from the 1979–2007 control run (see Table 5).

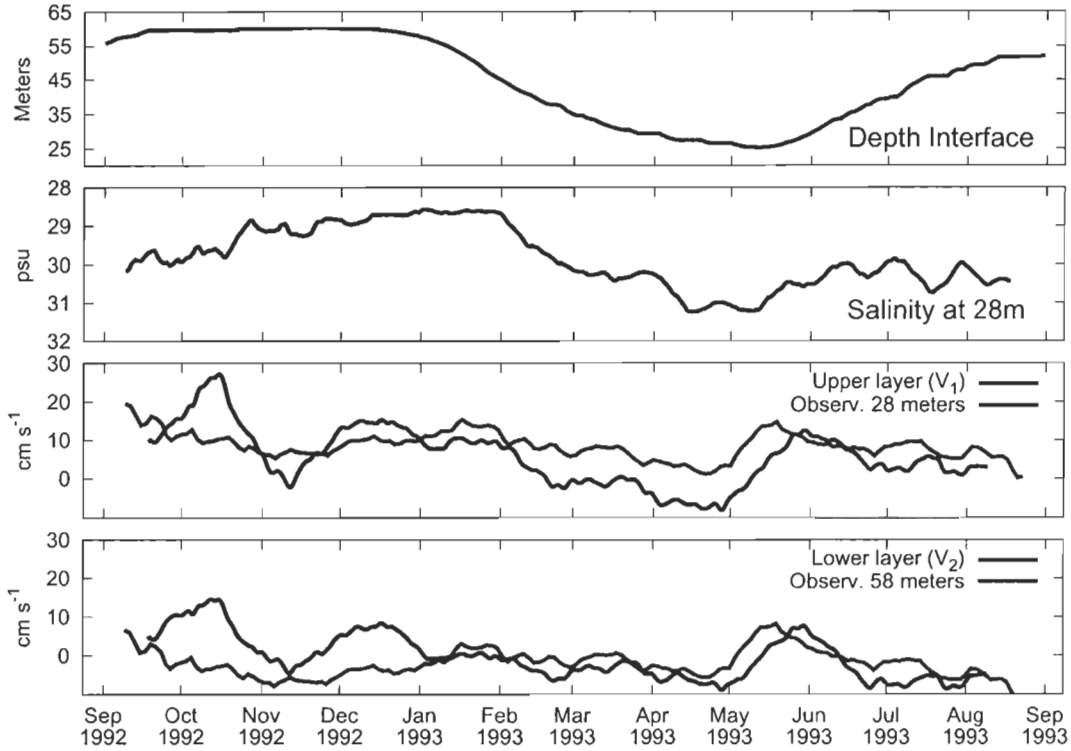

Figure 27: Comparison between observations from Saucier et al. (1994) (red curves) and model results (blue curves) downstream of the boundary current (station B in Fig. 24). The vertical axis for the depth of the interface is reversed to ease the comparison with the salinity record. The model results are an excerpt from the 1979–2007 control run (see Table 5).

next sections, this model will be used to examine the long-term variability in the freshwater balance and its controls.

3.4.2 Storage and Export of Freshwater in Hudson Bay

In this section we turn our attention from the mean and seasonal variability of the freshwater balance (section 3.4.1) to its interannual variability. This long-term variability is likely to be controlled by the fluctuating hydrologic and atmospheric forcing, in particular the river runoff and the wind stress over the basin. Fig. 28 shows how the river runoff varies over the 28 years of the simulation (data obtained from the website described in Déry et al., 2009). The runoff fluctuates by ±20% of its mean value and notably includes an abrupt decrease around 1980 and 1987, and an abrupt increase in 2005. This variability in the runoff is known to be closely related to variations in the Arctic Oscillation index (Déry and Wood, 2004). The changes occurring in 1980 and 2005 are sufficiently abrupt to have a visible effect on the volume of freshwater within the boundary current (fourth panel from top) which is otherwise constant over the 28 years.

Another source of variability is the curl of the wind stress (second panel from top) that sets the transport upstream of the boundary current and the exchange of freshwater with the interior region (through Ekman transport). The figure shows a smoothed version of the curl but the values used by the model vary considerably and often shift in sign (see section 3.3). The curl timeseries notably shows a strong and broad cyclonic period around 1990, and an extended period of anticyclonic curl in 2005. Again, these changes in the forcing are immediately visible in the volume of freshwater within the interior (fifth panel from the top). The interior releases about $200\,km^3$ of freshwater around 1990, and stores a similar volume in 2005. These variations are dictated by Ekman transport that sets the cross-shore exchange of freshwater between the boundary and interior.

The validation of these long-term changes in storage would require a correspondingly

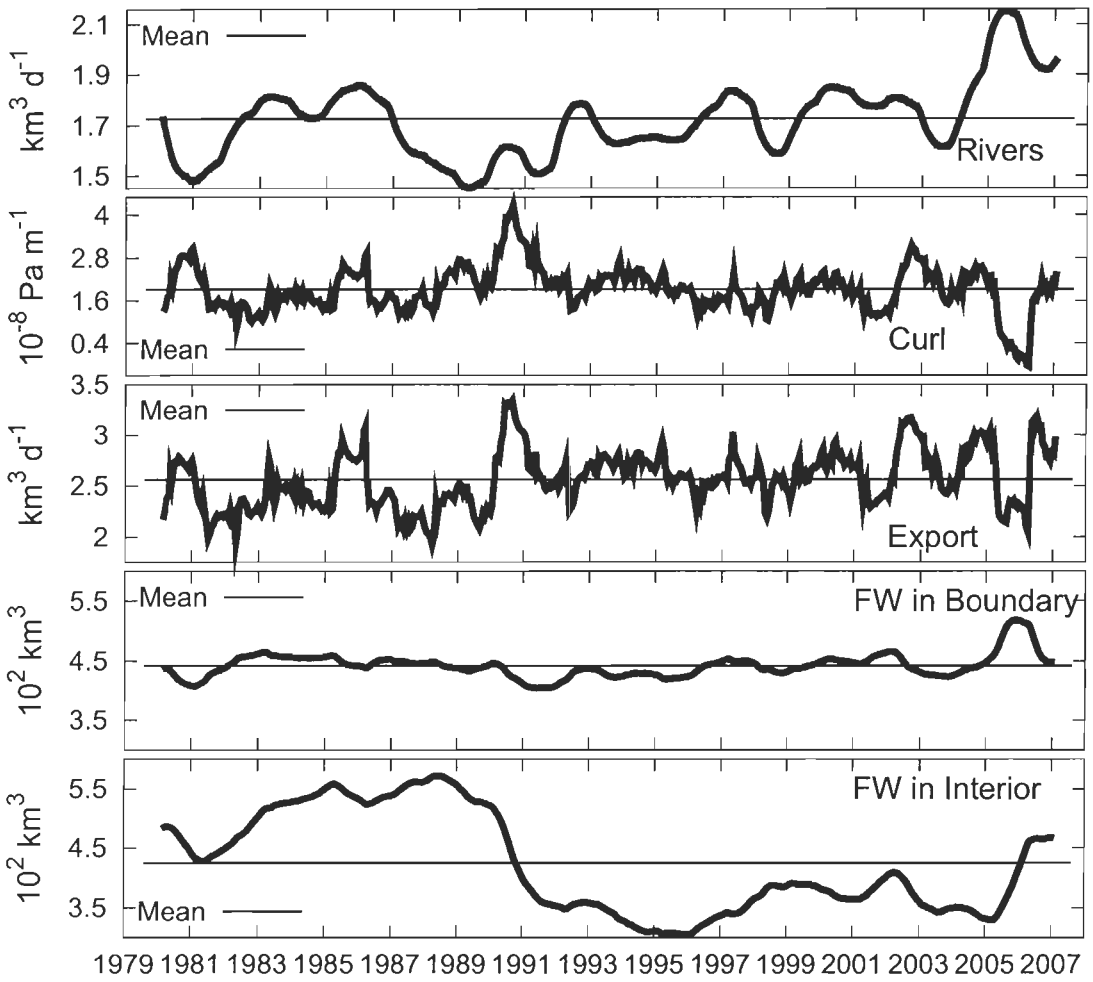

Figure 28: Interannual variability the river runoff, curl of the wind stress, export of freshwater out of the basin, and volume of freshwater within the boundary region and interior. All values are referenced to a salinity $S_0 = 33$ psu. A moving average of one year was applied to the curves to filter the seasonal variability and to highlight the interannual variability. These results are taken from the control run (see Table 5).

long-term monitoring of the system, which is not available. Nevertheless, the model results can be compared to a zonal section along 61°N that was sampled in August/September of the years 2003–2006 (Saucier et al., 2004b). The salinity profiles from this section are used to calculate the freshwater concentration over the four years (Fig. 3.4.2). The profiles are similar over the years 2003–2004, while a substantial freshening occurred over the top 20 m in 2005. The fourth year (2006) still shows a relatively fresh profile but with a more uniform distribution over depth. Although the data from a single section is not representative of the whole interior region, the profiles still show that an important freshening occured over the year 2005, which supports the model prediction that freshwater was stored in the interior over this year.

The export of freshwater is shown on the third panel of Fig. 28. Its variability mostly follows that of the wind stress curl (second panel), with a slight modulation by the interannual river runoff (first panel). The existence of a strong relation between winds, storage, and export, is best visible between 2005 and 2006. This period is characterized by an anomalously high river runoff but a very small export since freshwater is diverted to the interior of the basin (as expected from the low curl values; see Fig. 28). This model prediction can be compared to a unique timeseries of the freshwater flux measured downstream of Hudson Bay (station C, Fig. 24) over the period 2004–2007 (data from Straneo et al., 2010). This freshwater outflow is shown in Fig. 30, and it has a clear annual cycle dominated by fresh bursts over the fall season. It can be seen that the export predicted by the model agrees well with the observations. Both modeled and observed outflow follow a variability that is not consistent with the river input over these years (Fig. 28, first panel), again supporting the model prediction that part of the 2005 river input was stored in the interior.

This section showed the substantial variability in the freshwater balance of Hudson Bay over the last 28 years. The model notably demonstrates the capability of the system to store freshwater during years of low wind stress curl, leading to a complex interannual variability visible both in the modeled and observed export. In the next section, we will examine in more

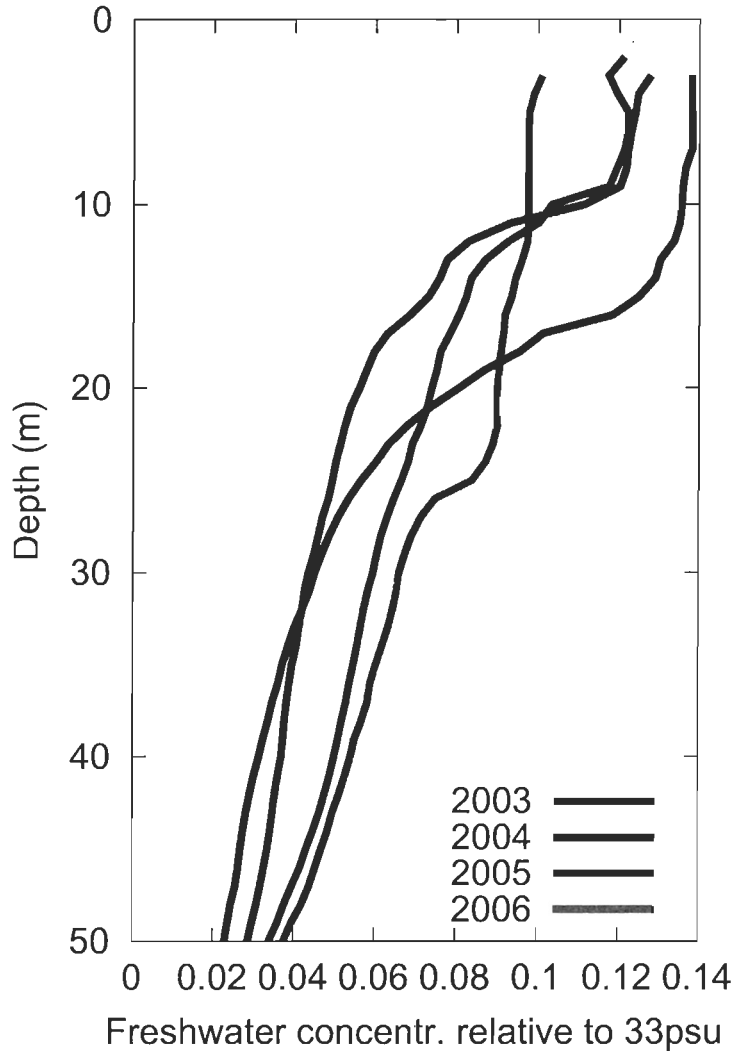

Figure 29: Vertical profiles of freshwater concentration derived from a zonal transect along 61°N in the interior region of Hudson Bay during August/September (ice-free period) of years 2003–2006.

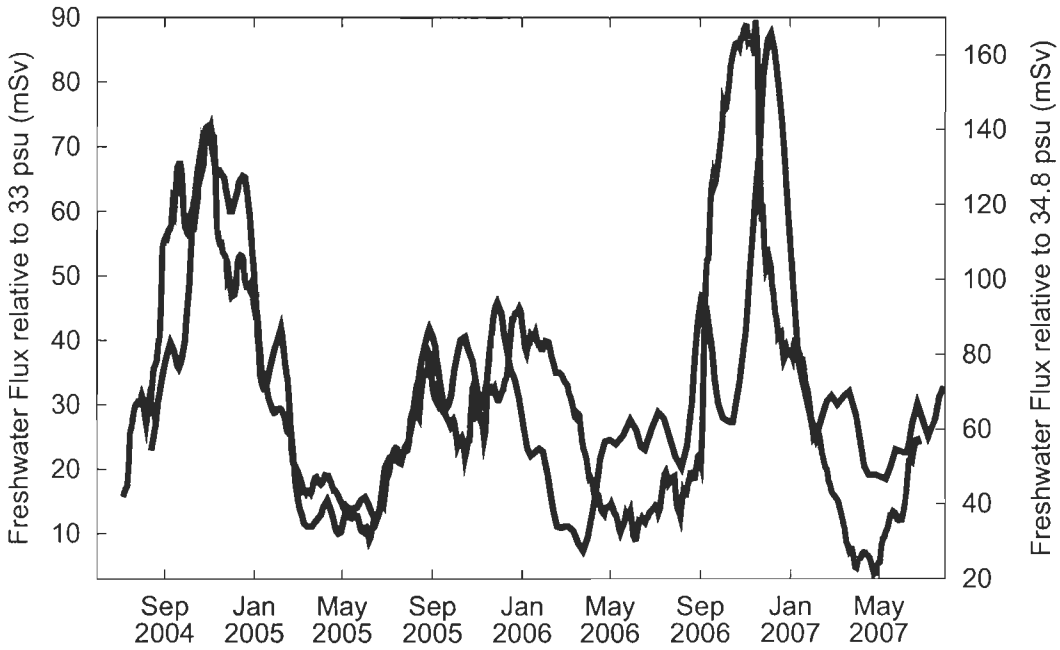

Figure 30: Comparison between the modeled (blue curve) and observed (red curve) freshwater flux downstream of the boundary current (station C in Fig. 24). Observations are from Straneo et al. (2010). Note that the observed flux was only available for a reference salinity of 34.8 psu. The model results are an excerpt from the 1979–2007 control run (see Table 5).

detail the role of the hydrologic, cryospheric and atmospheric forcing in the formation of the fresh bursts that dominate this freshwater outflow.

3.4.3 The Formation of the Fresh Bursts

The previous section showed the skill of the idealized model in capturing the variability of the freshwater outflow of Hudson Bay. This freshwater export from the system integrates the effect of the different freshwater sources (river runoff, sea ice growth/melt cycle, net precipitation), the exchanges between the boundary and interior regions, and the boundary current that fluctuates according to winds and density gradients. Although all these processes are likely to play a significant role in shaping the fresh bursts, it is desirable at this point to identify which one of these processes is the most important. For this purpose, we conduct a series of experiments that highlight the role of each component.

We specifically consider four experiments that differ from the control simulation (run #1) by the use of: a constant wind stress curl (run #2); a constant wind stress curl and no ice growth/melt cycle (run #3); a constant wind stress curl and constant river runoff (run #4); a constant river runoff and no ice/growth melt cycle (run #5, see Table 5). Note that with constant winds, the volume inflow at the northwestern boundary, as well as the exchange between the interior and boundary, become fixed in time. Thus run #2 highlights the role of the variable buoyancy inputs (rivers and ice cycle) in the seasonal freshening of the basin (e.g., Fig. 27, top panel) and in the formation of the fresh bursts. The top panel of Fig. 31 shows that the seasonal freshening is well reproduced in absence of time-varying winds. It means that rivers and the ice cycle are largely responsible for the annual oscillation of the freshwater content. However, the shape of the fresh bursts (bottom panel of Fig. 31) is heavily modified by the use of constant winds. The bursts now spread over summer and fall of each year so that the variability of the freshwater outflow is much reduced. The top panel of Fig. 31 makes it clear that this is not caused by changes in the seasonal freshwater content, but rather by changes in the advective velocities (that became more constant over the year by removing the

wind variability, see middle panel).

The next experiment (run #3) is similar to the previous one (constant winds, run #2) except that the ice growth/melt cycle is also removed. This specifically highlights the role of the rivers in the seasonality. From Fig. 31 (top panel), the amplitude of the annual freshening is approximately reduced by half by removing the ice cycle. The remaining seasonality has a maximum in August that is associated with the spring freshet signal coming from James Bay. The fresh bursts (lower panel) are similar to those from run #2 except for a reduced variance (resulting from the weaker freshening, upper panel).

Run #4 has both constant winds and constant river runoff so that only the ice cycle contributes to the seasonality. The annual freshening (upper panel) is again reduced compared to the control simulation (run #1) because of the lack of a river freshet signal. The lower panel of Fig. 31 shows that run #4 produces the bursts with the least variability. This is first due to the relatively weak seasonality in freshwater (upper panel), but also to velocities that are essentially constant when constant winds and constant runoff are used (middle panel).

The last experiment (run #5) has all the sources of buoyancy constant in time in order to isolate the role of the variable winds. The freshwater concentration (upper panel) remains essentially constant over the year in this experiment with constant buoyancy inputs. However, the bursts produced are closest in shape to those from the control simulation (run #1). This means the variability in the winds is the most important factor in shaping the fresh bursts exported by the system. The variability in the winds controls the formation of the bursts in two ways, by determining the storage/release from the interior region, and by modulating the advective velocity of the boundary current. We see from Fig. 31 that the velocity of the current plays a leading role in shaping the bursts.

Despite the strong role played by the winds, the fresh bursts produced in the last experiment (run #5) are still substantially smaller than those from the control simulation, meaning that the variability in the buoyancy inputs still plays a significant role in the formation of the

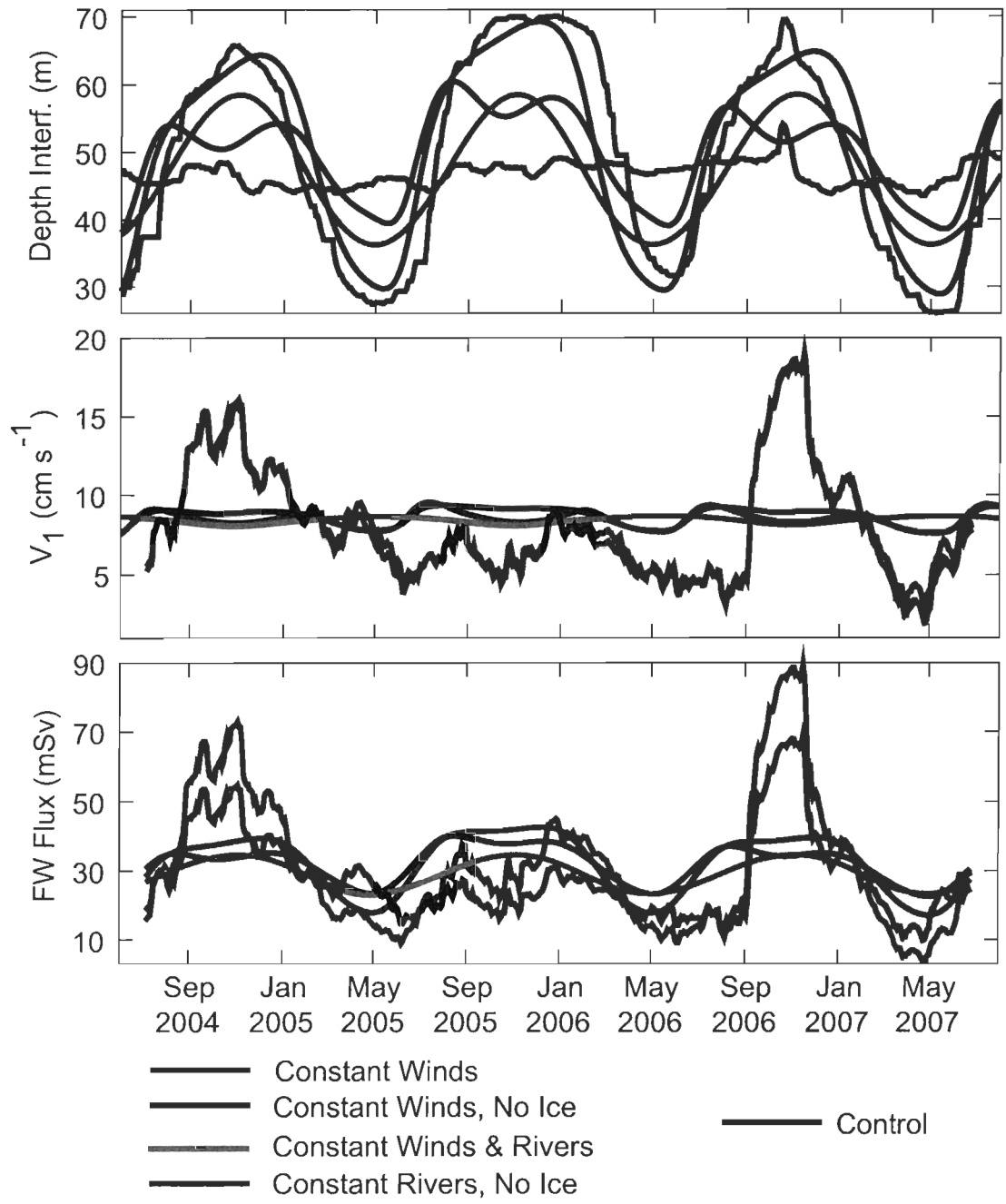

Figure 31: Sensitivity of the model to changes in hydrological and atmospheric forcing. The results are shown for the 2004–2007 period when observations are available for comparison (see Fig. 30). The panel shows the depth of the interface (top), the velocity of the fresh layer (middle), and the resulting freshwater flux (bottom) at the downstream boundary of the model (northeastern Hudson Bay) for the control simulation and experiments. See Table 5 for a detailed description of the model runs. The vertical axis for the depth of the interface is reversed so that increasing (decreasing) freshwater content is associated with an upward (downward) curve.

bursts. Interestingly, we note that the ice melt, river freshet, and seasonal winds all act to increase the magnitude of the fresh burst during the early fall (lower panel). Although this is probably a coincidence, it nevertheless contributes to the pulsatory aspect of Hudson Bay's fresh outflow.

In summary, these four experiments highlight the specific role of the rivers (run #3), sea ice growth/melt cycle (run #4), and winds (run #2 and 5) in the annual freshening of the boundary current and in the formation of the fresh bursts exported from the basin. It is found that the annual freshening is about equally due to the ice cycle and to the seasonality of the rivers. The formation of the bursts is most importantly caused by the seasonal winds even though the seasonal buoyancy inputs also play a significant role. The importance of winds in these results raises the question whether the long-term freshwater balance could be correlated to the large-scale modes of atmospheric variability such as the North Atlantic Oscillation. This hypothesis will be examined in the next section.

3.4.4 Is the Freshwater Balance in Phase with Climatic Indices?

The previous sections showed that the atmospheric forcing can account for a substantial fraction of the changes in storage and export of freshwater in Hudson Bay (Fig. 28). This atmospheric forcing is related to large-scale pressure patterns through geostrophy, and so the forcing could be correlated with climate indices such as the Arctic Oscillation (AO) index. If it is the case, then knowledge of the relevant climate index could provide an indication of long-term changes in the freshwater balance of the basin.

Following the work of Hochheim and Barber (2010) on the ice cover of Hudson Bay and its linkage to climate indices, we specifically consider three indices: the NAO, the Arctic Oscillation (AO), and the East Pacific/North Pacific index (EP/NP). Monthly values of the three indices are obtained for the simulation period (1979–2007) from the Climate Prediction Center of the National Oceanic and Atmospheric Administration (NOAA) at

http://www.cpc.noaa.gov/data/teledoc/telecontents.shtml. As a first attempt, we compare in Fig. 32 the climate indices with the atmospheric forcing used in the simulation (wind stress curl).

The figure shows that the timeseries strongly vary at yearly timescales, and no correlation is visible at these short timescales. This is expected since the high-frequency variability is most likely related to regional processes that cannot be captured by the climate indices and the large-scale variability they represent. At longer timescales however, a low-high-low pattern emerges from the indices and curl (1979–1988, 1989–1996, and 1997–2007 respectively). This pattern in the curl is best captured by the AO index, followed by the NAO and EP/NP indices. The correlation between the AO index and the atmospheric forcing is $R = 0.495$, significant at the 95% level with $N = 21$ effective degrees of freedom (e.g., Emery and Thomson, 1997).

The implication of such correlation between Hudson Bay and the Arctic Oscillation is best interpreted by looking at the storage of freshwater. The storage S in the interior is given by the time-accumulation of Ekman pumping events, the latter being proportional to the wind stress curl $\overline{\nabla \times \tau_w}$ (e.g., Pedlosky, 1996; St-Laurent, 2010, Appendix A, Eq. 5.31). Thus the storage corresponds to the time-integrated curl or, considering the correlation noted above, the integration over time of the AO index I_{AO}:

$$S(t) \propto -\int_0^t \overline{\nabla \times \tau_w}\, dt',$$

$$\text{if} \quad \overline{\nabla \times \tau_w} \propto I_{AO} \quad \text{then} \quad S(t) \propto -\int_0^t I_{AO}(t')\, dt'. \tag{3.1}$$

The storage and the time-integrated indices are compared in the lower panel of Fig. 32. As expected, the low-high-low curl identified previously translates into an upward-downward-upward pattern in the storage. This storage is particularly well represented by the AO index, again followed by the NAO and EP/NP indices. Note that the indices were multiplied by -1 for the lower panel to take into account the fact that storage decreases when the curl increases

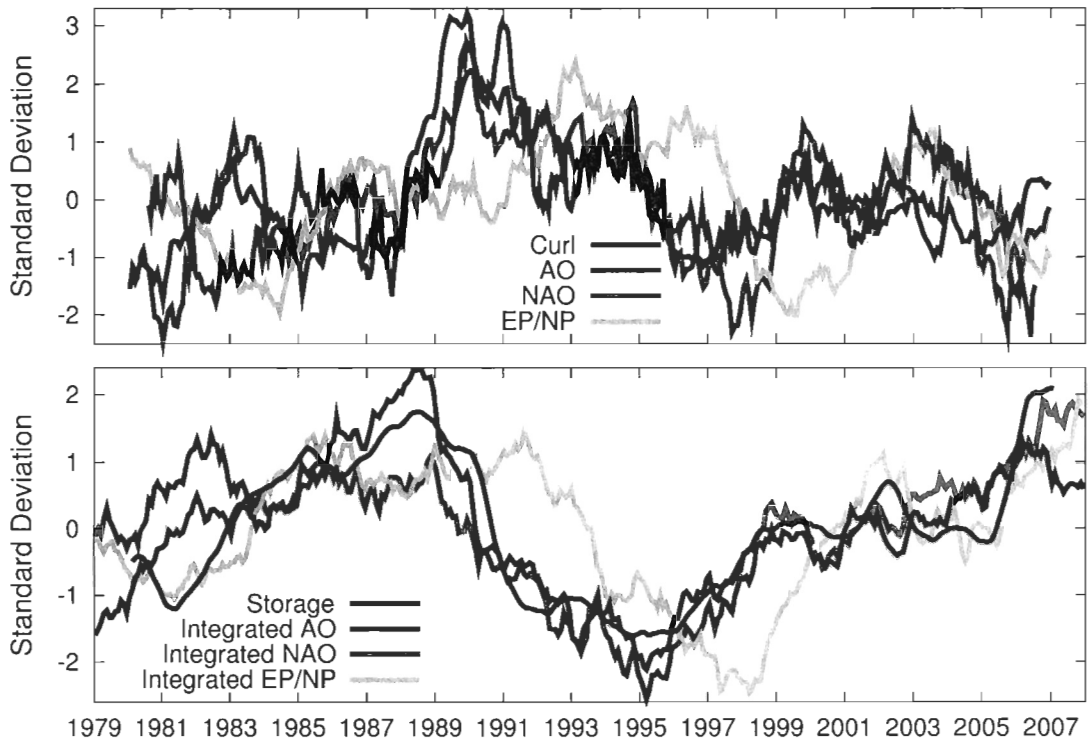

Figure 32: Comparison between climate indices, the wind stress curl, and the storage of freshwater in the interior of Hudson Bay. All curves are detrended and divided by their standard deviation. Climate indices include the Arctic Oscillation (AO) index, the North-Atlantic Oscillation (NAO) index, and the East Pacific/North Pacific (EP/NP) index. The model results are from the 1979–2007 control run (see Table 5).

(and vice versa, see Eq. 3.1).

In summary, the atmospheric forcing of Hudson Bay is significantly correlated to one of the large-scale modes of the atmosphere (the Arctic Oscillation). This index correctly describes the changes in the storage of freshwater over the course of the simulation. The implications of these results will be discussed in the next section.

3.5 Discussion

The objective of this study was to simulate the freshwater balance of Hudson Bay on decadal timescales. This was accomplished using a conceptual model that, admittedly, involves a number of idealizations. One potentially significant process that is neglected is the seasonal modulation of the flow by the seasonal ice cover. For instance, the model uses a year-long constant friction coefficient for the boundary current, while friction is expected to be higher during the ice-thick period. Such effects mainly occur in the nearshore regions where the ice is landfast or sufficiently packed to resist wind and ocean forcing (e.g., Figs. 12b and 18d). The neglection of these effects could explain the bias (overestimation) in the velocity of the upper layer over the Feb.–May period (Figs. 26 and 27).

Notwithstanding these simplifications, the model showed substantial skill in capturing the variability from the observations, in particular that of the freshwater export. We believe that the model is a useful tool for understanding the connections between the hydrologic, cryospheric, and atmospheric forcing and their role in the freshwater balance of Arctic seas. The model may also be an attractive and intuitive framework for the interpretation of results from observations and from more complex primitive equations models.

One of the key results of the study is the strong relation between winds, storage and export that gives rise to a complex interannual variability in the fresh outflow (e.g. in 2004–2007). This storage/export capability could lead to the formation of fresh bursts that disturb the winter convection in the subarctic areas downstream. A definite assessment of this would

of course require a more complete view of the problem that includes the subarctic seas. Nevertheless, the study provides an understanding of what controls the release of freshwater upstream, which is arguably an important component within the chain of events.

Another interesting result is the relation between the storage in the interior of Hudson Bay and the Arctic Oscillation. It was seen that a high (low) AO index yields a high (low) value for the wind stress curl, with impacts upon the freshwater content of Hudson Bay. Other components of the Arctic freshwater budget are correlated with the AO or NAO indices though (Déry and Wood 2004; Melling et al. 2008, their Fig. 9.8; Hochheim and Barber 2010). The study from Déry and Wood (2004) notably show that the river runoff in Hudson Bay is anti-correlated with the AO index, meaning that a high (low) AO index yields low (high) river runoff to the basin. Fig. 33 summarizes these ideas and show how the AO index can act to modulate the freshwater content of Hudson Bay.

Regarding climate change and global warming, the sensitivity experiments show that the system is most of all sensitive to changes in the atmospheric forcing. Such changes in the wind regime are likely to occur over the present or future winter seasons. The development of winter-time polar lows, associated with strong cyclonic winds, is very sensitive to the shape and extent of the ice cover (Gachon et al., 2003), and this ice cover has been clearly decreasing over the last 25 years (Hochheim and Barber, 2010). Moreover, the weaker ice cycle, the acceleration of the hydrological cycle, and future hydroelectric developments, would all tend toward a reduced seasonality in the freshwater inputs of Hudson Bay. The sensitivity experiments show that the flatter inputs will mostly impact the seasonal freshening of the boundary region (upper panel of Fig. 31), while the fresh outflow would still show fresh bursts but of reduced magnitude (lower panel).

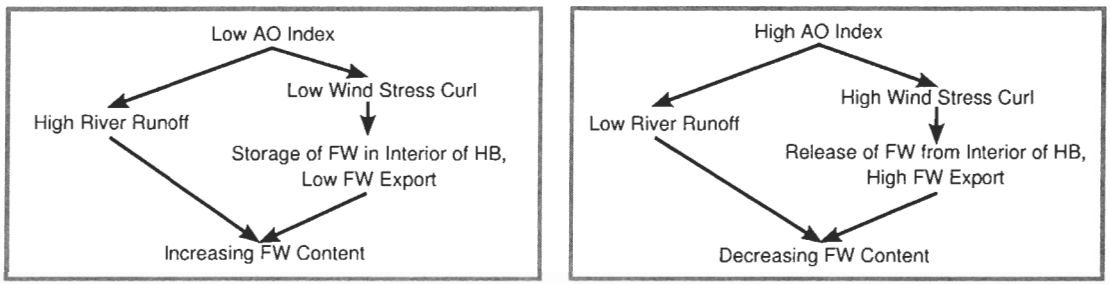

Figure 33: Schematic for the relations between the Arctic Oscillation (AO) index, river runoff in Hudson Bay (Déry and Wood, 2004), and the storage/release of freshwater (FW) in Hudson Bay (HB, see Fig. 32).

3.6 Conclusions

The observations and model results presented in the study describe an oceanographic system strongly influenced by its freshwater inputs. As a result of these fresh sources, the pycnocline deepens around the basin and the flow reverses with depth within the boundary current (Fig. 27). The pycnocline also has a substantial annual cycle (Fig. 27) that is found to be caused by growth/melt of sea ice and also by the large river freshet signal advected along the basin (Fig. 31).

The goal of this study was to simulate the storage/export of freshwater on decadal timescales and to examine its controls. In agreement with observations from the Beaufort Sea (Proshutinsky et al., 2009) and comprehensive numerical simulations of Hudson Bay (St-Laurent et al., 2010), the simulated storage in the interior is primarily controlled by the wind stress curl through Ekman pumping. This relation with the atmospheric forcing is extended to the large-scale Arctic Oscillation. Its index correctly describes the variability in storage over the period of the simulation (Fig. 32).

The export of freshwater shows more complex dependencies than the storage in the interior. Sensitivity experiments show that accurate prediction of the fresh outflow requires the knowledge of atmospheric, oceanic, hydrologic, and cryospheric parameters. First, the outflow depends upon the winds as they control the storage/release of freshwater from the interior, and the advective velocity of the boundary current. This boundary current is also modified by the cross-shore density gradients, thus requiring knowledge of the hydrographic conditions. Last, the variability in the hydrologic and cryospheric inputs (rivers and ice melt/growth) is found to play a significant role in setting the magnitude of the fresh bursts exported from the system (Fig. 31).

This complexity of the outflow is particularly visible around the 2004–2007 period. Despite record high freshwater inputs from the rivers (Fig. 28), the winds act to store the excess freshwater and delay its export, resulting in a non-intuitive pattern in the fresh outflow

(Fig. 30). This clearly demonstrates the capability of the system to store a substantial volume of freshwater, and also the complex dependence of the system on the various forcings.

Finally, the study presents a number of historical and previously unpublished observations that validate several assumptions of an idealized model. This new conceptual model represents an intuitive description of the large-scale oceanography of Hudson Bay that is consistent with a realistic but more complex primitive equations model (Saucier et al., 2004a). The study also showed that the conceptual model is a predictive tool for the kinematics of the freshwaters of Hudson Bay.

3.7 Acknowledgements

This work is a contribution to the Freshwater–Marine Coupling project of the ArcticNet network of Canada. We thank NSERC and the Canada Research Chairs program for funding. FS acknowledges support from NSF OCE-0751554. We want to thank the Department of Fisheries and Oceans (DFO) of Canada, their technicians, the captains and crews of the CCGS Radisson, DesGroseillers, Martha Black, and Amundsen. We also thank S. Senneville and J. Caveen for technical support. Data from 1992 were downloaded from DFO's SGDO (Système de Gestion des Données Océanographiques).

CONCLUSION GÉNÉRALE

[1]This study was motivated by the significant changes occurring in the Arctic seas (e.g., Peterson et al., 2006; Bernstein et al., 2007) and the several challenges to be faced before we understand the controls and impacts of the variability in Arctic seas' freshwaters (e.g., Dickson et al., 2008). Accordingly, the goal of the thesis was *to better understand the controls and impacts of the variability in Hudson Bay's freshwaters*. Several new results from the thesis contribute to this goal, and the most significant ones are highlighted in the following paragraphs.

The first chapter shows that the presence of the seasonal ice cover leads to significant changes in the barotropic tidal currents throughout the Hudson Bay System (Hudson Bay, Hudson Strait, and Foxe Basin). These changes are recurrent according to multi-year observations. The regions where the ice resists the most to the ocean forcing are identified as James Bay, southeastern Hudson Bay, and southeastern Foxe Basin. These areas correspond to those with the thickest and strongest ice.

The second chapter shows that winds play a significant role in diverting the river waters from the nearshore regions to the interior of the basin. The wind stress switches from a cyclonic to an anticyclonic curl over the seasons, which controls the substantial cross-shore exchange of freshwater between the boundary and interior regions. Another result is that sea ice growth and melt are relatively uniform over the domain so that the net annual effect of the ice cycle is smaller than atmospheric and hydrologic contributions.

The third chapter shows that Ekman pumping leads to significant long-term changes in the volume of freshwater stored within the interior of the basin. This notably includes a large release event around 1990, and a large storage event around 2005. The variable winds

[1]Notez que les sections Résumé, Introduction Générale, et Conclusion Générale, sont présentées en anglais et en français dans la thèse. Dans toutes ces sections la version anglaise précède celle en français, le passage d'une langue à l'autre étant souligné par le symbôle ∴.

largely control the formation of fresh bursts in the export during the fall season, although the seasonality in the sources of freshwater (rivers and ice melt) also contribute to the fall maximum.

Through these novel results, the thesis represents a significant advance in our understanding of the Arctic seas. The implications, limitations, and outlooks from these results will now be collectively discussed for the first time in the thesis.

Some Implications of the Thesis' Results

The section Introduction Générale introduced the various implications or impacts of the variability in Arctic's freshwaters. One of these implications is the potential role played by the fresh outflow from Hudson Bay in the modulation of the deep convection in the Labrador Sea (e.g., Lazier, 1980). As noted by LeBlond et al. (1996), the impact of Hudson Bay's fresh outflow depends on several parameters, notably the magnitude of the fresh burst, whether the disturbance reaches the convective sites, and when it does (timing). The thesis offers interesting new results regarding these questions. Fig. 30 (data from Straneo et al., 2010) shows that Hudson Bay's outflow is more like a series of bursts (one every fall season) than a constant stream (in the most part because of the variability in the winds, Fig. 31). Therefore, an evaluation of the potential impact of the export from Hudson Bay upon deep convection in the Labrador Sea should take into account the fact that most freshwater is released as a large pulse during the fall season, rather than being gradually released over the year.

Another result from the thesis seems relevant to this topic. In one of the first studies on the fresh outflow of Hudson Bay, Myers et al. (1990) examined the statistical relationship between the salinity within the Labrador Current (see Fig. 1) and yearly timeseries of ice thickness in Hudson Bay. For instance, if the ice melt occurred over only a very small part of the bay, it would be likely to produce a distinct burst within the outflow, and the magnitude of the burst would be somewhat related to the volume of ice from the preceding winter. We note

however that Myers et al. (1990) could not find a significant correlation between these two variables (ice melt and salinity). Interestingly, this may be related to our observation that the sea ice growth and melt are relatively uniform over Hudson Bay proper (see section 2.4.2) so that the formation of a large burst of ice melt water is not likely to take place.

One interesting advance from the thesis is the development of a simple conceptual model for an Arctic sea (Hudson Bay). These systems are a priori complex as they include significant stratification, sea ice cover, river runoff, winds, tides, bathymetry, and they are strongly influenced by the rotation of the Earth. Despite this complexity, a number of key features were identified in the simulations conducted with the realistic 3–D model in the first two chapters. These key features were implemented in the conceptual model, and its comparison with observations from Hudson Bay suggests that it is a simplified but appropriate description of its freshwater balance.

The simple model could also be relevant for other Arctic seas. For instance, the geometry of the model, that includes a boundary current and an interior, seems quite general and adaptable to other stratified, rotating seas. Further comparison with observations from different basins (e.g. Beaufort and Baltic seas) would be very helpful in understanding the similarities and differences between these systems. Differences may include the mean depth (e.g., the Beaufort Sea is much deeper than the other Arctic shelf seas), stratification (Hudson Bay has a fairly shallow halocline/pycnocline), spatial or temporal pattern of sea ice growth/melt (which may lead to spatial redistribution of freshwater), spatial and temporal pattern of river runoff (a spatially distributed runoff leads to a smoother freshwater export), and partial or nearly complete enclosure by isobaths/coastlines (and their role in steering the flow through conservation of potential vorticity). In the next section I propose a procedure to quantitatively assess the potential effect of these differences.

Discussion and Suggestions for Future Research

The advances made in the thesis raise a number of new questions regarding the role of the Arctic freshwaters. These recommendations for future research are discussed below. Similarly, some topics could not be covered within the thesis even though they would merit attention; those are also presented in this section.

The third chapter showed a significant correlation between an index of large-scale atmospheric variability (the Arctic Oscillation, AO) and the wind stress curl over Hudson Bay. Through this correlation with the wind stress curl, the AO index can be related to Ekman pumping and the long-term (decadal) variability of storage of freshwater (Fig. 32). As mentioned in the chapter, the AO index is also a proxy for the river runoff of Hudson Bay (the index and the runoff are anticorrelated). These correlations illustrate that the Arctic Oscillation is likely to affect the freshwaters of Arctic seas in more than one way; the AO modulates the winds, precipitation (and then river runoff), and potentially the ice cover and air-sea exchanges (e.g., Fig. 33 from chapter 3). Amongst all these changes that follow the AO index, the results from chapter 3 show that, at interannual to decadal timescales, the changes in the winds are most likely to determine the changes in storage and release of freshwater within Hudson Bay.

On longer timescales, the latest projections of global warming (Bernstein et al., 2007) show a particularly large increase in air temperature over Hudson Bay (similar to what is projected for the seas above the Arctic Circle). Complex feedback processes between the atmosphere and the ocean are likely to emerge at these long timescales, and the variability of the winds may no longer play the dominant role in the freshwater storage/export of Hudson Bay. How will the freshwater balance of the Arctic seas evolve in these conditions? One change that is expected is the reduction of the sea ice cover over these seas. Such scenario was examined by Joly et al. (2010), who conducted a numerical experiment with a warmer atmosphere in a coupled sea ice-ocean model of Hudson Bay. For simplicity, their experiment

made use of present-day forcings for river runoff, precipitation and winds. The simulation showed a much reduced ice cover and deep water formation, and increased salinities over the basin (lower freshwater content). Unfortunately, the physics behind this lower freshwater content was not investigated by these authors.

One can envision that, with a thinner and mechanically weaker ice cover, the ocean underneath is more closely driven by the winds, and less prone to deceleration (spin-down) because of damping against the thick motionless ice cover (see chapter 1 of this thesis). This would result in a faster ocean circulation, and according to simple models, a lower freshwater content (as in the experiment of Joly et al., 2010). For instance, an idealized mixed-box estuarine model includes a salty inflow (salinity S_{in} and volume flux Q_{in}), a river runoff (salinity $S = 0$ and volume inflow Q_{riv}), and a brackish outflow of salinity S_{basin} and volume flux $Q_{\text{in}} + Q_{\text{riv}}$. In steady state, conservation of volume and salinity yields:

$$S_{\text{basin}} = \frac{Q_{\text{in}} S_{\text{in}}}{Q_{\text{in}} + Q_{\text{riv}}} = \frac{S_{\text{in}}}{1 + Q_{\text{riv}}/Q_{\text{in}}}, \tag{4.1}$$

which shows how a faster circulation (higher Q_{in}) leads to a lower freshwater content in the basin (higher S_{basin}). It can be verified that the conceptual model described in chapter 3 of this thesis has a qualitatively similar response in steady state (see Appendix A from this thesis). However, as I mentioned previously, it is not clear whether the physics of these simple models is applicable when we consider changes over long timescales and the complex feedback processes that may intervene. Clearly, future research whose objective is to understand the consequences of global warming should take into account the potentially important interactions between the different components (air, sea, ice, and land) of the climate.

As noted in the Introduction Générale, Hudson Bay is also subject to hydroelectric developments. Production of electricity requires a relatively constant stream of water, which is obtained through the use of a dam and a reservoir, and results in an artificially high (low) discharge of river water during the winter (summer) season (the annual mean discharge is assumed to be preserved). How do these hydroelectric developments affect the freshwater

balance of Hudson Bay? Although this topic was not specifically examined in the thesis, the results suggest that the regulation of a few rivers would have a limited impact on the large-scale freshwater content and export of freshwater, since these two variables depend on the alongshore-integrated river discharge (see Eqs. 5.33 and 5.32, respectively) rather than the local river discharge[2]. The integration tends to minimize the importance of individual rivers, meaning that the regulation of a few rivers is likely to be unnoticeable in the large-scale freshwater balance. For the same reasons, the idealized hydrologic forcing used in chapter 3 (see Appendix B of the thesis) should not be considered as an important caveat; in the end, the large-scale freshwater content and export depend more on the integrated contribution of the rivers, than on their individual variability.

The large-scale freshwater balance of Hudson Bay might be more sensitive to global warming than to hydroelectric developments since the former is likely to affect the whole system. Scenarios of climate change show a general modification in the seasonality of the river runoff, notably an earlier freshet due to snow melt and ice melt occurring earlier over the continent. The discussion surrounding the sensitivity experiments of chapter 3 (e.g., Fig. 31) suggests that modifying the seasonality of all rivers would have an important effect on the salinity of the basin over seasons. The effect of such modification on the freshwater outflow would be, however, relatively small when compared to the modulation induced by winds over the year (Fig. 31).

Numerical simulations of global warming also show increased precipitation over the Arctic regions (Plummer et al., 2006), which is consistent with the increasing river runoff observed over these areas (Déry et al., 2009). Increasing precipitation, river runoff, and evaporation, is often described collectively as the acceleration of the hydrological cycle. This acceleration could be caused, for instance, by the shrinking sea ice cover and the increased air-sea exchanges that result. Increased precipitation and river runoff act to increase the fresh-

[2]This conclusion of course depends on which spatial scale we consider. At small spatial scales, say in the vicinity of a given river outlet, the regulation of the river discharge will obviously have a detectable effect. But on a larger scale, say beyond an internal Rossby radius, the horizontally-averaged salinity depends more on the cumulated discharge of the rivers upstream than on the local river discharge; see Eq. 5.33.

water content of Arctic seas, while increased evaporation acts to lower the freshwater content. It is difficult to predict which of these changes will occur in Hudson Bay since complex feedback processes may be important. Nevertheless, the results from the thesis show that the river runoff is by far the largest source of freshwater over the year, and that changes in precipitation or evaporation would have a relatively small impact on the freshwater balance (notably because the area drained by the rivers of Hudson Bay is much larger than the bay itself). This would result in a larger freshwater outflow in order to balance the larger river runoff. One could also expect the mean salinity of the basin to decrease in response to the higher river runoff, but the opposite could be true if the mean ocean circulation accelerates in response to the reduced ice cover (Eq. 4.1). From these considerations, it seems clear that accurate projections over multidecadal timescales would require further research that take into account the complex interactions between the land, sea, and atmosphere.

A different topic explored in the thesis was the export of freshwater from Hudson Bay to the subarctic areas, that could play a significant role in the modulation of the convection in the Labrador Sea. The thesis focused on what controls the export at the mouth of Hudson Bay and did not examine the fate of this freshwater once it left the bay. A definite assessment of the role played by Hudson Bay's fresh outflow would require a more complete view that includes the Arctic and subarctic seas, e.g. a model covering this whole area. Such a model would have to include Hudson Bay since its outflow was seen in the thesis to largely depend on oceanographic processes occuring within the bay (and not only on the variability of its freshwater inputs, e.g. river runoff). The model should also be of sufficient resolution to explicitely resolve the exchange of freshwater between the Labrador Current and the convective sites in the interior (Spall, 2004; Straneo, 2006), something that is sometimes overlooked (Rennermalm et al., 2007).

A subject of importance in the Arctic seas is the dynamical role of the sea ice cover. It can act as a frictional layer that damps the ocean currents, or as an insulator that limits the momentum transfer from the winds to the ocean. Such dynamical impact of the ice

cover was examined in chapters 1 and 2 but further investigations (e.g., that of Steiner, 2001) are required to closely constrain the role of ice in the low-frequency wintertime ocean circulation. Observations would be particularly helpful, notably year-long velocity profiles that resolve the ice-ocean boundary layer. Studies of the momentum transfer from winds to Hudson Bay's ice cover would be very helpful too, and fortunately, this work is underway (D. Barber, pers. comm.).

Some of the results from the thesis are particularly interesting for the ecology of Arctic seas in general and Hudson Bay in particular. One of these new results is the significant role played by winds in the nearshore/offshore exchange of the river waters of Hudson Bay (e.g., Macdonald et al., 1999). It contributes to an increased stability of the waters offshore (by bringing buoyancy in the upper layers), and it is also likely to contribute to the dispersion of light-absorbing materials (CDOM, see Granskog et al., 2007) and pollutants. The pathway of CDOM and pollutants is, however, more complicated because of its interactions with the biogeochemical environment. For this kind of study, extensive field measurements and a ice-ocean-biogeochemical model would be probably required. Ideally, the model should also have high-resolution in the vicinity of the river plume and be coupled to a regional model of the bay. In this way the small-scale processes and the large-scale dispersion (e.g., chapter 2) would be included.

Finally, one approach that seems promising for the understanding of the differences and similarities between different Arctic seas would be to describe them through a set of non-dimensional parameters (e.g., Garvine, 1999). These parameters are formed through the combination of the constants describing the geometry, hydrography and forcing of the basins, and the non-dimensional parameters characterize the response of these seas (see Wåhlin and Johnson, 2009, for an example). Such a study would be very helpful to illustrate, for instance, whether a basin will be more influenced by rivers than by the atmosphere (and why), or

whether the horizontal advection of the freshwaters would be buoyancy- or more wind-driven.

∴

Cette étude fut motivée par les changements importants se produisant actuellement dans les mers arctiques et ceux qui sont prévus pour les décennies à venir (e.g., Peterson et al., 2006; Bernstein et al., 2007), ainsi que par les nombreux défis auxquels on doit faire face avant de bien comprendre les tenants et aboutissants de la variabilité des eaux douces arctiques (e.g., Dickson et al., 2008). Ainsi, le but de la thèse était de *mieux comprendre les processus contrôlant la variabilité des eaux de la baie d'Hudson, et les impacts de cette variabilité*. Plusieurs résultats nouveaux obtenus dans le cadre de la thèse contribuent à ces objectifs, et résultats les plus significatifs sont soulignés dans les paragraphes qui suivent.

Le premier chapitre montre que la présence de la couverture glacielle saisonnière mène à des changements significatifs dans les courants barotropes de marée, et ce partout dans le système de la baie d'Hudson (baie et détroit d'Hudson, bassin de Foxe). Ces changements sont récurrents tel que le montre des observations pluriannuelles inédites. Les régions où la glace résiste le plus à la traction occasionnée par l'écoulement océanique sont identifiées : la baie James, le sud-est de la baie d'Hudson, et le sud-est du bassin de Foxe. Ces régions correspondent à celles où la glace est la plus épaisse et la plus rigide.

Le second chapitre montre que les vents jouent un rôle significatif dans la diversion des eaux des rivières, des régions côtières vers l'intérieur du bassin. La contrainte exercée par les vents au fil des saisons passe d'un état où son rotationnel est cyclonique à un état anticyclonique, ces transitions contrôlant le substantiel échange d'eau douce entre les régions bordières et intérieures du bassin. Un autre résultat clef est que la formation et la fonte de la glace sont relativement uniformes sur le domaine, signifiant que l'effet annuel net du cycle glaciel est beaucoup plus faible que les contributions atmosphériques et hydrologiques.

Le troisième chapitre montre que le pompage d'Ekman mène à des changements à long

terme significatifs pour le volume d'eau douce stocké à l'intérieur du bassin. Ceci inclut notamment un important export autour de 1990, et un important stockage autour de 2005. Les vents variables contrôlent en grande partie la formation à l'automne d'un large maximum dans l'export d'eau douce, bien que la saisonnalité des sources d'eau douce (rivières et fonte des glaces) contribuent aussi à ce maximum automnal.

De par ces résultats novateurs, la thèse représente une avancée substantielle dans la compréhension des mers arctiques. Les implications, limitations, et perspectives relatives à ces résultats seront maintenant discutées collectivement pour la première fois dans la thèse.

Quelques implications des résultats de la thèse

La section Introduction Générale présenta un certain nombre d'implications ou d'impacts relatifs à la variabilité des eaux douces arctiques. L'une de ces implications est le rôle potentiel joué par l'export d'eau douce de la baie d'Hudson dans la modulation de la convection profonde dans la mer du Labrador (e.g., Lazier, 1980). Tel que noté par LeBlond et al. (1996), l'impact de l'export de la baie d'Hudson dépend de plusieurs paramètres, notamment l'amplitude de cet export d'eau douce, si la perturbation atteint ou non les sites de convection profonde, et à quel moment de l'année. La thèse offre des résultats novateurs concernant ces questions. La Fig. 30 (observations tirées de Straneo et al., 2010) montre que l'export de la baie d'Hudson est davantage analogue à une série de pics (un pic à chaque automne) qu'à un écoulement constant, et ce en grande partie à cause de la variabilité des vents (Fig. 31). Ainsi, une évaluation de l'impact potentiel de l'export de la baie d'Hudson sur la convection profonde devrait prendre en compte le fait qu'une grande partie de l'eau douce est expulsée à l'automne plutôt que d'être expulsée graduellement au fil de l'année.

D'autres résultats de la thèse semblent pertinents à ce sujet. Dans l'une des premières études portant sur l'export d'eau douce de la baie d'Hudson, Myers et al. (1990) s'intéressa à une éventuelle corrélation entre la salinité du courant du Labrador (voir Fig. 1) et une série

temporelle d'épaisseur de glace dans la baie d'Hudson. Ainsi, si la fonte glacielle se produisait principalement dans une région restreinte du bassin, cela produirait un signal aisément détectable dans l'export de l'eau douce, et l'amplitude de ce signal serait en quelque sorte proportionnelle au volume de glace ayant fondu lors du printemps précédent. Toutefois, même en prenant en compte un éventuel délai entre la fonte et la salinité, Myers et al. (1990) n'ont pu trouver de corrélation significative entre ces deux variables. Il est intéressant de noter que cette observation peut s'expliquer par l'un de nos résultats : la production et la fonte de la glace de mer étant relativement uniformes sur la baie d'Hudson (voir la section 2.4.2) la formation d'un large signal associé à la fonte de la glace est improbable.

Une avancée intéressante de la thèse correspond au développement d'un modèle conceptuel simple d'une mer arctique (la baie d'Hudson). Ces systèmes sont a priori complexe puisqu'il comportent une stratification significative, une couverture glacielle saisonnière, un apport d'eau douce dû aux rivières, un forçage dû aux vents et aux marées, une bathymétrie complexe, et ils sont finalement fortement influencés par la rotation de la Terre. Malgré cette complexité, un certain nombre d'éléments clefs ont été identifiés dans les simulations effectuées avec le modèle réaliste 3–D dans les deux premiers chapitres. Ces éléments clefs ont été implantés dans le modèle conceptuel, et sa comparaison avec des observations de la baie d'Hudson suggèrent qu'il s'agit d'une description simplifiée mais appropriée de la cinématique des eaux douces du système.

Le modèle simple pourrait aussi être approprié pour d'autres mers arctiques. Par exemple, la géométrie du modèle, qui inclut un courant bordier et une région intérieure, semble assez générale dans son emploi et adaptable à d'autre mers polaires stratifiées. De plus amples comparaisons avec des observations provenant de différents bassins (e.g. la mer de Beaufort ou la mer Baltique) serait très utile pour la compréhension des similitudes et des différences entre ces systèmes. Ces différences peuvent inclure la profondeur moyenne (e.g., la mer de Beaufort est beaucoup plus profonde que les autres mers arctiques), la stratification (la baie d'Hudson a une halocline/pycnocline particulièrement prononcée et peu profonde),

des patrons spatiaux ou temporaux particuliers pour la formation/fonte glacielle (qui peuvent mener à une redistribution spatiale des eaux douces) ou pour l'apport des rivières (un apport spatiallement distribué mène à un export d'eau douce plus constant), et une isolation partielle ou quasi-complète par les isobathes/côtes (celles-ci jouant un rôle dans la direction de l'écoulement par conservation de la vorticité potentielle). Dans la prochaine section, je proposerai une procédure pour examiner de façon quantitative le rôle joué par ces différences.

Discussion et suggestions pour les recherches à venir

Les avancées faites dans le cadre de la thèse soulèvent un certain nombre de questions concernant le rôle des eaux douces des mers arctiques. Des recommendations pour des études à venir sont discutées ci-bas. De façon similaire, certains sujets n'ont pu être couverts dans le corps de la thèse malgré le fait qu'ils auraient mérité une attention particulière ; ces sujets sont aussi abordés dans cette section.

Le troisième chapitre a montré l'existence d'une corrélation significative entre un indice de la variabilité atmosphérique de grande échelle (l'oscillation arctique, AO) et le rotationnel de la contrainte des vents au dessus de la baie d'Hudson. De par cette corrélation avec le rotationnel, l'indice AO peut être relié au pompage d'Ekman et à la variabilité temporelle à longue échelle (décennale) du stockage de l'eau douce (Fig. 32). Tel que mentionné dans ce chapitre, l'indice AO est aussi un proxi pour l'apport des rivières de la baie d'Hudson (l'indice et le débit des rivières sont anticorrelés). Ces corrélations illustrent le fait que l'oscillation arctique est susceptible d'influencer les eaux douces des mers arctiques de différentes manières ; l'AO module les vents, les précipitations (et donc l'apport des rivières), et potentiellement la couverture glacielle et les échanges air-océan (e.g., Fig. 33 du chapitre 3). Parmi tous ces changements qui suivent l'indice AO, les résultats du chapitre 3 montrent que, aux échelles interannuelles à décennales, ce sont les changements dans les vents qui sont les plus susceptibles de déterminer la variabilité du stockage et de l'export des eaux douces de la baie

d'Hudson.

Sur de plus longues échelles temporelles, les dernières projections en rapport au réchauffement global (Bernstein et al., 2007) montrent une augmentation particulièrement marquée des températures de l'air au dessus de la baie d'Hudson (similaire à ce qui est prévu pour les mers situées au nord du Cercle arctique). Des processus de rétroaction (feedback) complexes entre l'atmosphère et l'océan sont susceptibles d'émerger à ces longues échelles temporelles, et la variabilité des vents peut dans ces conditions jouer un rôle secondaire dans le stockage et l'export des eaux douces. Comment le bilan des eaux douces des mers arctiques évoluera-t-il dans ces conditions ? Un des changements attendus est la réduction de la couverture glacielle sur ces mers. Un tel scénario fut examiné par Joly et al. (2010), qui ont effectué une expérience numérique avec un atmosphère plus chaud dans un modèle couplé océan–glace de mer de la baie d'Hudson. Par soucis de simplicité, leur expérience faisait usage de forçages de vents, rivières et précipitations qui étaient représentatifs des conditions actuelles (seule la température de l'air était modifiée). La simulation effectuée montre une couverture glacielle et une formation d'eaux denses fortement diminuées, et des salinités plus élevées au dessus du bassin (i.e. un contenu en eau douce moins élevé). Malheureusement, les processus sous-jacents à cette diminution du contenu en eau douce n'ont pas été explorés par ces auteurs.

On peut envisager qu'avec une couverture de glace plus mince, déformable et mobile, l'océan serait davantage sensible au forçage du vent, et moins sensible à la friction se produisant dans les régions où la glace est épaisse et immobile (voir le chapitre 1 de la thèse). Cela résulterait en une circulation océanique plus rapide, et selon des modèles simples, à une diminution du contenu en eau douce (tel que dans l'expérience de Joly et al., 2010). Par exemple, un modèle estuarien en boîte comprend un intrant d'eau salée (salinité S_{in} et débit Q_{in}), un apport des rivières (salinité $S = 0$ et débit Q_{riv}), et un export saumâtre de salinité S_{basin} et de débit $Q_{\text{in}} + Q_{\text{riv}}$. En régime stationnaire, la conservation du volume et du sel mènent à l'Eq. 4.1, qui montre comment une circulation plus rapide (Q_{in} plus élevé)

mène à un contenu en eau douce inférieur dans le bassin (S_{basin} supérieur). Il peut être vérifié que le modèle conceptuel décrit au chapitre 3 de cette thèse a une réponse qualitativement similaire en régime stationnaire (voir l'Appendice A). Toutefois, tel qu'il a été mentionné précédemment, il n'est pas clair à savoir si la physique de ces modèles idéalisés s'applique lorsque l'on considère des changements sur de longues échelles temporelles susceptibles de mener à des rétroactions complexes. Il est apparent que des recherches visant à éclaircir les conséquences du réchauffement global devraient prendre en compte les interactions potentiellement importantes entre les différentes composantes (air, mer, glace et terre) du climat.

Tel que noté dans l'Introduction Générale, la baie d'Hudson est aussi sujette à des développements hydroélectriques. La production d'électricité nécessite un débit d'eau relativement constant, qui est obtenu par la mise en place et l'usage d'un barrage et d'un réservoir. Cela se traduit par un cycle saisonnier altéré, soit un débit artificiellement élevé (faible) pendant les mois d'hiver (été). Le débit annuel moyen est supposé préservé. Comment ces développements hydroélectriques affectent-ils le bilan des eaux douces de la baie d'Hudson ? Malgré que ce sujet n'ait pas été spécifiquement examiné dans la thèse, les résultats suggèrent que l'harnachement de quelques rivières aurait un impact limité sur le contenu en eau douce à grande échelle et sur l'export, puisque ces variables dépendent du cumul du débit des rivières en amont (voir les Eqs. 5.33 et 5.32, respectivement) plutôt que du débit des rivières locales[3]. Cette intégration (ou ce cumul) tend à minimiser l'importance des rivières individuelles, ce qui signifie que l'harnachement de quelques rivières est peu probable de mener à des changements significatifs dans le bilan à grande échelle des eaux douces. Pour les mêmes raisons, le forçage hydrologique idéalisé utilisé au chapitre 3 (voir l'Appendice B de la thèse) ne devrait pas être considéré comme une limitation importante de l'étude ; au final, le contenu en eau douce à grande échelle et l'export dépendent davantage de la contribution intégrée/cumulée des rivières que de leur variabilité individuelle.

[3]Cette conclusion est évidemment dépendante de l'échelle spatiale considérée. Aux plus petites échelles spatiales, disons immédiatement à l'embouchure d'une certaine rivière, l'harnachement de cette-ci mènera bien sûr à un changement mesurable. Mais à des échelles spatiales plus grandes, soit au delà d'un rayon de déformation interne de Rossby, la salinité moyennée sur l'horizontale dépendra davantage du cumul du débits des rivières situées en amont que du débit de la rivière locale ; voir l'Eq. 5.33.

Le bilan des eaux douces de la baie d'Hudson pourrait être beaucoup plus sensible au réchauffement global qu'aux développement hydroélectriques, puisque le premier est susceptible d'agir sur l'ensemble du système. Des scénarios de changements climatiques montrent une modification générale de la saisonnalité des rivières, notamment un maximum plus précoce dû à une fonte des neiges plus précoce sur le continent. La discussion entourant les expériences de sensibilité du chapitre 3 (e.g., Fig. 31) suggère que la modification de la saisonnalité de l'ensemble des rivières aurait un effet important sur la salinité du bassin au fil des saisons. L'effet d'une telle modification sur l'export d'eau douce, toutefois, serait limité en comparaison de la modulation naturelle associée aux vents (Fig. 31).

Les simulations numériques du réchauffement global montrent aussi des précipitations accrues au dessus des régions arctiques (Plummer et al., 2006), ce qui est cohérent avec les débits de rivière accrus observés dans ces régions (Déry et al., 2009). L'augmentation des précipitations, du débit des rivières, et de l'évaporation, sont souvent associés collectivement au concept d'accélération du cycle hydrologique. Cette accélération pourrait être causée par, notamment, la réduction de la couverture glacielle et des échanges air–océan accrus. L'augmentation des précipitations et du débit des rivières tendent à augmenter le contenu en eau douce des mers arctiques, alors que l'augmentation de l'évaporation a un effet contraire. Il est difficile à ce stade de prédire laquelle de ces tendance s'observera dans la baie d'Hudson, car des processus de rétroaction complexes peuvent jouer un rôle important. Néanmoins, les résultats de la thèse montrent que le débit des rivières est de loin la principale source d'eau douce pendant l'année, et que des changements aux précipitations et à l'évaporation auraient un impact relativement faible sur le bilan des eaux douces (notamment parce que la superficie drainée par les rivières est beaucoup plus importante que celle de la baie elle même). Cela résulterait en un export d'eau douce accru afin de balancer l'augmentation du débit des rivières. On pourrait aussi s'attendre à ce que la salinité moyenne du bassin diminuerait en réponse à l'augmentation du débit des rivières, mais l'inverse pourrait tout aussi bien se produire si la circulation des eaux du bassin accélère en réponse à la décroissance de la couverture glacielle (Eq. 4.1). De ces considérations, il semble clair que des projections sur

des échelles multidécennales nécessiterait des recherches supplémentaires où les interactions complexes entre la terre, l'eau et l'atmosphère seraient prises en compte.

Un autre sujet exploré dans la thèse est l'export d'eau douce de la baie d'Hudson vers les mers subarctiques, qui pourrait jouer un rôle significatif dans la modulation de la convection profonde dans la mer du Labrador. La thèse a principalement porté sur les processus contrôlant l'export à l'embouchure de la baie d'Hudson, et le parcours subséquent des eaux douces n'a pas été abordé. Un examen approfondi et définitif du rôle joué par l'export des eaux douces de la baie d'Hudson exigerait une vue plus complète, incluant aussi bien les mers arctiques que subarctiques ; e.g. un modèle couvrant tous ces territoires. Un tel modèle devrait nécessairement inclure la baie d'Hudson car il a été vu dans la thèse que l'export de la baie dépend largement des processus océanographiques ayant lieu dans la baie (et non pas seulement la variabilité des sources d'eau douce, e.g. le débit des rivières). Le modèle devrait aussi être d'une résolution suffisante pour résoudre de façon explicite les échanges d'eau douce entre le courant du Labrador et les sites convectifs au large (Spall, 2004; Straneo, 2006), un fait qui est souvent négligé (Rennermalm et al., 2007).

La couverture glacielle joue aussi un rôle important dans la dynamique des mers arctiques. Elle peut agir telle une surface rugueuse qui amortit les courants océaniques, ou comme un isolant qui limite le transfert de momentum des vents à l'océan. De tels effets dynamiques de la couverture de glace ont été examinés dans les chapitres 1 et 2, mais des recherches plus poussées (e.g., celles de Steiner, 2001) sont nécessaires pour clairement circonscrire le rôle de la glace dans la variabilité saisonnière de la circulation océanique. Des observations de ces processus seraient particulièrement souhaitables, notamment des profils de l'écoulement sur une année complète et avec une résolution suffisante pour résoudre la couche limite à l'interface glace–océan. Des études portant sur le transfert de momentum des vents à la couverture glacielle de la baie d'Hudson seraient aussi très utiles, et heureusement, ce travail est déjà en cours (D. Barber, comm. pers.).

Certains résultats de la thèse sont particulièrement intéressants pour l'écologie des mers

arctiques en général et pour celle de la baie d'Hudson en particulier. Le rôle joué par les vents dans l'échange d'eau des rivières entre les côtes et le large (e.g., Macdonald et al., 1999) représente un de ces résultats novateurs. Ce processus contribue à une stabilité accrue des eaux situées au large (en apportant de la flottabilité dans la partie supérieure de la colonne d'eau), et il est aussi susceptible de contribuer à la dispersion des substances absorbant la lumière (voir Granskog et al., 2007) et des polluants. Le cheminement de ces substances est, toutefois, relativement complexe de par leurs interactions avec l'environnement biogéochimiques. Pour ce genre d'étude, des campagnes d'échantillonnage poussées et un modèle glace-océan-biogéochimie seraient probablement requis. Idéalement, le modèle devrait avoir une résolution fine à proximité des plumes des rivières et être couplé à un modèle régional couvrant l'ensemble de la baie. Ainsi, les processus à petites échelles et la dispersion à grande échelle (e.g., chapitre 2) seraient en bonne partie résolus.

Finalement , une approche qui semble prometteuse pour la compréhension des différences et des similitudes entre les différentes mers arctiques serait de décrire celles-ci par un ensemble de paramètres adimensionaux (e.g., Garvine, 1999). Ces paramètres sont formés par la combinaison des constantes décrivant la géométrie, l'hydrographie et le forçage de ces bassins, et les paramètres obtenus caractérisent la réponse physique de ces mers (voir Wåhlin and Johnson, 2009, par exemple). Une telle étude serait fort utile pour illustrer, par exemple, si un bassin est davantage influencé par la flottabilité des eaux des rivières ou par l'atmosphère (et pourquoi).

RÉFÉRENCES

Adcroft, A., Hill, C., Marshall, J., 1997. Representation of topography by shaved cells in a height coordinate ocean model. Mon. Weather Rev. 125, 2293–2315.

Backhaus, J. O., 1983. A semi-implicit scheme for the shallow water equations for application to shelf sea modelling. Cont. Shelf Res. 2, 243–254.

Backhaus, J. O., 1985. A three-dimensional model for the simulation of shelf sea dynamics. Dtsch. Hydrogr. Z. 38, 165–187.

Barber, D. G., Massom, R. A., 2007. The role of sea ice in Arctic and Antarctic Polynyas. In: Smith, W. O., Barber, D. G. (Eds.), Polynyas: Windows to the World. Vol. 74. Elsevier Oceanography Series, pp. 1–54.

Barber, F. G., 1965. Current observations in Fury and Hecla Strait. J. Fish. Res. Bd. Can. 22, 225–229.

Bernstein, L., Bosch, P., Canziani, O., Chen, Z., Christ, R., Davidson, O., Hare, W., Huq, S., Karoly, D., Kattsov, V., Kundzewicz, Z., Liu, J., Lohmann, U., Manning, M., Matsuno, T., Menne, B., Metz, B., Mirza, M., Nicholls, N., Nurse, L., Pachauri, R., Palutikof, J., Parry, M., Qin, D., Ravindranath, N., Reisinger, A., Ren, J., Riahi, K., Rosenzweig, C., Rusticucci, M., Schneider, S., Sokona, Y., Solomon, S., Stott, P., Stouffer, R., Sugiyama, T., Swart, R., Tirpak, D., Vogel, C., Yohe, G., 2007. Climate change 2007: Synthesis report. Tech. Rep. 4, Intergovernmental Panel on Climate Change.

Britannica, E., 1984. Arctic Ocean. In: The new Encyclopaedia Britannica, 15th Edition. Vol. 1. Encycl. Brit., Inc., pp. 1118–1121.

Chapman, D. C., Beardsley, R. C., 1989. On the origin of shelf water in the Middle Atlantic Bight. J. Phys. Oceanogr. 19, 384–391.

Côté, J., Gravel, S., Méthot, A., Patoine, A., Roch, M., Staniforth, A., 1998. The operational CMC/MRB Global Environmental Multiscale (GEM) model: Part I–Design considerations and formulation. Mon. Weather Rev. 126, 1373–1395.

Crabs, W. E., Portmann, F., de Couet, T., 2000. Discharge observation networks in Arctic regions: computation of the river runoff in the Arctic Ocean, its seasonality and variability. In: Lewis, E. L. (Ed.), The freshwater budget of the Arctic Ocean. Kluwer Academic Publishers, pp. 249–268.

Déry, S. J., Hernandez-Henriquez, M. A., Burford, J. E., Wood, E. F., 2009. Observational evidence of an intensifying hydrological cycle in northern canada. Geophys. Res. Lett. 36 (L13402), doi:10.1029/2009GL038852.

Déry, S. J., Stieglitz, M., McKenna, E. C., Wood, E. F., 2005. Characteristics and trends of river discharge into Hudson, James, and Ungava Bays, 1964–2000. J. Clim. 18, 2540–2557.

Déry, S. J., Wood, E. F., 2004. Teleconnection between the Arctic Oscillation and Hudson Bay river discharge. Geophys. Res. Lett. 31 (L18205), doi:10.1029/2004GL020729.

Dickson, R., Rudels, B., Dye, S., Karcher, M., Meincke, J., Yashayaev, I., 2007. Current estimates of freshwater flux through Arctic and subarctic seas. Prog. Oceanogr. 73, 210–230, doi:10.1016/j.pocean.2006.12.003.

Dickson, R. R., Meincke, J., Malmberg, S. A., Lee, J., 1988. The "Great Salinity Anomaly" in the northern North Atlantic 1968–1982. Prog. Oceanogr. 20, 103–151.

Dickson, R. R., Meincke, J., Rhines, P., 2008. Arctic-Subarctic ocean fluxes, 1st Edition. Springer Science.

Ekman, V. W., 1905. On the influence of the Earth's rotation on ocean-currents. Arkiv för Matematik, Astronomi och Fysik 2, 1–53.

Emery, W. J., Thomson, R. E., 1997. Data analysis methods in physical oceanography, 2nd Edition. Elsevier.

Foreman, M., 1978. Manual for tidal currents analysis and prediction. Tech. rep., Inst. Ocean Sci., Patricia Bay, Sidney, B.C. (Canada).

Freeman, N., Murty, T., 1976. Numerical modeling of tides in Hudson Bay. J. Fish. Res. Board Can. 33, 2345–2361.

Gachon, P., Laprise, R., Zwack, P., Saucier, F. J., 2003. The effects of interactions between surface forcings in the development of a model-simulated polar low in Hudson Bay. Tellus 55A, 61–87.

Garvine, R. W., 1999. Penetration of buoyant coastal discharge onto the continental shelf: A numerical model experiment. J. Phys. Oceanogr. 29, 1892–1909.

Gill, A., 1982. Atmosphere-ocean dynamics. Academic Press, London (UK).

Godin, G., 1986. Modification by an ice cover of the tide in James Bay and Hudson Bay. Arctic 39, 65–67.

Godin, G., Barber, F., 1980. Variability of the tide at some sites in the Canadian Arctic. Arctic 33, 30–37.

Granskog, M. A., Macdonald, R. W., Kuzyk, Z. A., Senneville, S., Mundy, C. J., Barber, D. G., Stern, G. A., Saucier, F. J., 2009. Coastal conduit in southwestern Hudson Bay (Canada) in summer: Rapid transit of freshwater and significant loss of colored dissolved organic matter. J. Geophys. Res. 114 (C08012), doi:10.1029/2009JC005270.

Granskog, M. A., Macdonald, R. W., Mundy, C. J., Barber, D. G., 2007. Distribution, characteristics and potential impacts of chromophoric dissolved organic matter (CDOM) in Hudson Strait and Hudson Bay, Canada. Cont. Shelf Res. 27, 2032–2050, doi:10.1016/j.csr.2007.05.001.

Hare, A., Stern, G. A., Macdonald, R. W., Kuzyk, Z., Wang, F., 2008. Contemporary and preindustrial mass budgets of mercury in the Hudson Bay Marine System: The role of sediment recycling. Sci. Total Environ. 406, 190–204.

Heil, P., Hutchings, J., Worby, A., Johansson, M., Launiainen, J., Haas, C., Hibler, III, W., 2008. Tidal forcing on sea-ice drift and deformation in the western Weddell Sea in early austral summer, 2004. Deep-Sea Res. II 55, 943–962.

Hibler, III, W. D., 1979. A dynamic thermodynamic sea ice model. J. Phys. Oceanogr. 9, 815–846.

Hochheim, K. P., Barber, D., 2010. Atmospheric forcing of sea ice in Hudson Bay during the fall period, 1980–2005. J. Geophys. Res. 115 (C05009), doi:10.1029/2009JC005334.

Holloway, G., Proshutinsky, A., 2007. Role of tides in Arctic Ocean/ice climate. J. Geophys. Res. 112 (C04S06), doi:10.1029/2006JC003643.

Huisman, S. E., Dijkstra, H. A., von der Heydt, A., de Ruijter, W. P. M., 2009. Robustness of multiple equilibria in the global ocean circulation. Geophys. Res. Lett. 36 (L01610), doi:10.1029/2008GL036322.

Hunke, E. C., Dukowicz, J. K., 1997. An elastic-viscous-plastic model for sea ice dynamics. J. Phys. Oceanogr. 27, 1849–1867.

IHO, 1953. Limits of Oceans and Seas. Tech. Rep. 23, International Hydrographic Organization.

Ingram, R., Prinsenberg, S., 1998. Coastal oceanography of Hudson Bay and surrounding eastern Canadian Arctic waters. In: Robinson, A., Brink, K. (Eds.), The Sea. Vol. 11. Chichester UK Wiley, pp. 835–861.

Jahn, A., Tremblay, B., Mysak, L. A., Newton, R., 2009. Effect of the large-scale atmospheric circulation on the variability of the Arctic Ocean freshwater export. Clim. Dyn.Doi:10.1007/s00382-009-0558-z.

Jahn, A., Tremblay, B., Newton, R., Holland, M. M., Mysak, L. A., Dmitrenko, I. A., 2010. A tracer study of the Arctic Ocean's liquid freshwater export variability. J. Geophys. Res.In press.

Johnson, W., Kowalik, Z., 1986. Modeling of storm surges in the Bering Sea and Norton Sound. J. Geophys. Res. 91, 5119–5128.

Joly, S., Senneville, S., Caya, D., Saucier, F. J., 2010. Sensitivity of Hudson Bay sea ice and ocean climate to atmospheric temperature forcing. Clim. Dyn.Doi:10.1007/s00382-009-0731-4.

Kagan, B., Romanenkov, D., Sofina, E., 2008. Tidal ice drift and ice-generated changes in the tidal dynamics/energetics on the Siberian continental shelf. Cont. Shelf Res. 28, 351–368.

Kalnay, E., Kanamitsu, M., Kistler, R., Collins, W., Deaven, D., Gandin, L., Iredell, M., Saha, S., White, G., Woollen, J., Zhu, Y., Leetmaa, A., Reynolds, R., Chelliah, M., Ebisuzaki, W., Higgins, W., Janowiak, J., Mo, K., Ropelewski, C., Wang, J., Jenne, R., Joseph, D., 1996. The NCEP/NCAR 40-year reanalysis project. Bull. Amer. Meteor. Soc. 77, 437–470.

Kwok, R., Rothrock, D. A., 2009. Decline in Arctic sea ice thickness from submarine and ICESat records: 1958–2008. Geophys. Res. Lett. 36 (L15501), doi:10.1029/2009GL039035.

Lammers, R. B., Shiklomanov, A. I., Vörösmarty, C. J., Fekete, B. M., Peterson, B. J., 2001. Assessment of contemporary Arctic river runoff based on observational discharge records. J. Geophys. Res. 106, 3321–3334.

Langleben, M., 1982. Water drag coefficient of first-year sea ice. J. Geophys. Res. 87, 573–578.

Lapoussière, A., Michel, C., Gosselin, M., Poulin, M., 2009. Spatial variability in organic material sinking export in the Hudson Bay system, Canada, during fall. Cont. Shelf Res. 29, 1276–1288.

Lazier, J. R., 1980. Oceanographic conditions at ocean weather ship Bravo, 1964–1974. Atmos.-Ocean 18, 227–238.

LeBlond, P. H., Lazier, J. R., Weaver, A. J., 1996. Can regulation of freshwater runoff in Hudson Bay affect the climate of the North Atlantic? Arctic 49, 348–355.

Lentz, S. J., 2004. The response of buoyant coastal plumes to upwelling-favorable winds. J. Phys. Oceanogr. 34, 2458–2469.

Levitus, S., Burgett, R., Boyer, T. P., 1994. World ocean atlas 1994. U.S. Department of Commerce, NOAA, NESDIS.

Li, Z., Chao, Y., McWilliams, J. C., 2006. Computation of the streamfunction and velocity potential for limited and irregular domains. Mon. Wea. Rev. 134, 3384–3394.

Lind, O. C., Oughton, D. H., Salbu, B., Skipperud, L., Sickel, M. A., Brown, J. E., Fifield, L. K., Tims, S. G., 2006. Transport of low $^{240}Pu/^{239}Pu$ atom ratio plutonium-species in the Ob and Yenisey Rivers to the Kara Sea. Earth and Planetary Science Letters 251, 33–43.

Macdonald, R. W., Carmack, E. C., McLaughlin, F. A., Falkner, K. K., Swift, J. H., 1999. Connections among ice, runoff and atmospheric forcing in the Beaufort Gyre. Geophys. Res. Lett. 26, 2223–2226.

Madsen, O., Bruno, M., 1986. A methodology for the determination of drag coefficients for ice floes. In: Proceedings of the Fifth international offshore mechanics and Arctic engineering symposium. Vol. 4. Am. Soc. Mech. Eng., pp. 410–417.

Mailman, M., Stepnuk, L., Cicek, N., Bodaly, R. A., 2006. Strategies to lower methyl mercury concentrations in hydroelectric reservoirs and lakes: A review. Science of the Total Environment 368, 224–235.

Markham, W., 1986. The ice cover. In: Martini, I. (Ed.), Canadian Inland Seas. Elsevier oceanogr. series, pp. 101–116.

Marshall, J., Schott, F., 1999. Open-ocean convection: Observations, theory, and models. Rev. Geophys. 37, 1–64.

Martin, P. J., 1985. Simulation of the mixed layer at OWS November and Papa with several models. J. Geophys. Res. 90, 903–916.

Martin, S., Polyakov, I., Markus, T., Drucker, R., 2004. Okhotsk Sea Kashevarov Bank polynya: Its dependence on diurnal and fortnightly tides and its initial formation. J. Geophys. Res. 109 (C09S04), doi:10.1029/2003JC002215.

Martinson, D. G., Wamser, C., 1990. Ice drift and momentum exchange in winter Antarctic pack ice. J. Geophys. Res. 95, 1741–1755.

Matsumoto, K., Takanezawa, T., Ooe, M., 2000. Ocean tide models developed by assimilating Topex/Poseidon altimeter data into a hydrodynamical model: A global model and a regional model around Japan. J. Oceanogr. 56, 567–581.

Maxwell, J. B., 1986. A climate overview of the Canadian inland seas. In: Martini, I. (Ed.), Canadian Inland Seas. Elsevier oceanogr. series, pp. 79–99.

McPhee, M. G., Proshutinsky, A., Morison, J. H., Steele, M., Alkire, M. B., 2009. Rapid change in the freshwater content of the Arctic Ocean. Geophys. Res. Lett. 36 (L10602), doi:10.1029/2009GL037525.

Melling, H., Agnew, T. A., Falkner, K. K., Greenberg, D. A., Lee, C. M., Münchow, A., Petrie, B., Prinsenberg, S. J., Samelson, R. M., Woodgate, R. A., 2008. Fresh-water fluxes via Pacific and Arctic outflow across the Canadian Polar Shelf. In: Dickson, R., Meincke, J., Rhines, P. (Eds.), Arctic-Subarctic ocean fluxes. Springer Science, pp. 193–247.

Mellor, G. L., Kantha, L., 1989. An ice-ocean coupled model. J. Geophys. Res. 94, 10937–10954.

Mesinger, F., DiMego, G., Kalnay, E., Mitchell, K., Shafran, P. C., Ebisuzaki, W., Jovic, D., Woollen, J., Rogers, E., Berbery, E. H., Ek, M. B., Fan, Y., Grumbine, R., Higgins, W., Li, H., Lin, Y., Manikin, G., Parrish, D., Shi, W., 2006. North American Regional Reanalysis: A long-term, consistent, high-resolution climate dataset for the North American domain, as a major improvement upon the earlier global reanalysis datasets in both resolution and accuracy. Bull. Amer. Meteor. Soc. 87, 343–360.

Mofjeld, H., 1986. Observed tides on the Northeastern Bering Sea Shelf. J. Geophys. Res. 91, 2593–2606.

Müller, P., 2006. The Equations of Oceanic Motions, 1st Edition. Cambridge University Press.

Murty, T., 1985. Modifications of hydrographic characteristics, tides, and normal modes by ice cover. Mar. Geod. 9, 451–468.

Myers, R. A., Akenhead, S. A., Drinkwater, K., 1990. The influence of Hudson Bay runoff and ice-melt on the salinity of the inner Newfoundland Shelf. Atmos.-Ocean 28, 241–256.

Newton, R., Tremblay, B., Cane, M. A., Schlosser, P., 2006. A simple model of the Arctic Ocean response to annular atmospheric modes. J. Geophys. Res. 111 (C09019), doi:10.1029/2004JC002622.

NOAA, 2006. 2-minute gridded global relief data (Etopo2v2). Tech. rep., U.S. Department of Commerce, National Geophysical Data Center.

Pawlowicz, R., Beardsley, B., Lentz, S., 2002. Classical tidal harmonic analysis including error estimates in Matlab using T-Tide. Comput. Geosci. 28, 929–937.

Pease, C., Salo, S., Overland, J., 1983. Drag measurements for first-year sea ice over a shallow sea. J. Geophys. Res. 88, 2053–2862.

Pedlosky, J., 1996. Ocean Circulation Theory, 1st Edition. Springer-Verlag.

Peterson, B. J., McClelland, J., Curry, R., Holmes, R. M., Walsh, J. E., Aagaard, K., 2006. Trajectory shifts in the Arctic and Subarctic freshwater cycle. Science 313, 1061–1066.

Plummer, D., Caya, D., Frigon, A., Côté, H., Giguère, M., Paquin, D., Biner, S., Harvey, R., De Elia, R., 2006. Climate and climate change over North America as simulated by the canadian RCM. J. Clim. 19, 3112–3132.

Polyakov, I., Martin, S., 2000. Interaction of the Okhotsk Sea diurnal tides with the Kashevarov Bank polynya. J. Geophys. Res. 105, 3281–3294.

Prinsenberg, S., 1987. Seasonal current variations observed in western Hudson Bay. J. Geophys. Res. 92, 10756–10766.

Prinsenberg, S., 1988a. Damping and phase advance of the tide in western Hudson Bay by the annual ice cover. J. Phys. Oceanogr. 18, 1744–1751.

Prinsenberg, S., Hamilton, J., March 2005. Monitoring the volume, freshwater and heat fluxes passing through Lancaster Sound in the Canadian Arctic Archipelago. Atmos.-Ocean 43, 1–22.

Prinsenberg, S. J., 1980. Man-made changes in the freshwater input rates of Hudson and James bays. Can. J. Fish. Aquat. Sci. 37, 1101–1110.

Prinsenberg, S. J., 1984. Freshwater contents and heat budgets of James Bay and Hudson Bay. Cont. Shelf Res. 3, 191–200.

Prinsenberg, S. J., 1986a. The circulation pattern and current structure of Hudson Bay. In: Martini, I. (Ed.), Canadian Inland Seas. Elsevier oceanogr. series, pp. 187–203.

Prinsenberg, S. J., 1986b. Salinity and temperature distributions of Hudson Bay and James Bay. In: Martini, I. (Ed.), Canadian Inland Seas. Elsevier oceanogr. series, pp. 163–186.

Prinsenberg, S. J., 1988b. Ice-cover and ice-ridge contributions to the freshwater contents of Hudson Bay and Foxe Basin. Arctic 41, 6–11.

Prinsenberg, S. J., Loucks, R. H., Smith, R. E., Trites, R. W., 1987. Hudson Bay and Ungava Bay runoff cycles for the period 1963 to 1983. Tech. Rep. 92, Fisheries and Oceans Canada.

Proshutinsky, A., Bourke, R. H., McLaughlin, F. A., 2002. The role of the Beaufort Gyre in Arctic climate variability: Seasonal to decadal climate scales. Geophys. Res. Lett. 29 (23), 1–4, doi:10.1029/2002GL015847.

Proshutinsky, A., Krishfield, R., Timmermans, M.-L., Toole, J., Carmack, E., McLaughlin, F., Williams, W. J., Zimmermann, S., Itoh, M., Shimada, K., 2009. Beaufort Gyre freshwater reservoir: State and variability from observations. J. Geophys. Res. 114 (C00A10), doi:10.1029/2008JC005104.

Pugh, D., 1987. Tides, surges and mean sea-level. J. Wiley Chichester.

Rahmstorf, S., Crucifix, M., Ganopolski, A., Goosse, H., Kamenkovich, I., Knutti, R., Lohmann, G., Marsh, R., Mysak, L. A., Wang, Z., Weaver, A. J., 2005. Thermohaline circulation hysteresis: A model intercomparison. Geophys. Res. Lett. 32 (L23605), doi:10.1029/2005GL023655.

Rennermalm, A. K., Wood, E. F., Weaver, A. J., Eby, M., Déry, S. J., 2007. Relative sensitivity of the Atlantic meridional overturning circulation to river discharge into Hudson Bay and the Arctic Ocean. J. Geophys. Res. 112 (G04S48), doi:10.1029/2006JG000330.

Rothrock, D. A., Kwok, R., Groves, D., 2000. Satellite views of the Arctic Ocean freshwater balance. In: Lewis, E. L. (Ed.), The freshwater budget of the Arctic Ocean. Kluwer Academic Publishers, pp. 409–452.

Sadler, H. E., 1982. Water flow into Foxe Basin through Fury and Hecla Strait. Nat. Can. 109, 701–707.

Saucier, F., Larouche, P., D'Astous, A., Dionne, J., 1994. Moored physical oceanographic data from northeastern Hudson Bay between August 1992 and September 1993. Canadian data report of hydrography and ocean sciences 132, Fisheries and Oceans Canada, Maurice-Lamontagne Institute.

Saucier, F. J., Senneville, S., Prinsenberg, S. J., Roy, F., Smith, G., Gachon, P., Caya, D., Laprise, R., 2004a. Modelling the sea ice-ocean seasonal cycle in Hudson Bay, Foxe Basin and Hudson Strait, Canada. Clim. Dyn. 23, 303–326, doi:10.1007/s00382-004-0445-6.

Saucier, F. J., Starr, M., Harvey, M., Therriault, J. C., 2004b. Expédition MERICA 2003: Suivi et étude du climat et de la productivité de la baie d'Hudson. Nat. Can. 128, 108–110.

Semtner, A. J., 1976. A model for the thermodynamic growth of sea ice in numerical investigations of climate. J. Phys. Oceanogr. 6, 379–389.

Shiklomanov, I., Shiklomanov, A., Lammers, R., Peterson, B., Vorosmarty, C., 2000. The dynamics of river water inflow to the Arctic Ocean. In: et al., E. L. (Ed.), The freshwater budget of the Arctic Ocean. Vol. 7. Kluwer Acad., pp. 281–296.

Sibert, V., Zakardjian, B., Le Clainche, Y., Gosselin, M., Starr, M., Senneville, S., 2010. Spatial and temporal variability of primary production over the Hudson Bay, Foxe Basin and Hudson Strait marine system via coupled bio-physical models. J. Mar. Syst. xxx, xxx, under review.

Spall, M. A., 2004. Boundary currents and watermass transformation in marginal seas. J. Phys. Oceanogr. 34, 1197–1213.

St-Laurent, P., 2010. Seasonal and interannual variability of freshwaters in Arctic seas: The case of Hudson Bay. Ph.D. thesis, Université du Québec à Rimouski, Québec, Canada, available at http://pages.globetrotter.net/pierrestlau/thesis.pdf.

St-Laurent, P., Straneo, F., Dumais, J.-F., Barber, D. G., 2010. What is the fate of the river waters of Hudson Bay? J. Mar. Syst. xxx, xxx, under review.

Steele, M., Morley, R., Ermold, W., 2001. PHC: A global ocean hydrography with a high quality Arctic Ocean. J. Clim. 14, 2079–2087.

Steele, M., Zhang, J., Rothrock, D., Stern, H., 1997. The force balance of sea ice in a numerical model of the Arctic Ocean. J. Geophys. Res. 102, 21061–21079.

Steiner, N., 2001. Introduction of variable drag coefficients into sea-ice models. Ann. Glaciol. 33, 181–186.

Stern, M. E., 1975. Ocean Circulation Physics, 1st Edition. Academic Press.

Stouffer, R. J., Yin, J., Gregory, J. M., Dixon, K. W., Spelman, M. J., Hurlin, W., Weaver, A. J., Eby, M., Flato, G. M., Hasumi, H., Hu, A., Jungclaus, J. H., Kamenkovich, I. V., Levermann, A., Montoya, M., Murakami, S., Nawrath, S., Oka, A., Peltier, W. R., Robitaille, D. Y., Sokolov, A., Vettoretti, G., Weber, S. L., 2006. Investigating the causes of the response of the thermohaline circulation to past and future climate changes. J. Clim. 19, 1365–1387.

Straneo, F., 2006. On the connection between dense water formation, overturning, and poleward heat transport in a convective basin. J. Phys. Oceanogr. 36, 1822–1840.

Straneo, F., 2010. Interannual variations in the freshwater and heat transport from Hudson Bay 2004–2007. J. Mar. Syst. xxx, xxx, under review.

Straneo, F., Saucier, F. J., 2008a. The Arctic-subarctic exchange through Hudson Strait. In: Dickson, R., Meincke, J., Rhines, P. (Eds.), Arctic-Subarctic ocean fluxes. Springer Science, pp. 249–261.

Straneo, F., Saucier, F. J., 2008b. The outflow from Hudson Strait and its contribution to the Labrador Current. Deep Sea-Res. I 55, 926–946, doi:10.1016/j.dsr.2008.03.012.

Straneo, F., Sutherland, D. A., St-Laurent, P., Déry, S. J., 2010. Variability of the fresh water export from Hudson Bay: What are the controls? Eos trans. AGU 91(26), Ocean Sci. Meet. Suppl., Abstract PO34C-07.

Sutherland, D., Straneo, F., Lentz, S. J., St-Laurent, P., 2010. Observations of fresh, anticyclonic eddies in the Hudson Strait outflow. J. Mar. Syst. xxx, xxx, under review.

Sverdrup, H., 1927. Dynamics of tides on the North Siberian Shelf. Geofys. Publ. 4, 75.

Tucker, III, W., Perovich, D., 1992. Stress measurements in drifting pack ice. Cold Regions Science and Technology 20, 119–139.

Wåhlin, A. K., Johnson, H. L., 2009. The salinity, heat, and buoyancy budgets of a coastal current in a marginal sea. J. Phys. Oceanogr. 39, 2562–2580, doi:10.1175/2009JPO4090.1.

Yamamoto-Kawai, M., McLaughlin, F. A., Carmack, E. C., Nishino, S., Shimada, K., 2008. Freshwater budget of the Canada Basin, Arctic Ocean, from salinity, $\delta^{18}O$, and nutrients. J. Geophys. Res. 113 (C01007), doi:10.1029/2006JC003858.

Zedler, S. E., Niiler, P. P., Stammer, D., Terrill, E., Morzel, J., 2009. Ocean's response to Hurricane Frances and its implications for drag coefficient parameterization at high wind speeds. J. Geophys. Res. 114 (C04016), doi:10.1029/2008JC005205.

Zubov, N., 1943. Arctic ice. Izdatel'stvo Glavsermorputi, Moscow, trans. U.S. Navy Electronics Laboratory (1963).

APPENDICE A

EXPANDED DESCRIPTION OF THE CONCEPTUAL MODEL

This appendix provides a detailed description of the conceptual model used in the third article of the thesis. The first three sections (*Dynamics*, *Volume Conservation*, and *Buoyancy Conservation*) describe the assumptions and equations of the model. Then, the procedure used to solve the equations is presented. Finally, the section *Explicit Equations for the Storage, Export, and Spatial Distribution of Freshwater* provides explicit solutions obtained from linearization of the equations or other approximations.

Dynamics

Arctic seas are conceptualized as semi-enclosed, semi-circular basins with horizontal scales sufficiently large for rotational effects to be important, yet small enough for the use of a constant rotation rate (the f-plane approximation). We assume that at these scales the Rossby numbers and horizontal Ekman number are all small, leading to a depth-integrated momentum equation of the form (e.g., Müller, 2006, Chap. 13):

$$\int_{-H}^{\eta} \rho_0 f \mathbf{e}_3 \times \mathbf{v}_\mathrm{h}\, \mathrm{d}z = -\int_{-H}^{\eta} \nabla_\mathrm{h} p\, \mathrm{d}z + \int_{-H}^{\eta} \frac{\partial \boldsymbol{\tau}}{\partial z}\, \mathrm{d}z, \qquad \mathbf{M} = \int_{-H}^{\eta} \mathbf{v}_\mathrm{h}\, \mathrm{d}z,$$

$$\rho_0 f \mathbf{e}_3 \times \mathbf{M} = -\nabla_\mathrm{h} \int_{-H}^{\eta} p\, \mathrm{d}z + \underbrace{p(z=\eta)}_{0} \nabla_\mathrm{h}\eta + p(z=-H) \underbrace{\nabla_\mathrm{h} H}_{0} + \boldsymbol{\tau}_\mathrm{w} - \boldsymbol{\tau}_\mathrm{b}, \quad (5.1)$$

where ρ_0 is a reference density under the Boussinesq approximation, f the Coriolis parameter, $\mathbf{e}_3$ the unit vector pointing upward, $\mathbf{M}$ the horizontal (h) velocity integrated over the water column, p the hydrostatic pressure, η the sea surface deviation from geoid, and τ_w, τ_b the stress at the surface (winds) and bottom, respectively. For simplicity we assume a flat bottom ($\nabla_h H = 0$) and neglect deviations from a standard atmospheric pressure ($p(z = \eta) = 0$ everywhere).

The presence of rotation and buoyancy inputs leads to two distinct regions within the sea, a buoyant boundary current in the nearshore region (of fixed width L), and a denser interior region (of radius R, see Fig. 22). Stratification is represented in the model with two layers of density ρ_1 and ρ_2, the depth of the interface being allowed to vary in time and in space. The upper layer has a thickness $h_1(\theta, t)$ in the boundary region, and a thickness $(H - D)(t)$ in the interior region. The thickness of the lower layers is noted $h_2(\theta, t)$ in the boundary, and $D(t)$ in the interior region. From now on we also assume a rigid lid at the surface so that $h_1 + h_2 = H$ and $w(z = -H) = w(z = 0) = 0$.

The volume of water entering the boundary region upstream, $L\mathbf{M}(\theta = 0, R < r < R + L, t)$, is prescribed in the following way. First we assume the bottom stress to be a linearized friction in $\mathbf{M}$ with a constant spin-down timescale ϵ, so that $\tau_b \equiv \rho_0 \epsilon \mathbf{M}$. Applying the curl operator over Eq. 5.1 then yields (assuming constant f value and $\nabla_h \cdot \mathbf{M} = 0$ because of the rigid lid; also note that the curl of a gradient vanishes) :

$$\nabla \times \tau_w = \nabla \times \tau_b = \rho_0 \epsilon \nabla \times \mathbf{M}. \tag{5.2}$$

With our previous assumption of a strong along-shore flow in a semi-circular basin, the previous equation is spatially averaged to obtain the relation linking $\mathbf{M}$ to the domain-averaged

curl of the wind stress :

$$\begin{aligned}
\frac{1}{A}\int_0^R\int_0^\Theta \nabla\times\tau_w r\,d\theta\,dr &= \frac{\rho_0\epsilon}{A}\int_0^R\int_0^\Theta \nabla\times\mathbf{M}\,r\,d\theta\,dr,\\
\overline{\nabla\times\tau_w} &= \frac{\rho_0\epsilon}{A}\int_0^R\int_0^\Theta \frac{\mathbf{e}_3}{r}\left(\frac{\partial}{\partial r}rM_\theta-\frac{\partial M_r}{\partial\theta}\right)r\,d\theta\,dr,\\
&\approx \mathbf{e}_3\frac{\rho_0\epsilon\Theta R}{A}M_\theta\approx\mathbf{e}_3\frac{2\rho_0\epsilon}{R}M_\theta,
\end{aligned}$$

$$\boxed{\mathbf{M}(\theta=0,t)=R\mathbf{e}_3\cdot\frac{\overline{\nabla\times\tau_w}}{2\rho_0\epsilon}\mathbf{e}_\theta,} \tag{5.3}$$

where the overbar represents a spatial average and $\mathbf{e}_\theta$ is the azimuth unit vector. The Eq. 5.3 predicts a linear relationship between the wind stress curl and the transport $\mathbf{M}$, and such relation is supported by observations (Fig. 34).

The bottom stress coefficient ϵ is obtained through linearization of the usual quadratic formulation ($<\,.\,>$ denotes averaging in time, and $C_D\sim10^{-3}$):

$$\begin{aligned}
\|\tau_b\|=\rho_0C_D\frac{M_\theta^2}{H^2} &\approx \rho_0C_D\frac{\langle M_\theta\rangle}{H}\frac{M_\theta}{H}=\rho_0C_D\frac{R\mathbf{e}_3\cdot\left\langle\overline{\nabla\times\tau_w}\right\rangle}{2\rho_0\epsilon H}\frac{M_\theta}{H}=\rho_0\epsilon M_\theta,\\
\epsilon &= \sqrt{\frac{RC_D\mathbf{e}_3\cdot\left\langle\overline{\nabla\times\tau_w}\right\rangle}{2\rho_0H^2}}.
\end{aligned} \tag{5.4}$$

Equations 5.1, 5.2, and 5.3 together suggest a geostrophic balance for the along-shore component of the flow, and suggest that the surface and bottom Ekman transports act in the cross-shore direction to cancel each other (e.g., Newton et al., 2006, also note that the along-shore pressure gradient is assumed to be small). This leads to the thermal wind relation for

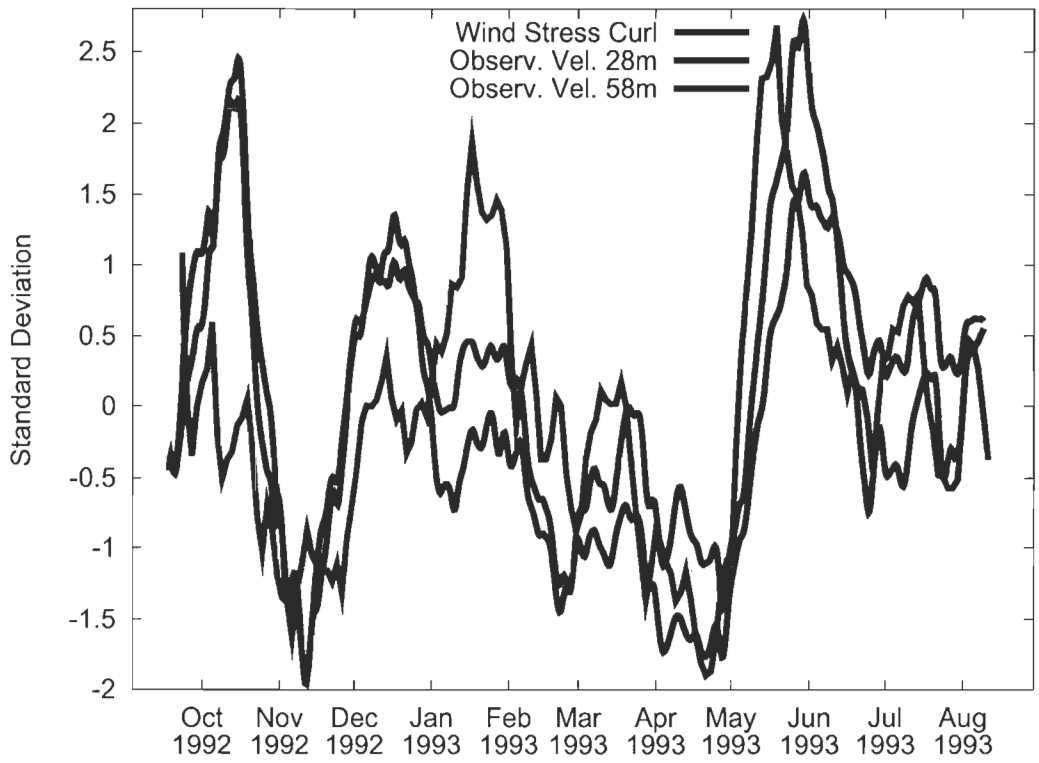

Figure 34: Comparison between the domain-averaged wind stress curl from Mesinger et al. (2006) and the observed along-shore velocity at two different depths at station B (see Fig. 24). All curves are detrended and divided by their standard deviation. Note that the wind stress curl and velocities show similar fluctuations at monthly timescales.

the along-shore component of the flow in the boundary region :

$$\begin{aligned} \frac{\partial v}{\partial z} &= -\frac{g}{f\rho_0}\frac{\partial \rho}{\partial r} \\ &= \frac{g}{f\rho_0}\frac{\partial Z_\rho}{\partial r}\frac{\partial \rho}{\partial z}, \end{aligned} \tag{5.5}$$

where $v(\theta, r, z, t)$ is the along-shore velocity, and Z_ρ is the vertical position of the isopycnal ρ. From Fig. 22,

$$\left[\frac{\partial Z_\rho}{\partial r}\right]_{r=R+L/2} = \begin{cases} 2\,(h_2 - D)\,/L & \text{if } z = h_1, \\ 0 & \text{otherwise,} \end{cases} \tag{5.6}$$

$$\begin{aligned} \int_{h_1^-}^{h_1^+} \frac{\partial v}{\partial z}\,\mathrm{d}z &= \frac{g}{f\rho_0}\frac{2}{L}(h_2 - D)\int_{h_1^-}^{h_1^+} \frac{\partial \rho}{\partial z}\,\mathrm{d}z, \\ V_1 - V_2 &= \frac{g}{f\rho_0}\frac{2}{L}(H - h_1 - D)(\rho_1 - \rho_2), \end{aligned} \tag{5.7}$$

$$\boxed{V_1 - V_2 = \frac{2g'}{fL}(D - H + h_1)} \tag{5.8}$$

where g' is the reduced gravity, and $(V_1, V_2)(\theta, t)$ the laterally- and layer-averaged velocities of the two layers forming the boundary current.

The stress τ contributes to surface ('s') and bottom ('b') Ekman transports in the cross-shore (radial) direction :

$$\mathbf{M}_\mathrm{s} = -\frac{\mathbf{e}_3}{f\rho_0} \times \tau_\mathrm{w}, \qquad \mathbf{M}_\mathrm{b} = \frac{\mathbf{e}_3}{f\rho_0} \times \tau_\mathrm{b}. \tag{5.9}$$

These Ekman transports are assumed to balance each other so that divergence in the upper layer is compensated by convergence in the lower layer :

$$\nabla \cdot \mathbf{M}_\mathrm{s} = \mathbf{e}_3 \cdot \frac{\nabla \times \tau_\mathrm{w}}{f\rho_0} = -\nabla \cdot \mathbf{M}_\mathrm{b}, \tag{5.10}$$

where we made use of Eq. 5.2.

Volume Conservation

We assume oceanic flows to be incompressible :

$$\boldsymbol{\nabla} \cdot \mathbf{v} = 0, \tag{5.11}$$

which leads to conservation of volume through the divergence theorem :

$$\iiint_V \boldsymbol{\nabla} \cdot \mathbf{v} \, \mathrm{d}V = \iint_S \mathbf{v} \cdot \mathrm{d}\mathbf{S} = 0. \tag{5.12}$$

Eq. 5.12 is separately applied to the interior and boundary regions. For a small slice $\delta\theta$ of the interior region, we get :

$$\int_0^R [w(z=0) - w(z=-H)] \, \mathrm{d}r \, \delta\theta = -\left[\int_{-H}^0 u \, \mathrm{d}z \, \delta\theta\right]_{r=R} - \int_0^R \int_{-H}^0 \frac{1}{r}\frac{\partial v}{\partial \theta} \, \mathrm{d}z \, \mathrm{d}r \, \delta\theta \tag{5.13}$$

where the left hand side is null given the flat bottom and rigid lid. We assume that $\partial v/\partial\theta \approx 0$, and that the interior region only exchanges volumes of water with the boundary region through Ekman transport in the surface and bottom Ekman layers. These two Ekman transports compensate each other (Eq. 5.10) so that the volume of the interior is constant over time :

$$\left[\int_{-H}^0 u \, \mathrm{d}z \, \delta\theta\right]_{r=R} = (\mathbf{M}_\mathrm{s} + \mathbf{M}_\mathrm{b}) \, \delta\theta = 0. \tag{5.14}$$

We now express volume conservation for a small slice $\delta\theta$ of the boundary region :

$$\int_R^{R+L} [w(z=0) - w(z=-H)]\, \mathrm{d}r\, \delta\theta = \left[\int_{-H}^{0} u\, \mathrm{d}z\, \delta\theta\right]_{r=R} - \left[\int_{-H}^{0} u\, \mathrm{d}z\, \delta\theta\right]_{r=R+L} - \int_{-H}^{0}\int_{R}^{R+L} \frac{1}{r}\frac{\partial v}{\partial \theta}\, \mathrm{d}r\, \mathrm{d}z\, \delta\theta \tag{5.15}$$

At $r = R + L$ there are rivers causing an across-shore transport :

$$\left[\int_{-H}^{0} u\, \mathrm{d}z\, \delta\theta\right]_{r=R+L} \equiv u_{\mathrm{riv}} h_{\mathrm{riv}} \delta\theta, \tag{5.16}$$

where $u_{\mathrm{riv}}(\theta, t) \leq 0$ since u is positive shoreward, and h_{riv} is the typical depth of a river (a constant). Thus for the boundary region we have :

$$u_{\mathrm{riv}} h_{\mathrm{riv}} \delta\theta = -\int_{-H}^{0}\int_{R}^{R+L} \frac{1}{r}\frac{\partial v}{\partial \theta}\, \mathrm{d}r\, \mathrm{d}z\, \delta\theta = -\frac{\partial}{\partial \theta}\int_{-H}^{0}\int_{R}^{R+L} \frac{v}{r}\, \mathrm{d}r\, \mathrm{d}z\, \delta\theta \tag{5.17}$$

Given reasonable values for R and L we have the following approximation (the so-called small gap approximation, Stern 1975, p. 71) :

$$-\frac{\partial}{\partial \theta}\int_{-H}^{0}\int_{R}^{R+L} \frac{v}{r}\, \mathrm{d}r\, \mathrm{d}z\, \delta\theta \approx -\frac{\partial}{\partial \theta}\int_{-H}^{0} \frac{VL}{R}\, \mathrm{d}z\, \delta\theta \tag{5.18}$$

where the uppercase velocity V represents the laterally-averaged (across the width L of the boundary region) velocity. We finally get :

$$\boxed{u_{\mathrm{riv}} h_{\mathrm{riv}} = -\frac{L}{R}\frac{\partial}{\partial \theta}(V_1 h_1 + V_2 h_2)} \tag{5.19}$$

Buoyancy Conservation

We define an equation for buoyancy conservation :

$$\frac{\partial b}{\partial t} = -\boldsymbol{\nabla} \cdot b\mathbf{v} + \boldsymbol{\nabla} \cdot \mathbf{F} \tag{5.20}$$

where b is buoyancy and $\mathbf{F}$ are eddy fluxes. This equation is obtained by replacing ρ by $\rho_2 - b$ in the continuity equation (e.g., Müller, 2006, Chap. 3), and by assuming an incompressible flow (Eq. 5.11). Applying Eq. 5.20 in its integral form to the interior region, we obtain :

$$\begin{aligned} A \int_{-H}^{0} \frac{\partial b}{\partial t} \,\mathrm{d}z &= -\int_0^R \int_0^{\Theta} \int_{-H}^{0} r\boldsymbol{\nabla} \cdot b\mathbf{v} \,\mathrm{d}z \,\mathrm{d}\theta \,\mathrm{d}r - Abw(z=0) \\ &\quad + Abw(z=-H) + AF_3(z=0) - AF_3(z=-H) \end{aligned} \tag{5.21}$$

$$Ab_1 \frac{\mathrm{d}}{\mathrm{d}t}(H-D) = -b_1 \int_0^R \int_0^{\Theta} r\boldsymbol{\nabla} \cdot \mathbf{M}_\mathrm{s} \,\mathrm{d}\theta \,\mathrm{d}r + Ab_0(P+M) \tag{5.22}$$

$$\frac{\mathrm{d}D}{\mathrm{d}t} = \frac{1}{A} \int_0^R \int_0^{\Theta} r\boldsymbol{\nabla} \cdot \mathbf{M}_\mathrm{s} \,\mathrm{d}\theta \,\mathrm{d}r - \frac{b_0}{b_1}(P+M) \tag{5.23}$$

where $b_0 = \rho_2 - \rho_0$, $b_1 = \rho_2 - \rho_1$, and $\rho_0 = 1000\,\mathrm{kg\,m^{-3}}$ is the density of rain, river waters, and ice melt water. Net precipitation $P(t)$ and net ice melt (ice melt minus ice grow, $M(t)$) act as diffusive fluxes of buoyancy, and they do not modify the volume of the basin. Lateral eddy fluxes are assumed negligible compared to their advective counterpart caused by Ekman pumping. Using Eq. 5.10, this can be rewritten in term of the domain-averaged curl of the wind stress :

$$\boxed{\frac{\mathrm{d}D}{\mathrm{d}t} = \mathbf{e}_3 \cdot \frac{\overline{\boldsymbol{\nabla} \times \boldsymbol{\tau}_\mathrm{w}}}{f\rho_0} - \frac{b_0}{b_1}(P+M)} \tag{5.24}$$

Now applying buoyancy conservation to a slice of the boundary region, we get :

$$\begin{aligned}\int_{-H}^{0}\int_{R}^{R+L}\frac{\partial b}{\partial t}\,\mathrm{d}r\,\mathrm{d}z\,\delta\theta \;=\; &-\int_{R}^{R+L} w\,(z=0)\,b\,\mathrm{d}r\,\delta\theta+\int_{R}^{R+L} w\,(z=-H)\,b\,\mathrm{d}r\,\delta\theta\\ &+\int_{R}^{R+L} F_3\,(z=0)\;\mathrm{d}r\,\delta\theta-\int_{R}^{R+L} F_3\,(z=-H)\;\mathrm{d}r\,\delta\theta\\ &+\left[\int_{-H}^{0} ub\,\mathrm{d}z\,\delta\theta\right]_{r=R}-\left[\int_{-H}^{0} ub\,\mathrm{d}z\,\delta\theta\right]_{r=R+L}\\ &-\int_{-H}^{0}\int_{R}^{R+L}\frac{1}{r}\frac{\partial vb}{\partial\theta}\,\mathrm{d}r\,\mathrm{d}z\,\delta\theta \end{aligned} \tag{5.25}$$

$$\frac{\partial h_1}{\partial t}=(P+M)\frac{b_0}{b_1}+\frac{\mathbf{M}_s\cdot\mathbf{e}_r}{L}-u_{\mathrm{riv}}\frac{b_0}{b_1}\frac{h_{\mathrm{riv}}}{L}-\frac{1}{R}\frac{\partial}{\partial\theta}V_1h_1 \tag{5.26}$$

which can be simplified by using Eq. 5.10, the divergence theorem, and assuming $\partial\mathbf{M}_s/\partial\theta$ to be small :

$$\mathbf{e}_3\cdot\frac{\overline{\nabla\times\tau_w}}{f\rho_0}=\frac{1}{A}\int_0^R\int_0^\Theta\nabla\cdot\mathbf{M}_s\,r\,\mathrm{d}\theta\,\mathrm{d}r=\frac{1}{A}\int_0^\Theta\mathbf{M}_s\cdot\mathbf{e}_r\,R\,\mathrm{d}\theta\approx\frac{R\Theta}{A}\mathbf{M}_s\cdot\mathbf{e}_r \tag{5.27}$$

so that we obtain :

$$\boxed{\frac{\partial h_1}{\partial t}=(P+M)\frac{b_0}{b_1}+\mathbf{e}_3\cdot\frac{A\overline{\nabla\times\tau_w}}{f\rho_0R\Theta L}-u_{\mathrm{riv}}\frac{b_0}{b_1}\frac{h_{\mathrm{riv}}}{L}-\frac{1}{R}\frac{\partial}{\partial\theta}V_1h_1} \tag{5.28}$$

In summary, these four equations together form the conceptual model:

$$V_1 - V_2 = \frac{2g'}{fL}(D - H + h_1) \tag{5.8}$$

$$u_{\text{riv}} h_{\text{riv}} = -\frac{L}{R}\frac{\partial}{\partial\theta}(V_1 h_1 + V_2 (H - h_1)) \tag{5.19}$$

$$\frac{\mathrm{d}D}{\mathrm{d}t} = \mathbf{e}_3 \cdot \frac{\overline{\nabla \times \tau_{\text{w}}}}{f\rho_0} - \frac{b_0}{b_1}(P + M) \tag{5.24}$$

$$\frac{\partial h_1}{\partial t} = (P + M)\frac{b_0}{b_1} + \mathbf{e}_3 \cdot \frac{A\overline{\nabla \times \tau_{\text{w}}}}{f\rho_0 R\Theta L} - u_{\text{riv}}\frac{b_0}{b_1}\frac{h_{\text{riv}}}{L} - \frac{1}{R}\frac{\partial}{\partial\theta}V_1 h_1 \tag{5.28}$$

Solution of the Steady State

Eqs. 5.8, 5.19, 5.24, and 5.28 can be solved for the steady state in the following way. First, the left hand side of Eq. 5.24 is set to zero, and the time-averaged forcing $\left(P, M, \overline{\nabla \times \tau_{\text{w}}}, u_{\text{riv}}\right)$ is assumed known. With these assumptions, the buoyancy of the upper layer, b_1, is obtained from Eq. 5.24. The mean wind stress curl is also used in Eq. 5.3 to obtain the transport upstream of the boundary current, $\mathbf{M}(\theta = 0)$. This inflow is assumed barotropic so that $V_1 = V_2 = M_\theta/H$ at $\theta = 0$. From Eq. 5.8, this means that the pycnocline must be flat at $\theta = 0$, and that $h_1(\theta = 0) = H - D$. Finally, the freshwater inflow upstream of the boundary current is assumed to be known, so that $h_1(\theta = 0)$ can be derived since $V_1(\theta = 0)$ is also known.

Now that all information is known at $\theta = 0$, Eqs. 5.19 and 5.28 can be integrated to yield $\mathbf{M}(\theta)$ and $V_1 h_1(\theta)$. Note that $V_2 h_2$ follows directly from Eq. 5.19. The last step is to multiply Eq. 5.8 by $h_1 h_2$ and solve the resulting quadratic algebraic equation for $h_1(\theta)$:

$$(V_1 h_1)(H - h_1) - (V_2 h_2) h_1 = \frac{2g'}{fL}(D - H + h_1) h_1 (H - h_1) \tag{5.29}$$

The velocity of the lower layer, $V_2(\theta)$, is obtained from V_1 and h_1 with the thermal wind equation (Eq. 5.8).

Solution of the Prognostic Case

The equation set 5.8, 5.19, 5.24, and 5.28 can be used with time-varying forcing $(P, M, \nabla \times \tau_w)(\theta, t)$ in a prognostic calculation. This calculation begins with the solution of the steady state case as the initial condition. The volume flux in the boundary region, **M**, is free to evolve and reverse depending on the sign of the wind stress curl (Eq. 5.3). The position of the interface at $\theta = 0$ (upstream) is prescribed as $h_1(t) = h_1(t = 0)$ on inflow, and the thermal wind relation (Eq. 5.8) is applied at every point of the boundary region.

Explicit Equations for the Storage, Export, and Spatial Distribution of Freshwater

For convenience, we define three variables describing the input from the different freshwater (F) sources (rivers, surface fluxes, and Ekman exchange between the boundary and interior, respectively):

$$F_{riv}(\theta, t) = -h_{riv} u_{riv}, \quad F_{surf}(t) = L(P + M), \quad F_{ekm}(t) = \frac{b_1}{b_0} \frac{A}{R\Theta} \mathbf{e}_3 \cdot \frac{\overline{\nabla \times \tau_w}}{f\rho_0}. \tag{5.30}$$

—Storage of Freshwater

The volume of freshwater stored in the interior is obtained by integrating Eq. 5.24 in time:

$$S(t) = S(t = 0) + \frac{Ab_1}{b_0} \left[-\frac{\mathbf{e}_3}{f\rho_0} \cdot \int_0^t \overline{\nabla \times \tau}\, dt' + \frac{b_0}{b_1} \int_0^t (P + M)\, dt' \right] \tag{5.31}$$

which quantitatively shows how Ekman pumping, net precipitation, and ice melt/growth modify the volume of freshwater stored in the interior.

—Export of Freshwater

An explicit equation for the freshwater outflow from the basin, $O(t)$, is obtained by assuming the volume of freshwater enclosed in the boundary region to be constant over time (e.g., Fig. 28). With this assumption, the integration of Eq. 5.28 along θ yields:

$$O(t) \approx F_{\text{in}} L + R\left(F_{\text{surf}}\Theta + F_{\text{ekm}}\Theta + \int_0^{\Theta} F_{\text{riv}}\, \mathrm{d}\theta'\right), \quad F_{\text{in}} = \frac{b_1}{b_0}\left(V_1 h_1\right)|_{\theta=0}, \tag{5.32}$$

where $F_{\text{in}}L$ is the flux of freshwater entering the boundary current upstream (a constant value in the simulations, e.g. Table 4).

—Spatial Distribution of Freshwater in the Boundary

The amount of freshwater within the boundary current is proportional to the thickness of the fresh upper layer, $h_1(\theta, t)$. An approximate but explicit equation for h_1 can be obtained for the steady state case in the following way. Eq. 5.28 is first integrated in θ and then combined with Eqs. 5.29 and 5.19. Then, a first-order development of h_1 around $\theta = 0$ yields:

$$\begin{aligned} h_1(\theta) &= h_1(\theta = 0) + \delta h_1, \quad (\delta h_1)^2 \to 0, \quad h_1(\theta = 0) \equiv h_1^0 = H - D, \\ \delta h_1 &\approx \frac{HR}{L}\frac{b_0}{b_1}\frac{F_{\text{surf}}\,\theta + F_{\text{ekm}}\,\theta + \int_0^{\theta} F_{\text{riv}}\, \mathrm{d}\theta'}{HV_1(\theta = 0) + 2g'(fL)^{-1}\left(H - h_1^0\right)h_1^0}. \end{aligned} \tag{5.33}$$

The numerator of Eq. 5.33 represents the different sources of freshwater that are collected by the boundary current: net precipitation and net ice melt (F_{surf}), freshwater originating from the interior region (F_{ekm}), and rivers (F_{riv}). In the special case where all the sources of freshwater are evenly distributed along the boundary region, the numerator increases linearly with θ. The denominator is a constant and it represents a spatial average of the velocity in the fresh upper layer of the boundary current. The value of h_1 can thus be seen as a competition

between the freshwater inputs that thicken the fresh layer, while the boundary flow tends to flush this freshwater and thus to thin the fresh upper layer. Similarly, it can be shown that:

$$\begin{aligned} \delta V_1 &\approx \frac{\delta h_1}{H}\frac{2g'}{fL}\left(H - h_1^0 - \delta h_1\right), \\ \delta V_2 &\approx -\frac{\delta h_1}{H}\frac{2g'}{fL}\left(h_1^0 + \delta h_1\right), \end{aligned} \tag{5.34}$$

meaning that V_1 does not indefinitely speed up with increasing h_1, but rather reach a plateau around $\delta h_1 = \left(H - h_1^0\right)/2$ (e.g., Fig. 25) and decrease afterward. V_2 monotonically decreases with increasing h_1.

APPENDICE B

CALCULATION OF RIVER RUNOFF WITHIN HUDSON BAY

This section describes how the river runoff of Hudson Bay is calculated from the river gauge timeseries provided by:

1. Hydrometric Database (HYDAT) of Water Survey of Canada; http://www.wsc.ec.gc.ca/
2. International Polar Year (IPY) Arctic Freshwater Systems database (Déry et al., 2009); http://nhg.unbc.ca/ipy/index.html
3. Ministère de l'Environnement du Québec database; http://cehq.gouv.qc.ca/suivihydro/default.asp
4. personal communications between Sylvain Joly and Hydro-Québec, Ontario Hydro, and Manitoba Hydro.

Spatial Coverage

Usually only a fraction of the drainage basin is gauged, and the total runoff must be estimated from a proxy. Following the work of Prinsenberg et al. (1987), Hudson Bay is divided into six regions and the proportion of gauged area to total area is given in Table 6. The runoff from the ungauged areas is estimated from adjacent gauged areas as in Prinsenberg et al. (1987). It can be seen in Table 6 that up to 77% of the total drainage basin is gauged

over the years, which represents a substantial fraction of the whole drainage basin.

Temporal Coverage, Daily Runoff, and Monthly Climatology

The numerical model of Chapters 1 and 2 uses observed daily river runoff obtained from the sources mentioned above. The temporal coverage of these daily data is shown in Fig. 35 for a sample (the ten largest rivers) of the whole river runoff dataset. It is seen that daily data were available for nearly all (eight out of 10) of the largest rivers during the period examined in Chapters 1 and 2 (August 2003 to August 2004). Furthermore, these data cover the rivers of Hudson Bay that are affected by dams, diversion or reservoirs (Fig. 35). We conclude that the hydrometric data used in the study are representative of the true runoff of Hudson Bay, and that the numerical simulations conducted in the study are as realistic as possible.

For rivers and years when daily runoff is not available, the model falls back to the temporal interpolation of a monthly climatology of river discharge. This climatology is built by averaging, for a given month and river, the data over all the years available. For rivers that are regulated (e.g. for hydroelectric production) the years prior to regulation are discarded so that the climatology is representative of the regulated runoff of Hudson Bay. The climatology thus includes 12 values (Jan. to Dec.) for each of the rivers around the basin.

River Runoff in Chapter 3

The monthly river runoff climatology described above provides a realistic description of: (1) the spatial distribution of the river runoff within the basin, and (2) the seasonal cycle of each river within the basin. This simple (yet realistic) climatology is thus appropriate for the idealized model described in Chapter 3. Unfortunately, if it is taken alone, the monthly climatology ignores the actual interannual variations in the river runoff of the basin. To add

Table 6: Size of gauged and ungauged areas within the drainage basin of Hudson Bay. See Prinsenberg et al. (1987) for a detailed map of the six regions defined in the table, and a list of the rivers they include.

Region		Gauged Area 10^3 km^2	Ungauged Area 10^3 km^2	Total Area 10^3 km^2
I	Prairies & NW Ont.	1542.5	166.6	1709.1
II	NW Territories	255.0	240.0	495.0
III & IV	North Québec	0.0	80.0	80.0
V	Mid-Qué. / NE Ont.	101.4	77.0	178.4
VIa	West James Bay	252.0	111.5	363.5
VIb	East James Bay	256.4	43.5	299.9
Sum		2407.3	718.6	3125.9

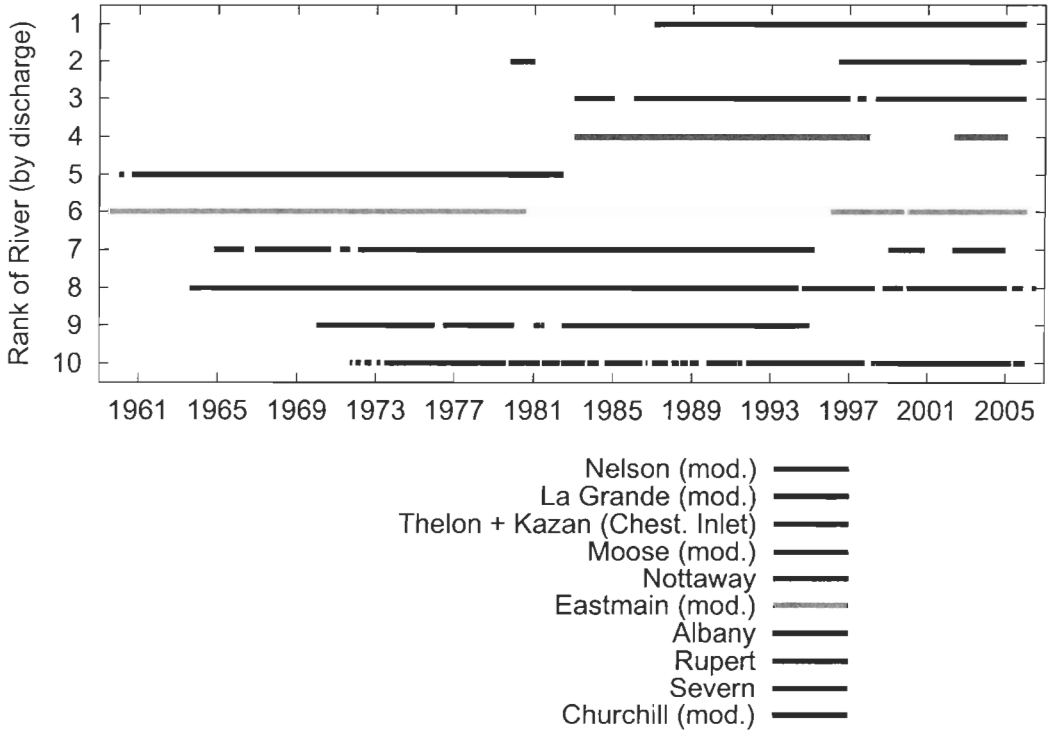

Figure 35: Period over which observed daily river runoff data is available for the ten largest rivers of Hudson Bay. Rivers affected by dams, diversion or reservoirs are identified (mod.).

this information about interannual variability into the idealized model, while at the same time keeping the model reasonably simple, we decide to multiply the monthly climatology by a yearly *scaling factor* $\phi(t)$. For instance, if during a given year t' the total runoff of Hudson Bay is 10% higher than its long-term mean value, then $\phi(t') = 1.1$ and thus the monthly climatology is scaled up by 10% during this year. With this procedure, both seasonal and interannual variability of the river discharge are introduced in the idealized model.

The scaling factor $\phi(t)$ (multiplied by the long-term mean runoff of Hudson Bay) is shown in the top panel of Fig. 28. The value of $\phi(t)$ is obtained in the following way. Yearly river runoff timeseries are first obtained from source 2 (IPY) for all the rivers of Hudson Bay that are available. Then, in the simple case where all the N rivers of Hudson Bay would be continuously gauged, the modulation $\phi(t)$ at year $t = t'$ would be calculated as:

$$\phi(t = t') = \frac{R(t')}{\mathrm{LTMR}}, \quad R(t') = \sum_{i=1}^{N} Q_i(t'), \quad \mathrm{LTMR} = \sum_{i=1}^{N} \langle Q_i(t) \rangle, \tag{6.1}$$

which is simply the ratio between the runoff from this particular year, $R(t')$, and the Long-Term Mean Runoff (LTMR) of Hudson Bay (about 635 $\mathrm{km^3\,y^{-1}}$, Lammers et al., 2001). The symbol $Q_i(t')$ represents the discharge from river i over the year t', and the brackets $< . >$ denote its time-average over all the years covered by the dataset.

In the more realistic case where the number of rivers gauged fluctuates over the years, the more general equation used is:

$$\phi(t = t') = \left(\sum_{i=1}^{N(t')} Q_i(t') \right) \left(\sum_{i=1}^{N(t')} \langle Q_i(t) \rangle \right)^{-1}, \tag{6.2}$$

where the index i now runs over the $N(t')$ rivers that are gauged at year t', and the brackets $< . >$ denote a time-average of the discharge $Q_i(t)$ over all the years available for this particular river. Note that $\langle \phi(t) \rangle = 1$, as expected.